AD-A060 153 ENVIRONMENTAL RESEARCH INST OF MICHIGAN ANN ARBOR IN--ETC F/G 17/5
STATISTICAL ANALYSES OF SELECTED TERRAIN AND WATER BACKGROUND M--ETC(U)
JUL 78 J R MAXWELL N00123-77-C-0682
UNCLASSIFIED ERIM-132300-1-F NL

1 OF 2
ADA
060153

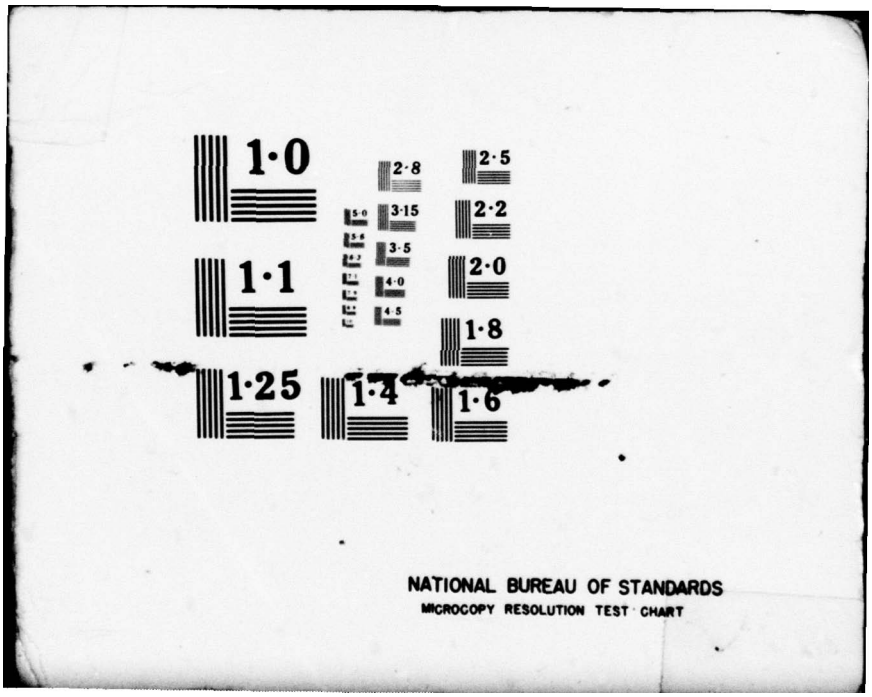
1·0
1·1
1·25
1·4
1·6
1·8
2·0
2·2
2·5
2·8
3·15
3·5
4·0
4·5
NATIONAL BUREAU OF STANDARDS
MICROCOPY RESOLUTION TEST CHART

LEVEL II

132300-1-F

Final Report

STATISTICAL ANALYSES OF SELECTED TERRAIN AND WATER BACKGROUND MEASUREMENTS DATA

J. ROBERT MAXWELL
Infrared and Optics Division

JULY 1978

Approved for Public Release
Distribution Unlimited

Optical Signatures Program
Naval Weapons Center
China Lake, California

ENVIRONMENTAL
RESEARCH INSTITUTE OF MICHIGAN
BOX 8618 • ANN ARBOR • MICHIGAN 48107

Notices

Sponsorship. The work reported herein was conducted by the Environmental Research Institute of Michigan (formerly the Willow Run Laboratory of The University of Michigan) for the Naval Weapons Center, China Lake, California under Contract Number N00123-77-C-0682. The Project Managers were Dr. Lowell Wilkins and Dr. Jon Wunderlich.

UNCLASSIFIED

SECURITY CLASSIFICATION OF THIS PAGE *(When Data Entered)*

REPORT DOCUMENTATION PAGE	READ INSTRUCTIONS BEFORE COMPLETING FORM
1 REPORT NUMBER: 132300-1-F ✓	2 GOVT ACCESSION NO
3 RECIPIENT'S CATALOG NUMBER	
4 TITLE *(and Subtitle)*: (6) Statistical Analyses of Selected Terrain and Water Background Measurements Data	5 TYPE OF REPORT & PERIOD COVERED: (9) Final Report,
6 PERFORMING ORG REPORT NUMBER: 132300-1-F	
7 AUTHOR(s): (10) J. Robert Maxwell	8 CONTRACT OR GRANT NUMBER(s): (15) N00123-77-C-0682 ✓
9 PERFORMING ORGANIZATION NAME AND ADDRESS: Infrared and Optics Division / Environmental Research Institute of Michigan / Ann Arbor, MI 48107	10 PROGRAM ELEMENT PROJECT TASK AREA & WORK UNIT NUMBERS
11 CONTROLLING OFFICE NAME AND ADDRESS: Dr. Lowell Wilkins / Naval Weapons Center, China Lake, CA 93555	(11) 12 REPORT DATE: July 1978 / 13 NUMBER OF PAGES: 154
14 MONITORING AGENCY NAME AND ADDRESS *(if different from Controlling Office)*: Receiving Officer / Naval Weapons Center / China Lake, CA 93555	15 SECURITY CLASS *(of this report)*: Unclassified / 15a DECLASSIFICATION/DOWNGRADING SCHEDULE: N/A

16 DISTRIBUTION STATEMENT *(of this Report)*

Approved for Public Release: Distribution Unlimited

(12) 152 p.

17 DISTRIBUTION STATEMENT *(of the abstract entered in Block 20, if different from Report)*

(14) ERIM-132300-1-F

18 SUPPLEMENTARY NOTES

19 KEY WORDS *(Continue on reverse side if necessary and identify by block number)*

Terrain backgrounds, IR imagery, statistical analyses

20 ABSTRACT *(Continue on reverse side if necessary and identify by block number)*

Terrain and water background measurement data in the mid-IR have been collected and analyzed in support of the Navy Optical Signature Program. This is a continuing program to provide representative backgrounds data for various system performance studies. Calibrated digital data tapes of the backgrounds data are maintained as part of the program.

Selected data over desert and mountainous terrain at Nellis AFB, over a rural and urban terrain in West Virginia, and over water at Pt. Mugu were → next page

DD FORM 1 JAN 73 1473 EDITION OF 1 NOV 65 IS OBSOLETE

UNCLASSIFIED

SECURITY CLASSIFICATION OF THIS PAGE *(When Data Entered)*

cont'd analyzed in several spectral bands in the IR and mid-IR including micrometer 2.0 - 2.6, 3.5 - 3.9, 3.9 - 4.7, 4.5 - 5.5, 5.1 - 5.7, and 9.0 - 11.4 μm. Of the extensive data available at Nellis, the data that were selected for statistical analysis provided a comparison of desert and mountainous terrain, downward and 35 degree depression angle data, morning and afternoon data and data at 1000 ft. and 5000 ft. altitude. Statistics and a discussion of the statistical analysis is presented in the report including means, standard deviations, histograms, hot spot (ellipse) analyses, spectral correlations, and power spectra.

TABLE OF CONTENTS

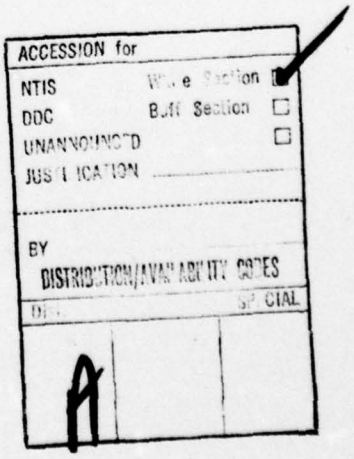

LIST OF TABLES

LIST OF FIGURES

1.0
INTRODUCTION AND SUMMARY

A backgrounds measurement and analysis program is being conducted for the Navy Optical Signatures Program for the purpose of generating calibrated digital imagery over various terrain backgrounds, generating statistics for these scenes useful for classifying various background types, and for developing statistical measures that can be related to various system performance characteristics.

Previous efforts on this program have included a literature search and bibliography of available backgrounds data [Reference 1]. In addition, selected terrain backgrounds data that were available that had been collected with the ERIM airborne multispectral scanner were analyzed and the results reported [References 2 and 3]. ERIM airborne multispectral scanner data are especially suitable for terrain backgrounds analysis because the data are multispectral, registered, calibrated, in digital format, are available with a ground spatial resolution of two to three feet, and provide a large coverage of the terrain. The data that were available for the early analysis efforts reported in References 2 and 3 were primarily data in spectral bands positioned between 1.0 and 2.5 μm and in the 8.0 - 13.5 μm spectral region.

The current program extends the work of last year with a data collection and analysis program. Airborne data were collected over an urban and a forested area in West Virginia in October 1977, over a desert and mountainous terrain at Nellis AFB in February 1978, and over water at Pt. Mugu in March 1978. Data were collected in the mid-IR in spectral bands from 2.0 - 2.6, 3.0 - 4.2, 3.5 - 3.9, 3.9 - 4.7, 4.5 - 5.5, and 5.1 - 5.7 μm as well as in the spectral band from 9.0 - 11.4 μm with the ERIM M-7 multispectral scanner.

An extensive series of flights at Nellis AFB was made in order to assess and compare the statistical characteristics of the desert and

mountainous terrain under a variety of conditions. A subset of the data was selected in order to compare the desert and mountainous terrain and to determine the effects of depression angle and time of day on the statistics. In addition, the altitude dependence of the measurements in the 5.1 - 5.7 μm band on the edge of the water vapor absorption at 6.3 μm was investigated.

Analysis of this subset of data collected at Nellis AFB in the 3.5 - 3.9, 3.9 - 4.7, 5.1 - 5.7, and 9.0 - 11.4 μm has been completed. The analysis has included measurement of means, standard deviations, spectral correlation coefficients, ellipse statistics, histograms, and power spectra. A number of significant findings result from the analysis:

- The 5.1 - 5.7 μm band is severely attenuated by atmospheric water vapor absorption. The mean apparent scene temperature and the clutter are lower at 5000 ft than at 1000 ft.
- The flat desert terrain is hotter and less cluttered than the mountainous desert terrain at Nellis.
- Shadows are the most prominent feature in the mountainous desert terrain at Nellis. This causes the clutter and the spectral correlations to be higher over the mountains than over the desert. This also causes the mean scene temperature over the mountains to be lower than over the desert.
- The 3.5 - 3.9, 3.9 - 4.7, and 9.0 - 11.4 μm data over the mountains are correlated with a correlation coefficient between 0.8 and 0.9. The correlation coefficients over the desert are significantly lower.

- The means and standard deviations of the data in the downward vs the 35° depression angle data were not found to be significantly different.
- The mean scene apparent temperatures at 1500 hrs were found to be about 5K higher than at 1000 hrs. Scene clutter was about the same at 1500 hrs as at 1000 hrs.
- Due to the solar reflection in the 3.5-3.9 μm band, the mean apparent temperatures and clutter are higher.
- There are a significant number of contiguous areas up to 200 m^2 at a one standard deviation above the mean threshold in all of the data.
- The moutainous desert terrain at Nellis showed more large areas at the one standard deviation above the mean than the other types of terrain analyzed.

Data collected over the urban and forested area of West Virginia in the 3.9 - 4.7 μm spectral band were also analyzed. The following findings have resulted from the analysis:

- No significant differences in scene mean apparent temperatures or standard deviations were observed for 90° vs 35° depression.
- The clutter over the urban area was significantly larger than over the rural area.

Finally, sunglint data at Pt. Mugu for fairly calm sea state conditions has been analyzed. For the prevailing conditions:

- The peak sunglint in the 2.0 to 2.6 μm band was 600 - 700 $\mu w/cm^2 \cdot sr \cdot \mu m$.

- The peak sunglint apparent temperature in the 3.9 - 4.7 μm band was observed to be 310 to 320K; in the 4.5 to 5.5 μm band, 292 to 293K.
- The sunglint was not observable in the 9.0 - 11.4 μm band.

Additional data collected at Nellis AFB in the 2.0 - 2.6 and 4.5 - 5.5 μm band is scheduled for reduction and statistical analysis along with further investigation into the effects of direction of flight and meteorological conditions.

In the material that follows, a very brief description of the ERIM M-7 multispectral scanner and data reduction procedures is given, and then a summary of the data and analysis completed to date for the specific purposes of collection described above are given.

2.0

MULTISPECTRAL SCANNER

Figure 1 is a schematic of the M-7 multispectral scanner. Radiation in the visible portion of the spectrum is collected in detector position number 3, dispersed, and sensed with 12 photo multipliers. By use of a dichroic beam splitter, energy beyond 0.9 μm is directed to detector position number 2. For the flights at Nellis AFB and Pt. Mugu a two or three element InSb detector array was placed in detector position 2 with each detector element appropriately filtered. The two element InSb array was filtered to 3.5 - 3.9 μm and 3.9 - 4.7 μm. The three element InSb array used for some flights was filtered to 2.0 - 2.6, 3.0 - 4.2, and 4.5 - 5.5 μm. A filtered HgCdTe detector was used in detector position 1A. On some flights a 5.1 - 5.7 μm filter was used, on others a 9.0 - 11.4 μm filter was used. It is important to note that the data in all 12 visible bands, the 2 (or 3) InSb mid-IR bands, and the filtered HgCdTe band are collected simultaneously and can be spatially registered by accounting for the delay between the two InSb detectors.

The InSb detectors are 2.5 mrad detectors and the HgCdTe detector is 2.9 mrad. The scanning motor scans 60 lines/sec. The detectors scan across up to six calibration sources located inside the scanner housing with each rotation of the scan mirror. The various IR channels are calibrated with two controlled blackbody sources located in the scanner housing. The scanner is mounted in a C-47 aircraft that flys with a typical ground speed of 202 ft/sec. Hence a scan line is recorded for every 3.4 feet of aircraft motion at a scan rate of 60 lines/sec. At an aircraft altitude of 1300 feet, with a detector resolution of 2.5 mrad, the imagery produced is contiguous with a ground resolution of 3.4 feet. At lower altitudes the data

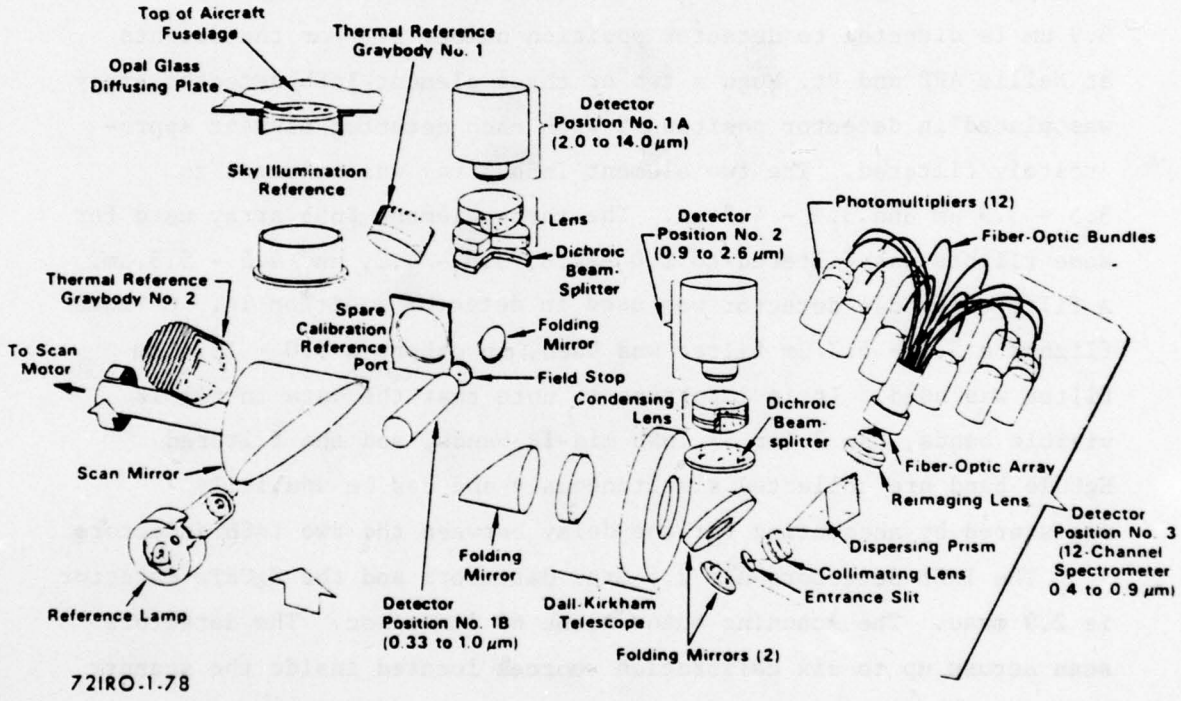

FIGURE 1. OPTICAL SCHEMATIC OF ERIM EXPERIMENTAL MULTISPECTRAL SCANNER, M-7

are somewhat under sampled, and at higher altitudes the data are over-sampled. As part of the calibration procedure an appropriate number of lines are averaged so that in the resulting image there is only one digital value for each resolution size (2.5 mrad) ground spot in the image. Calibrated data tapes are maintained for further analysis as necessary.

3.0
DISCUSSION OF RESULTS

3.1 HISTOGRAMS

Figure 2 shows samples of imagery obtained in four of the spectral bands of interest over the mountains at Nellis AFB. The 3.5 - 3.9, 3.9 - 4.7, and 9.0 - 11.4 μm images were obtained simultaneously at 0916 on February 25, 1978. The similarity of features in the imagery in these three spectral bands is typical of the imagery in the three spectral bands that are described below. The 5.1 - 5.7 μm band image was obtained at 1513 and is included to show the low signal-to-noise ratio in the imagery because of the water vapor absorption in the band.

Figure 3 shows imagery over the desert type terrain and a dry lake at Nellis AFB obtained at 1056 on February 25, 1978.

Table 1 summarizes the Nellis AFB data selected for analysis on this program. Data from four passes over the mountains and one over the desert are denoted by NEV B, NEV C, NEV D, NEV E, and NEV F. These data were all collected on February 25, 1978, under clear conditions with only high thin clouds at the time of data collection.

Figures 4a, 4b, and 4c are histograms of imagery over the mountains at Nellis AFB (NEV F) obtained at 1034 on February 25, 1978, with the scanner tilted 55° forward from nadir to achieve a 35° depression angle configuration with the aircraft approximately 1000 ft above the local terrain. These histograms have been constructed so that the vertical scale represents the fractional number of pixels in the scene at temperature T in an increment ΔT, where ΔT is the temperature quantization that is indicated in each histogram figure. The linear horizontal scale is apparent temperature from 260 to 330K. The calibration procedure employed in reducing the multispectral scanner data for this program has been designed to convert measured radiances in each IR

(a) 3.5 - 3.9 μm

(b) 3.9 - 4.7 μm

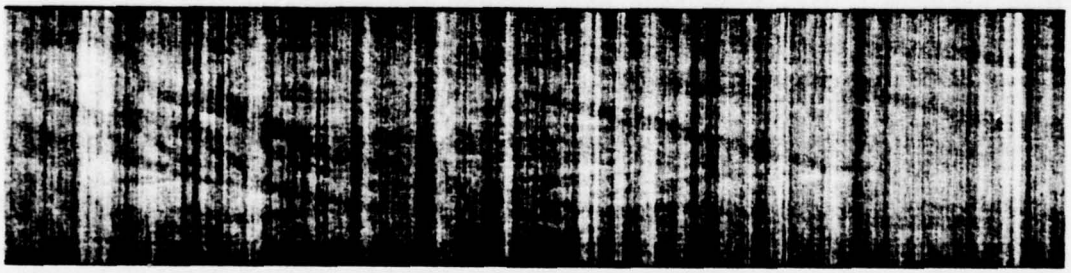

(c) 5.1 - 5.7 μm

(d) 9.0 - 11.4 μm

FIGURE 2. NELLIS AFB IMAGERY

(a) 3.5-3.9 μm

(b) 3.9-4.7 μm

(c) 9.0-11.4 μm

FIGURE 3. DESERT AND DRY LAKE NELLIS AFB IMAGERY

TABLE 1. NELLIS AFB DATA ANALYSIS

(Spectral Bands, Altitude, Depression Angle, Time, Flight Direction, and Approximate Ground Coverage)

NEV B	3.9 - 4.7, 3.5 - 3.9, 5.1 - 5.7 μm 1000 ft altitude - 35° depression angle 1511 hrs, E, mountains 1750 x 6750 ft
NEV C1	3.9 - 4.7, 3.5 - 3.9, 9.0 - 11.4 μm 1000 ft altitude - 35° depression angle 1056 hrs, W, desert east of dry lake 1750 x 3400 ft
NEV C2	Same but west of dry lake
NEV D	3.9 - 4.7, 3.5 - 3.9, 9.0 - 11.4 μm 1750 ft altitude - 90° depression angle 0914 hrs, W, mountains 1750 x 6750 ft
NEV E	3.9 - 4.7, 3.5 - 3.9, 5.1 - 5.7 μm 5000 ft altitude - 35° depression angle 1424 hrs, E, mountains 8700 x 6400 ft
NEV F	3.9 - 4.7, 3.5 - 3.9, 9.0 - 11.4 μm 1000 ft altitude - 35° depression angle 1034 hrs, E, mountains 1750 x 6750 ft

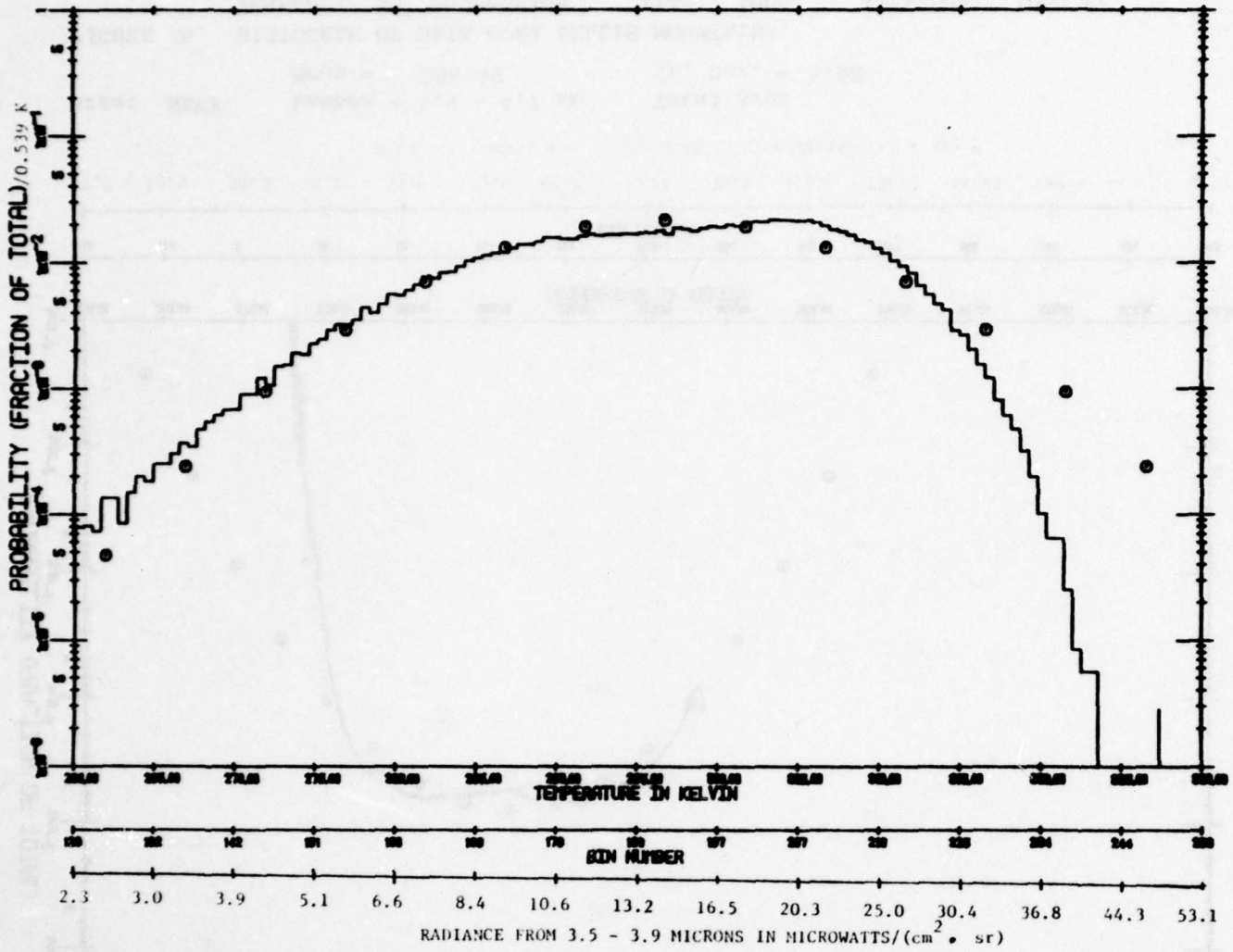

Area: NEVF Lambda = 3.5 - 3.9 μm Total Area
Mean = 296.76 Std. Dev. = 9.94

FIGURE 4a. HISTOGRAM OF DATA OVER NELLIS MOUNTAINS.
Scanner: 35° Depression Time: 1034 Altitude: 1000 Ft.

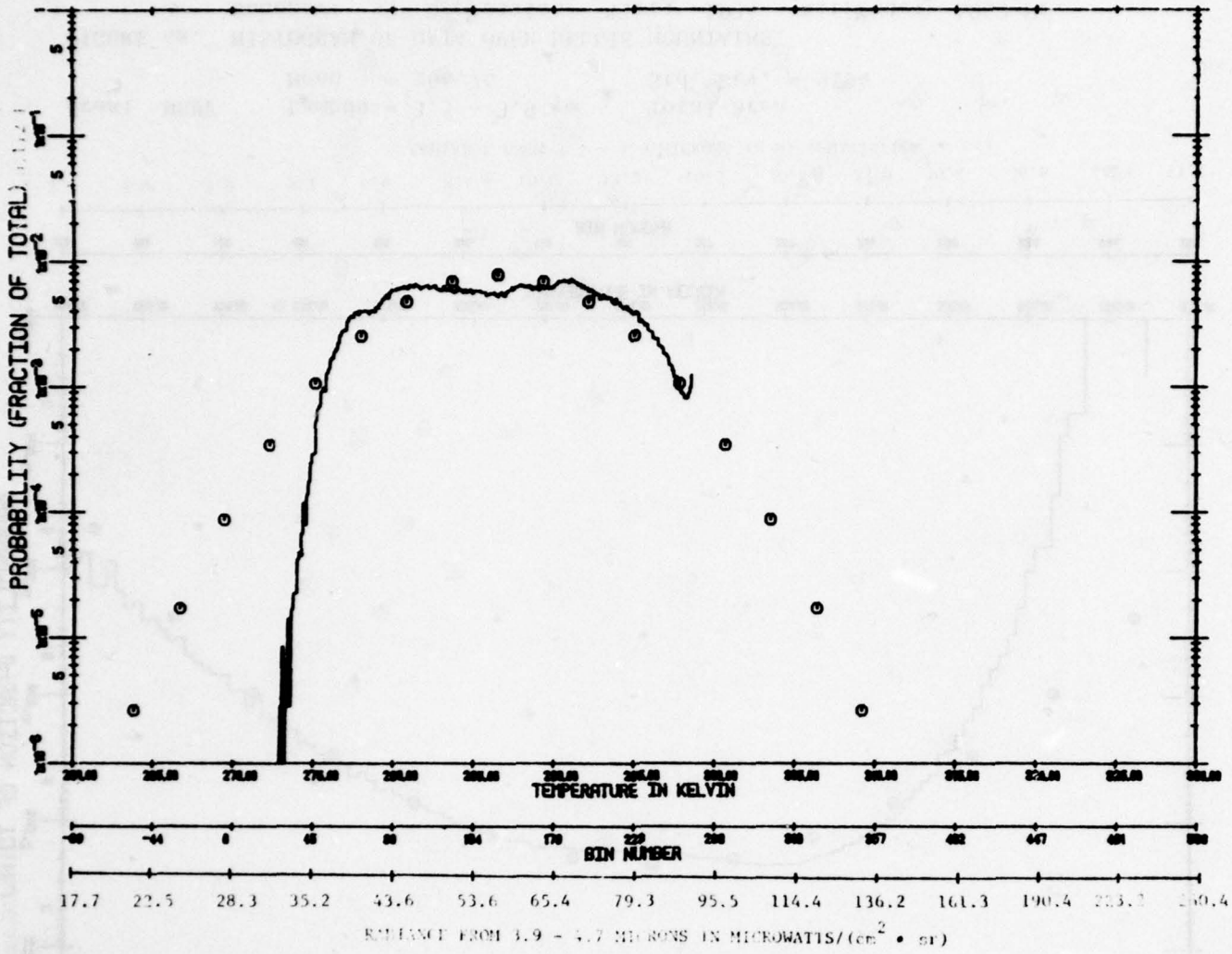

Area: NEVF Lambda = 3.9 - 4.7 μm Total Area
Mean = 286.49 St. Dev. = 5.68

FIGURE 4b. HISTOGRAM OF DATA OVER NELLIS MOUNTAINS.
Scanner: 35° Depression Time: 1034 Altitude: 1000 Ft.

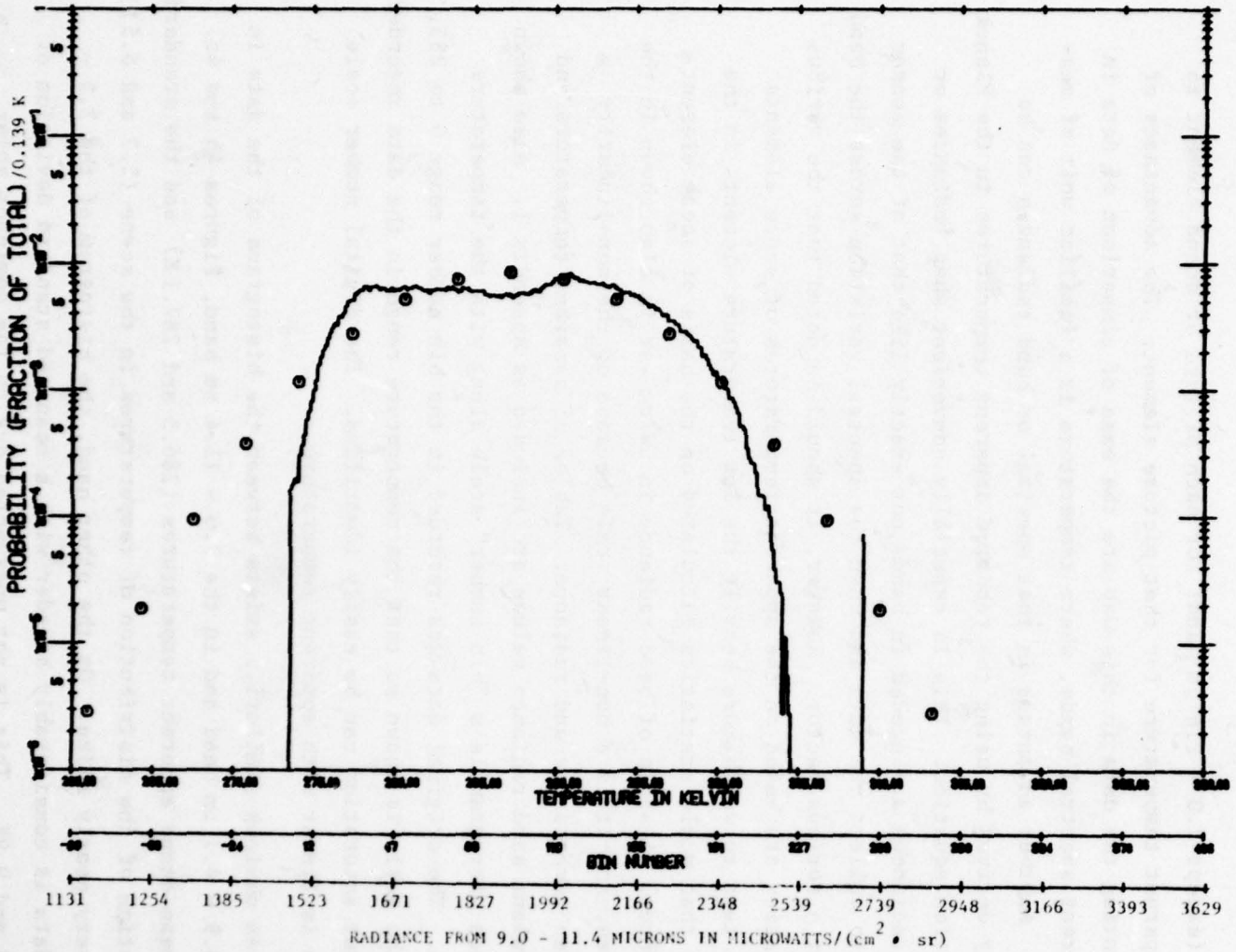

Area: NEVF Lambda = 9.0 - 11.4 μm Total Area
Mean = 287.08 Std. Dev. = 6.53

FIGURE 4c. HISTOGRAM OF DATA OVER NELLIS MOUNTAINS
Scanner: 35° Depression Time: 1034 Altitude: 1000 Ft.

band (except 2.0 - 2.6 μm band) for each picture or scene element to an apparent temperature for that picture element. The advantages of presenting the data in this way are the ease of comparison of data in different spectral bands, where temperature is a familiar unit of measure. Another advantage is that spectral or band radiances can be easily derived by using the reported apparent temperatures in the Planck radiation equation. This is especially convenient when radiances or band radiances are needed in bands not exactly like that of the sensor used to collect the data and when the spectral variation across the band is not a serious factor. However, it should be noted that the various statistics are based on the apparent temperatures of scene elements which tend to weigh more heavily the low temperature elements in the scene than would statistics calculated on the basis of scene element radiances. A scale of band radiance in $\mu W/cm^2 \cdot sr$ is also shown in the figures, and it is a non-linear scale because of the non-linearity between temperature and radiance. Tables of apparent temperature and equivalent band radiance values are included as Appendix 1. Also shown on each histogram is a "bin number" scale along with the temperature scale. The original data was recorded in the bin number range 0 to 255, and the scale is shown so that the temperature range in the data recorded without saturation can be easily identified. The digital number scale shown is linear with apparent temperature.

An obvious similarity exists between the histograms of the data in the 3.9 - 4.7 μm band and in the 9.0 - 11.4 μm band, Figures 4b and 4c. The mean scene apparent temperatures (286.5 and 287.1 K) and the standard deviation of the distribution of temperatures in the scene (5.7 and 6.5 K) are very nearly alike. On the other hand, the histogram of the 3.5 - 3.9 data is considerably broader with a mean and standard deviation of 296.8 and 9.9K. This is not unexpected due to the dominant solar reflection from 3.5 to 3.9 μm. Also shown in Figures 4a, 4b, and 4c are Gaussian distributions based on the measured mean and standard

deviation in the data. The Gaussian distribution is shown by the circle symbols on the plots at half-standard deviation increments.

Figures 5a and 5b show histograms of data in the 5.1 - 5.7 μm band at two different altitudes, 1000 ft in Figure 5a and 5000 ft in Figure 5b. These are histograms of data collected over the mountains at Nellis AFB in the mid-afternoon of February 25, 1978, with the scanner at a depression angle of 35°. There are two pronounced differences in the histograms, namely that the mean temperature at 5000 ft is 5K lower than at 1000 ft, and that there is more clutter at 1000 ft than at 5000 ft. The first difference is consistent with the fact that the atmospheric transmission in the 5.1 - 5.7 μm band is low so that the mean scene apparent temperature is strongly influenced by the atmosphere at the altitude of the aircraft, which decreases with altitude. Further, the standard deviation in the data at 1000 ft is 3.9K and at 5000 ft is 2.3K. A significant fraction of the variability in the measured apparent temperatures is due to detector noise which is so prominent because of the reduced sensitivity of the HgCdTe detector at the shorter wavelengths. The noise characteristics in the data have been analyzed by examining the noise in the calibration plate data recorded as part of each scan line. Assuming that the scene clutter and detector noise are both Gaussian, the residual scene clutter at 1000 ft is 1.7K, at 5000 ft is 1.1K. Qualitatively, these results are as expected and should form a basis for confirming spectral extrapolations with imagery in a window band (e.g., 9.0 - 11.4) to bands on the edges of absorption regions.

Figures 6a - 6f are histograms of data in the 3.5 - 3.9, 3.9 - 4.7, and 9.0 - 11.4 μm spectral bands collected over a rather flat desert area at Nellis AFB. Figures 6a, 6b, and 6c refer to the desert area to the east of the dry lake (left in Figure 3) and are denoted NEV C1. Figures 6d, 6e, and 6f refer to the desert area to the west of the dry lake (right in Figure 3) and are denoted NEV C2. The histograms are

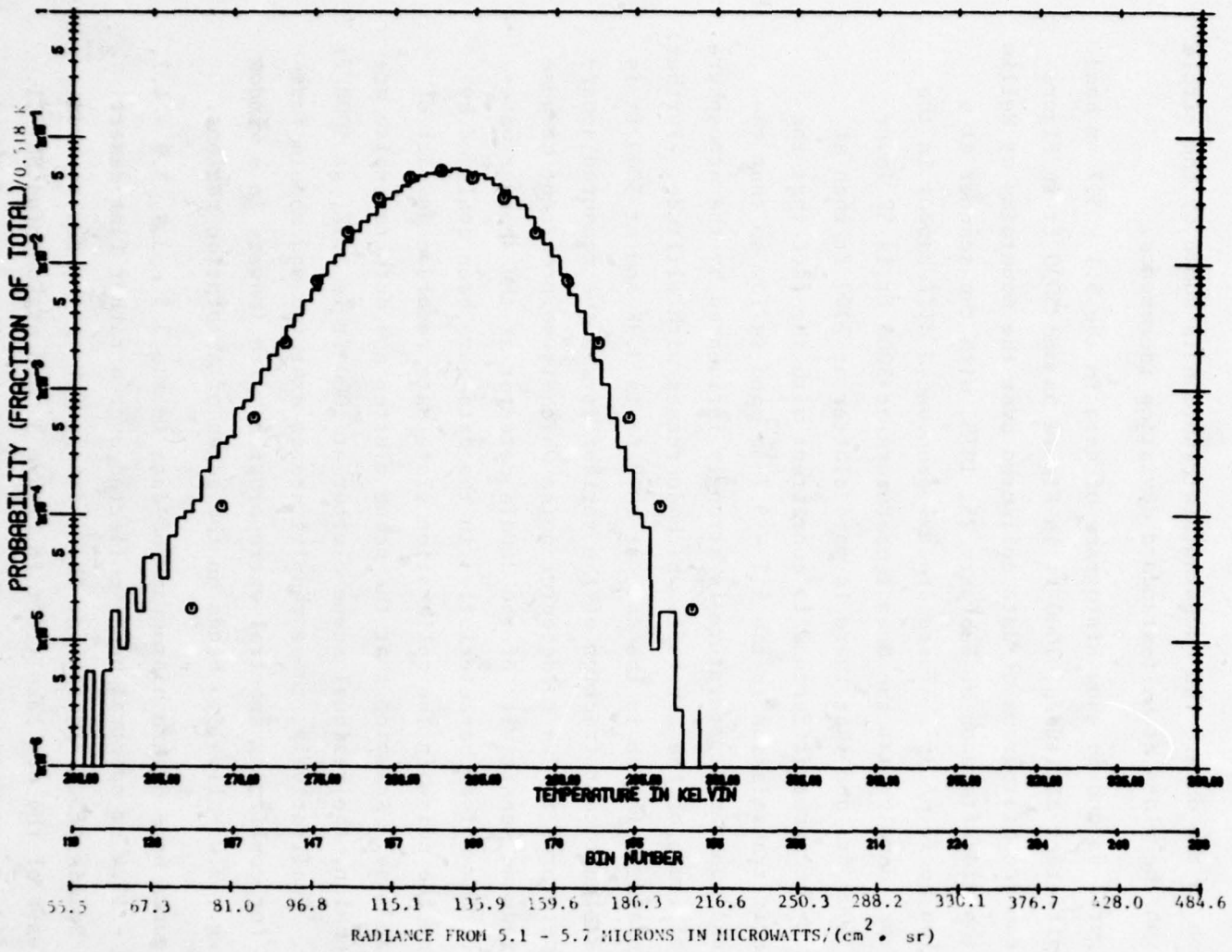

Area: NEVB Lambda = 5.1 - 5.7 μm Total Area
Mean = 282.88 St. Dev. = 3.90

FIGURE 5a. HISTOGRAM OF DATA OVER NELLIS MOUNTAINS.
Scanner: 35° Depression Time: 1511 Altitude: 1000 Ft.

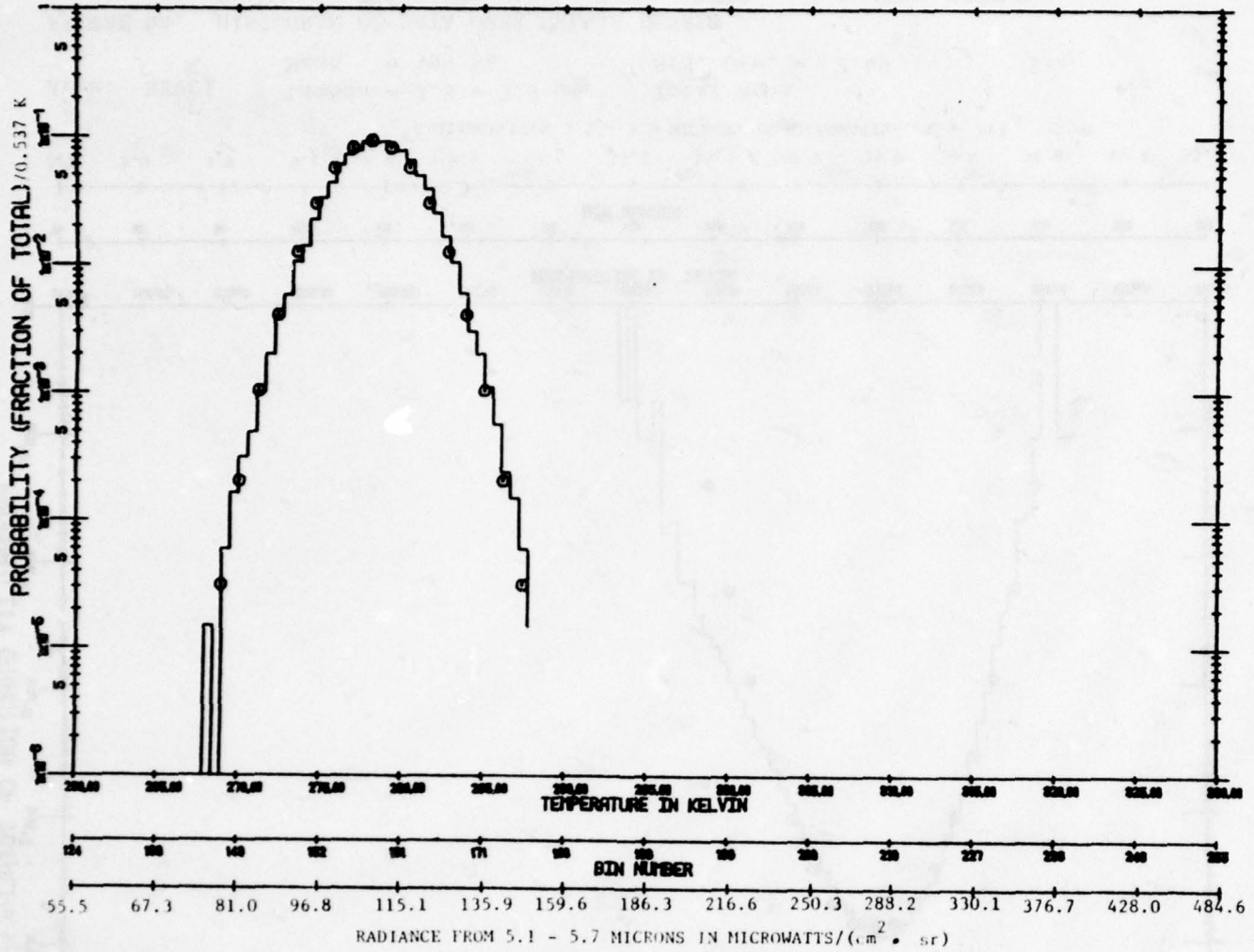

Area: NEVE Lambda = 5.1 - 5.7 μm Total Area
Mean = 278.15 Std. Dev. = 2.31

FIGURE 5b. HISTOGRAM OF DATA OVER NELLIS MOUNTAINS.
Scanner: 35° Depression Time: 1424 Altitude: 5000 Ft.

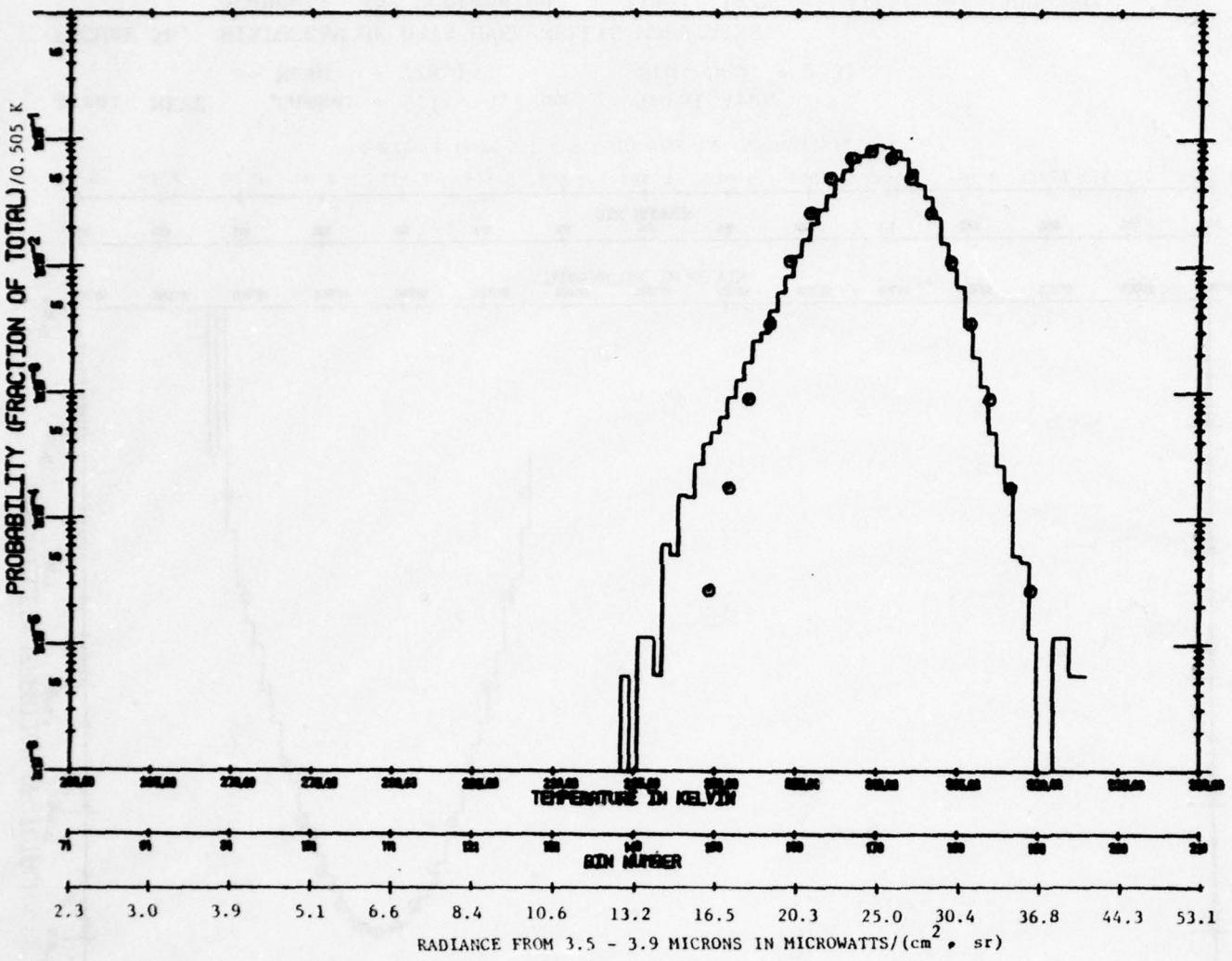

Area: NEVC1 Lambda = 3.5 - 3.9 μm Total Area
Mean = 309.56 Std. Dev. = 2.49

FIGURE 6a. HISTOGRAM OF DATA OVER NELLIS DESERT.
Scanner: 35° Depression Time: 1058 Altitude: 1000 Ft.

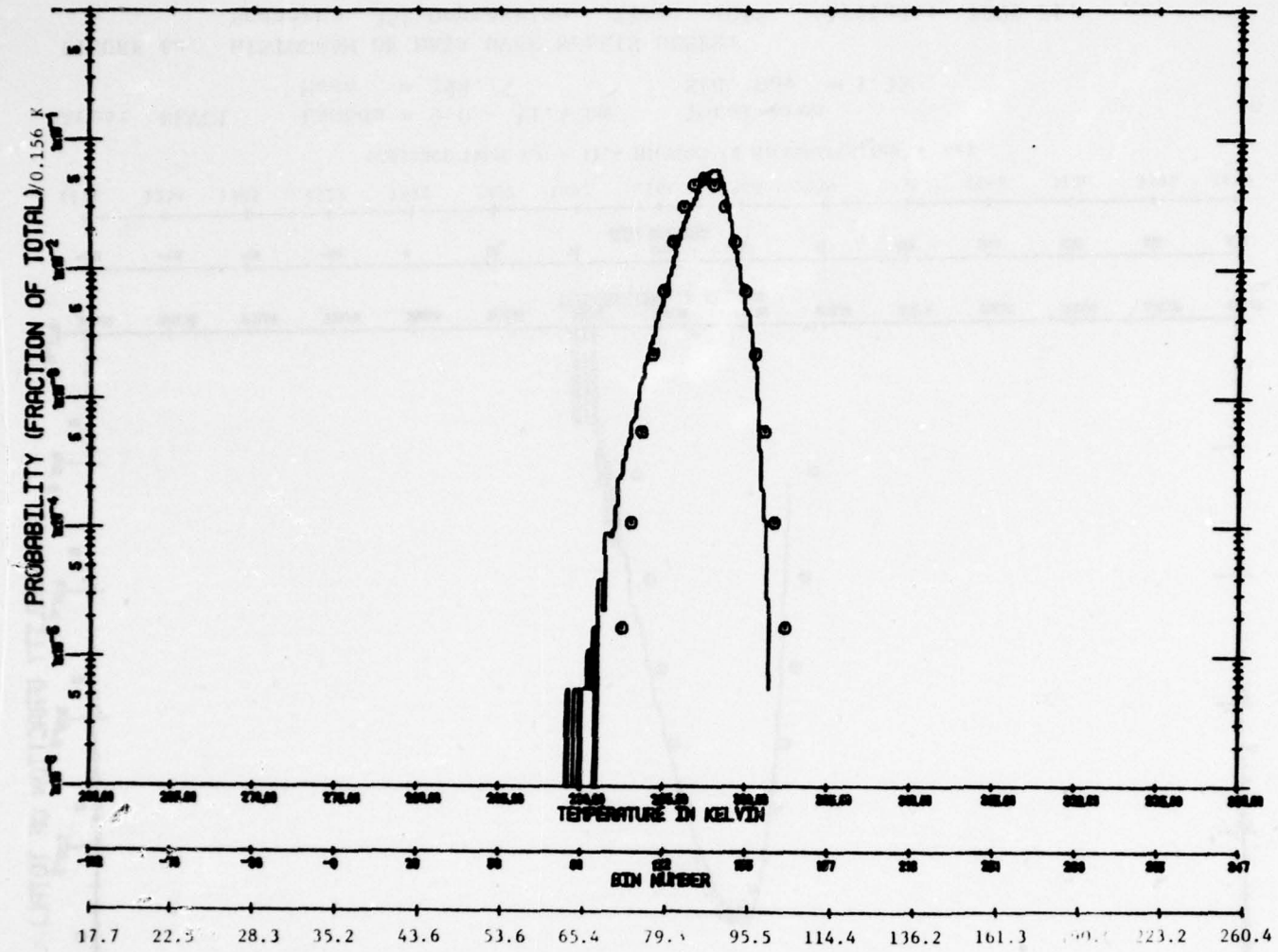

Area: NEVC1 Lambda = 3.9 - 4.7 μm Total Area
Mean = 297.41 Std. Dev. = 1.24

FIGURE 6b. HISTOGRAM OF DATA OVER NELLIS DESERT.
Scanner: 35° Depression Time: 1058 Altitude: 1000 Ft.

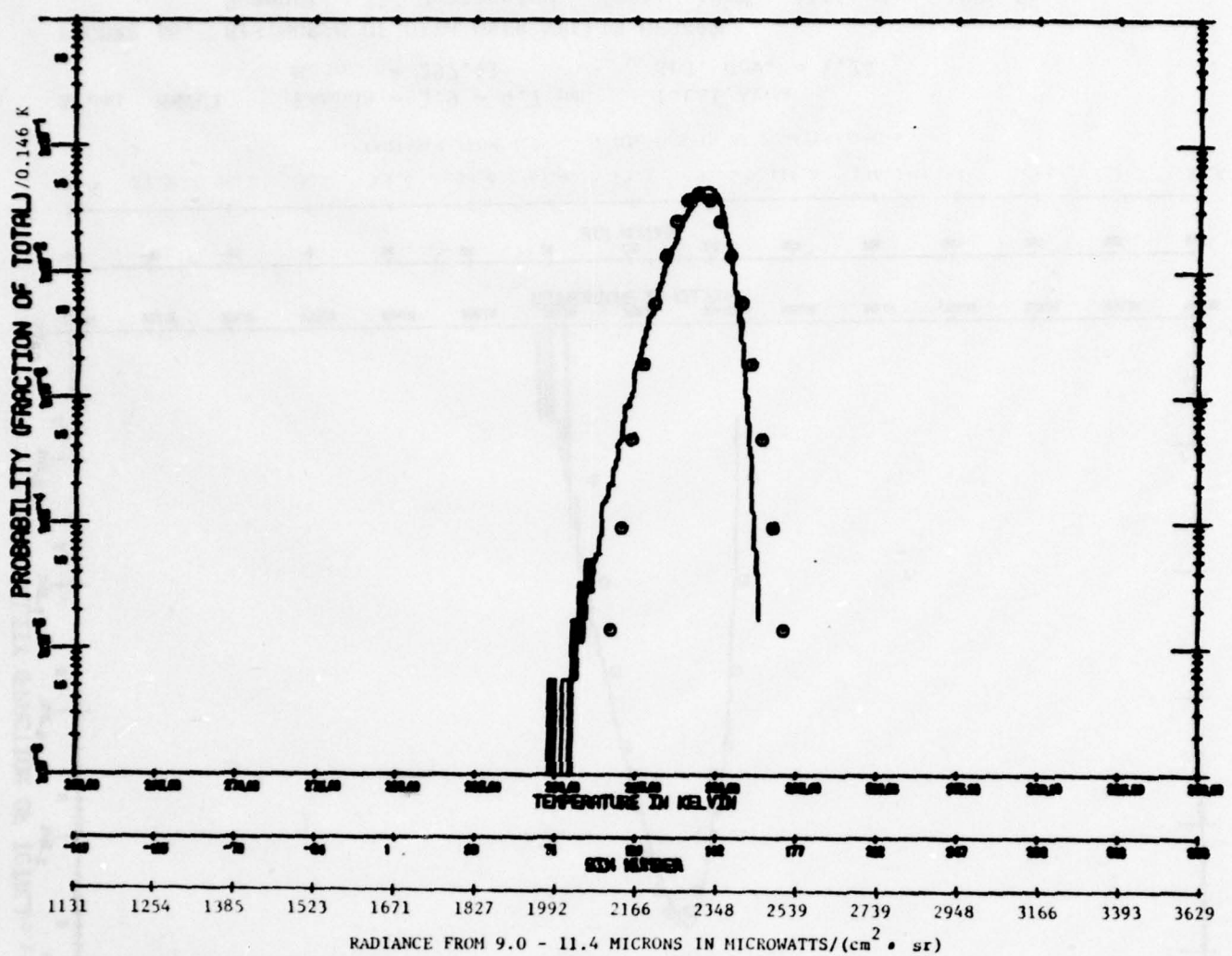

Area: NEVC1 Lambda = 9.0 - 11.4 μm Total Area
Mean = 298.75 Std. Dev. = 1.35

FIGURE 6c. HISTOGRAM OF DATA OVER NELLIS DESERT
Scanner: 35° Depression Time: 1058 Altitude: 1000 Ft.

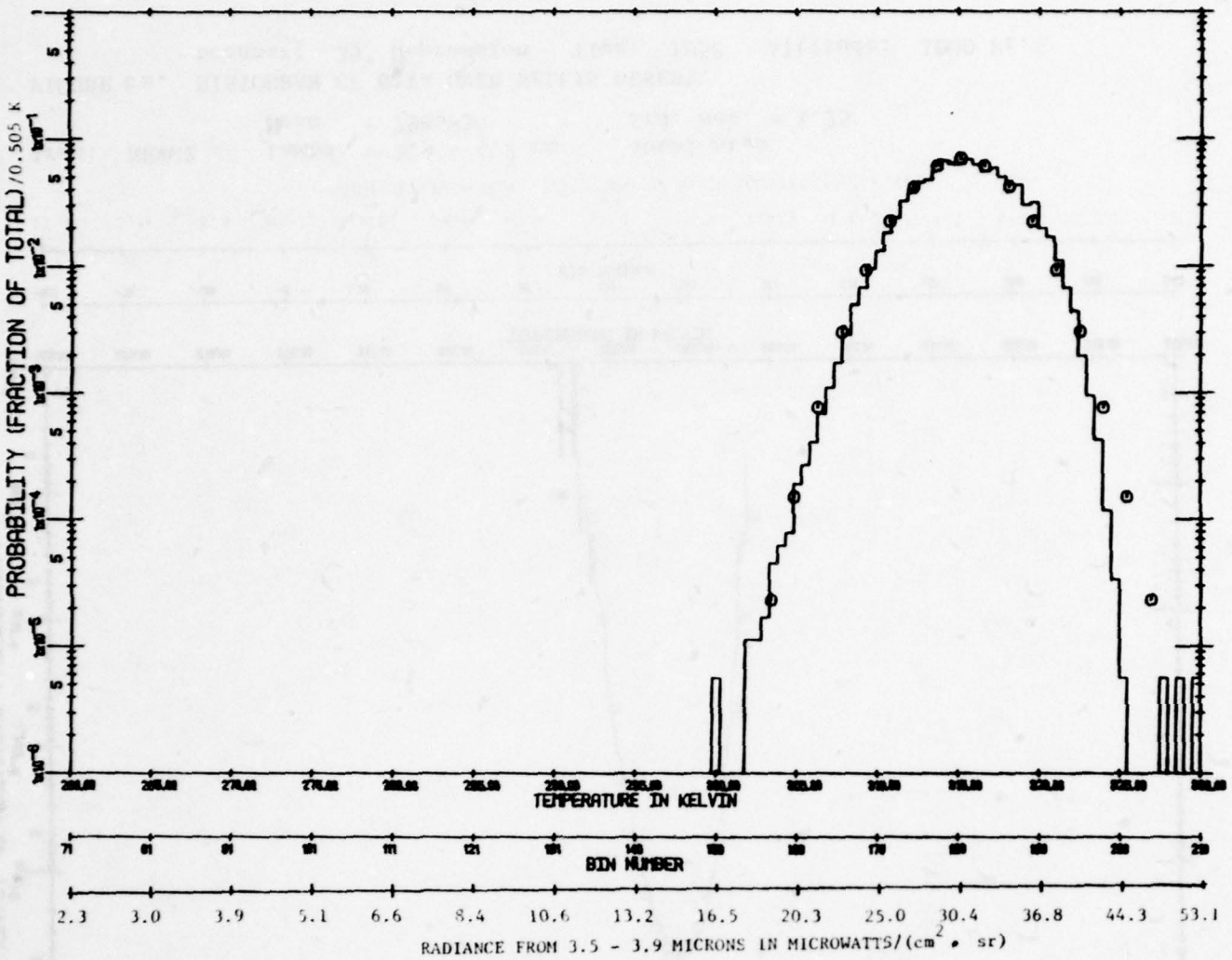

Area: NEVC2 Lambda = 3.5 - 3.9 μm Total Area
Mean = 315.14 Std. Dev. = 2.95

FIGURE 6d. HISTOGRAM OF DATA OVER NELLIS DESERT.
Scanner: 35° Depression Time: 1058 Altitude: 1000 Ft.

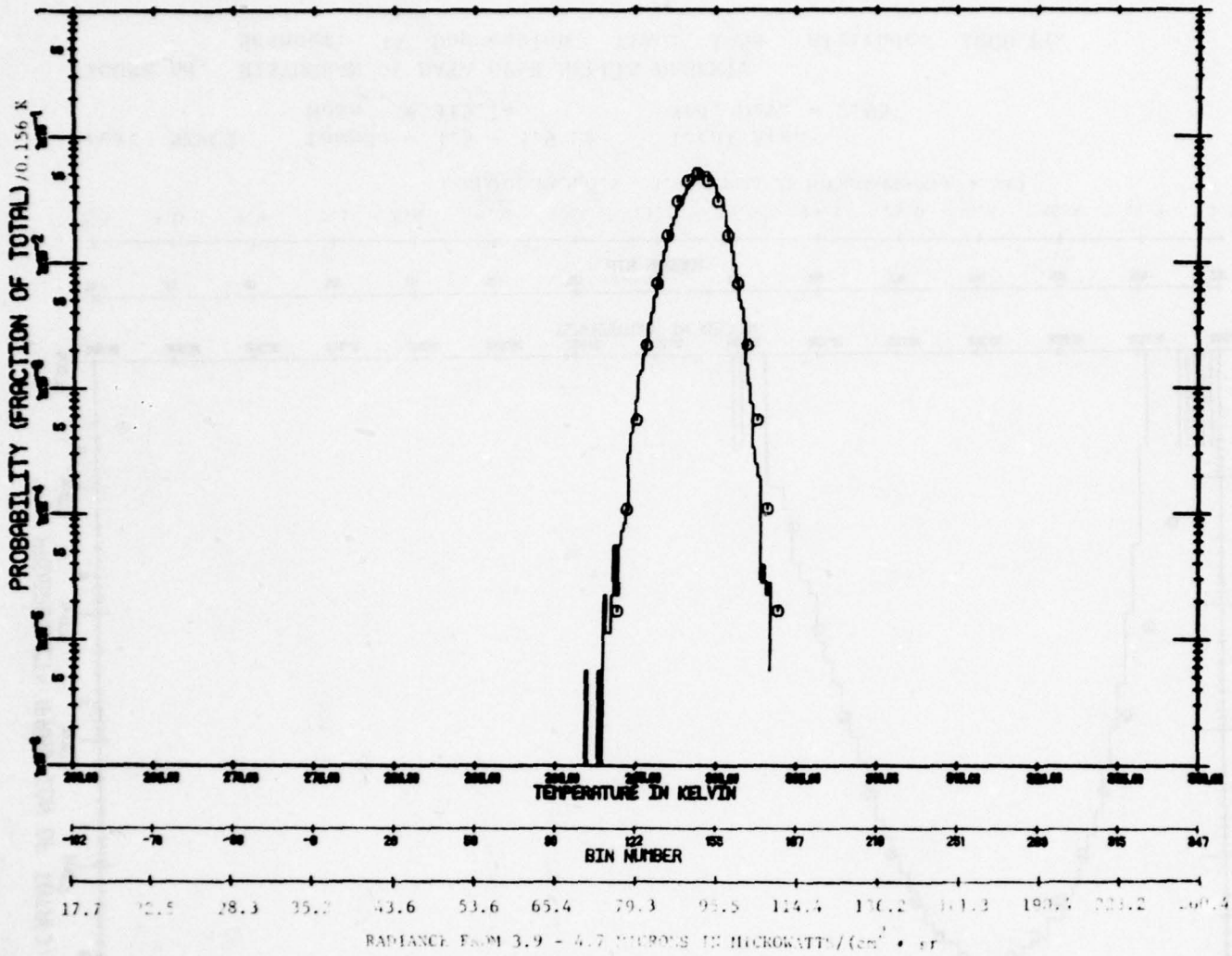

Area: NEVC2 Lambda = 3.9 - 4.7 μm Total Area
Mean = 298.85 Std. Dev. = 1.25

FIGURE 6e. HISTOGRAM OF DATA OVER NELLIS DESERT.
Scanner: 35° Depression Time: 1058 Altitude: 1000 Ft.

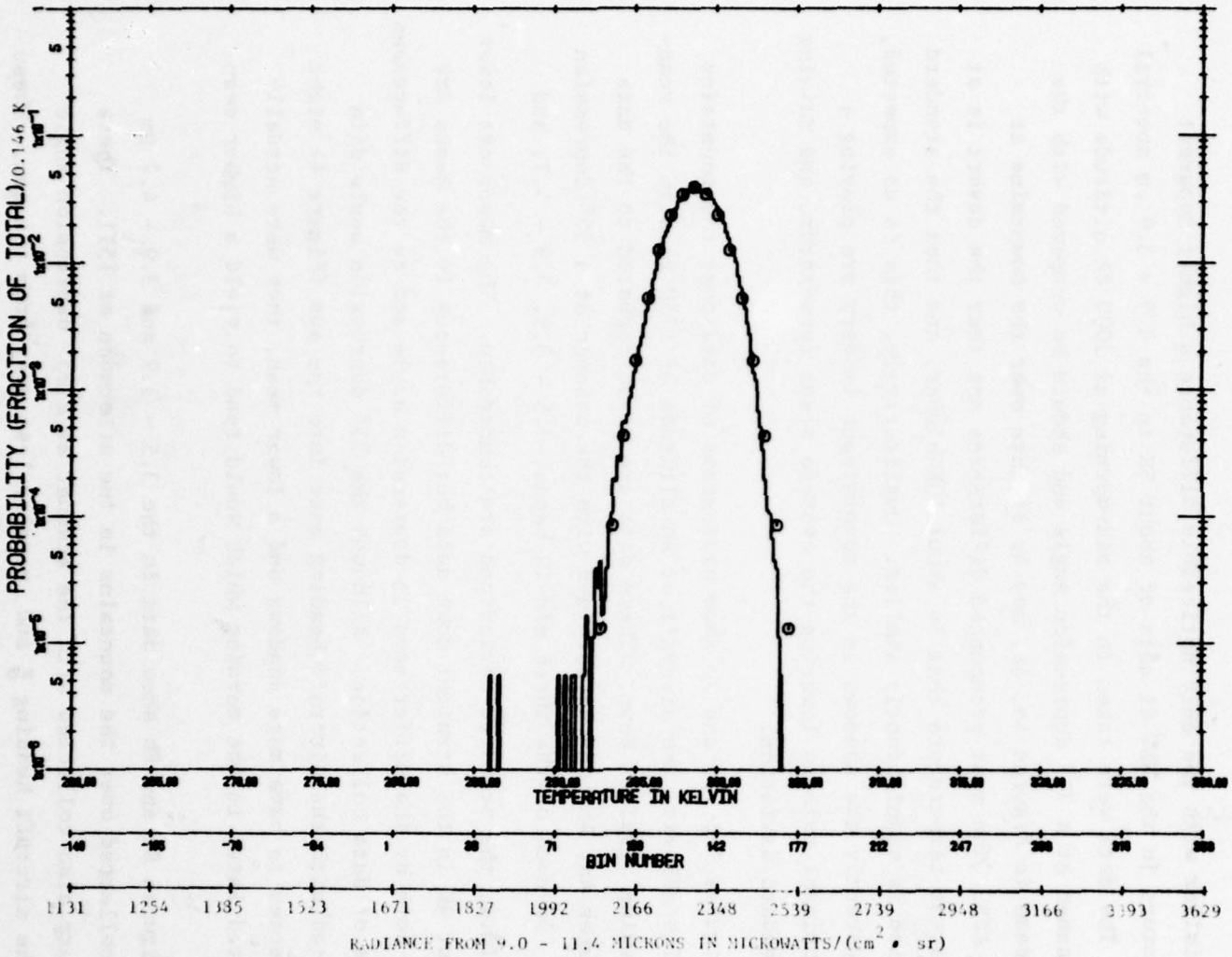

Area: NEVC2 Lambda = 9.0 - 11.4 μm Total Area
Mean = 298.58 Std. Dev. = 1.45

FIGURE 6f. HISTOGRAM OF DATA OVER NELLIS DESERT.
Scanner: 35° Depression Time: 1058 Altitude: 1000 Ft.

very similar with the only noticeable difference a higher apparent temperature in the NEV C1 data of about 5K in the 3.5 - 3.9 μm spectral band. The data were taken in the mid-morning at 1000 ft altitude with the scanner at a 35° depression angle and should be compared with the histograms in Figures 4a, 4b, and 4c of data over the mountains at Nellis AFB. The most pronounced differences are that the desert is at an apparent temperature that is about 10K higher, and that the standard deviation is significantly smaller. Qualitatively, this is as expected, and apparently the shadows in the mountainous imagery are playing a very dominant role in lowering the average scene temperature and raising the standard deviation.

Figures 7a, 7b, and 7c show histograms of data over the mountains at Nellis AFB with the aircraft at an altitude of 1750 ft with the scanner viewing straight down. These data are to be compared to the data in Figures 4a, 4b, and 4c obtained with the scanner at a 35° depression angle. In each of the three mid-IR bands, 3.5 - 3.9, 3.9 - 4.7, and 9.0 - 11.4, the standard deviations are comparable. The means are lower by about 4K in the straight down data but differences in the means are caused both by the differences in depression angle and to the differences in time of data collection. Although the 35° depression angle data collected with the aircraft heading east into the sun (Figure 4) might be expected to have more shadows and a lower mean, they were actually collected later in the morning which would tend to yield a higher mean.

Figures 8a and 8b show data in the 3.5 - 3.9 and 3.9 - 4.7 μm bands collected over the mountains in the afternoon at 1511. These data were also collected with the scanner at a 35° depression angle with the aircraft heading E and more or less away from the sun. These data should be compared with the data in Figures 4a and 4b. The mean scene apparent temperatures in the morning data are seen to be about 4K cooler than in the afternoon data which is as expected.

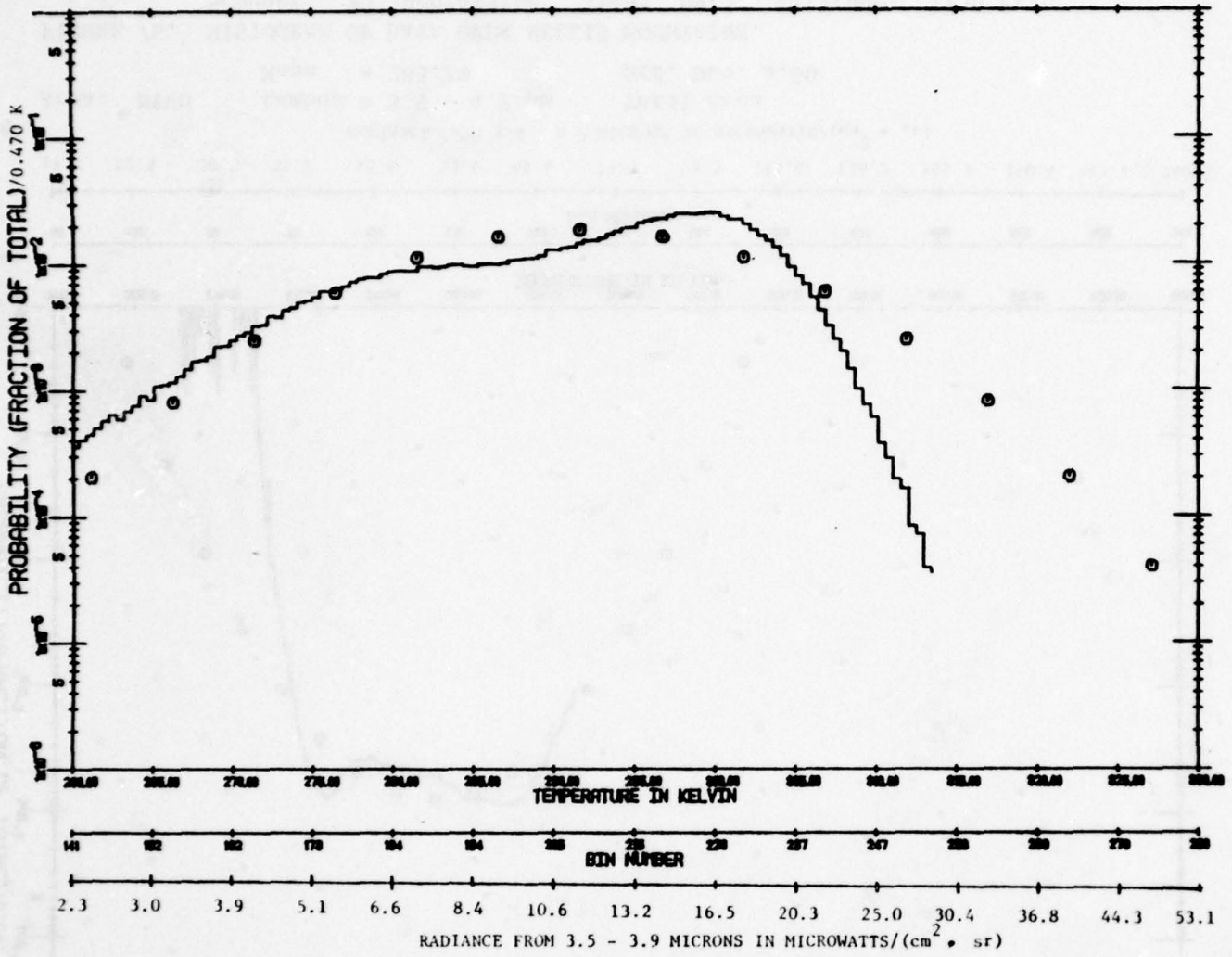

Area: NEVD Lambda = 3.5 - 3.9 μm Total Area
Mean = 291.58 Std. Dev. = 10.15

FIGURE 7a. HISTOGRAM OF DATA OVER NELLIS MOUNTAINS.
Scanner: 90° Depression Time: 0915 Altitude: 1750 Ft.

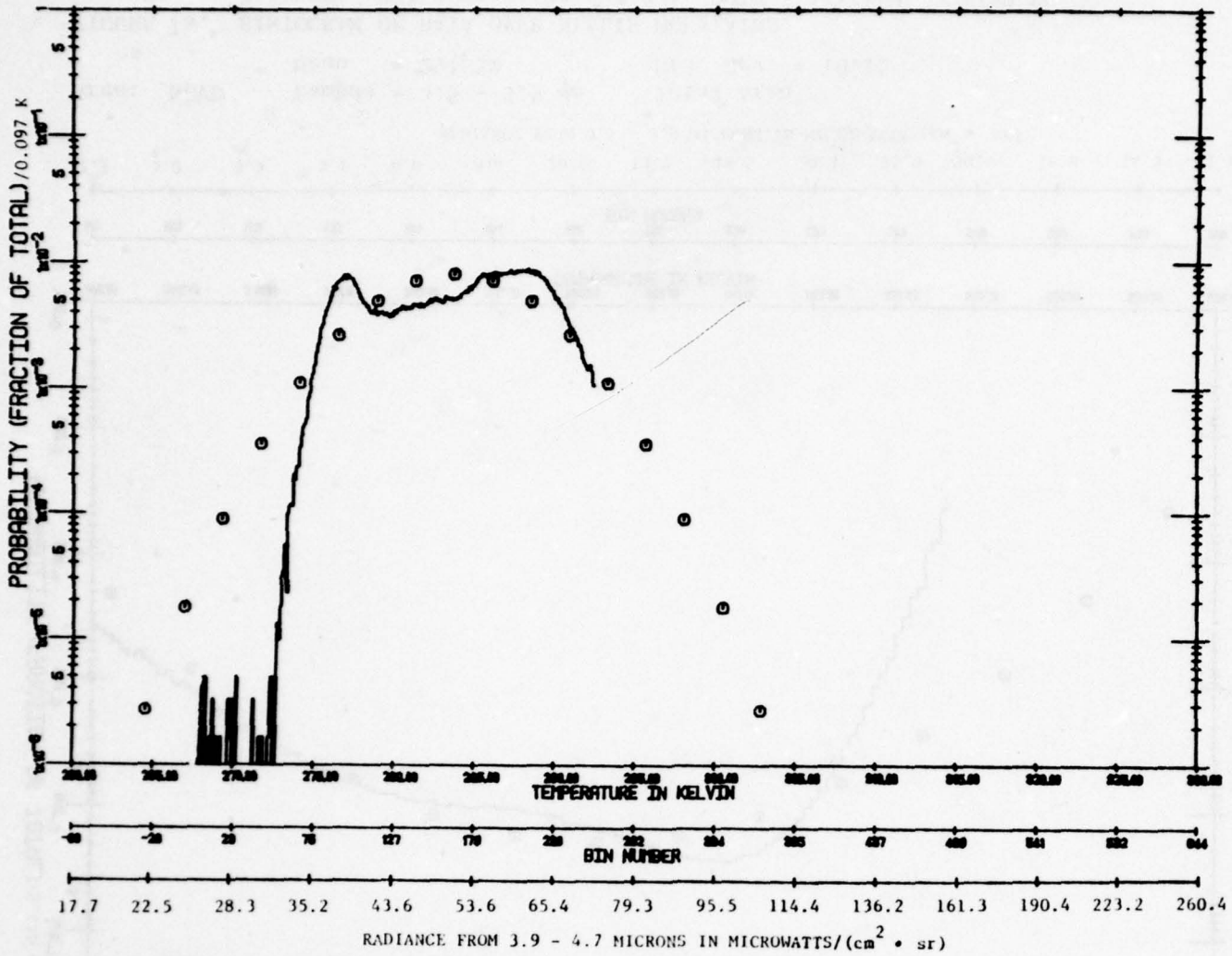

Area: NEVD Lambda = 3.9 - 4.7 μm Total Area
Mean = 283.70 Std. Dev. 4.80

FIGURE 7b. HISTOGRAM OF DATA OVER NELLIS MOUNTAINS.
Scanner: 90° Depression Time: 0915 Altitude: 1750 Ft.

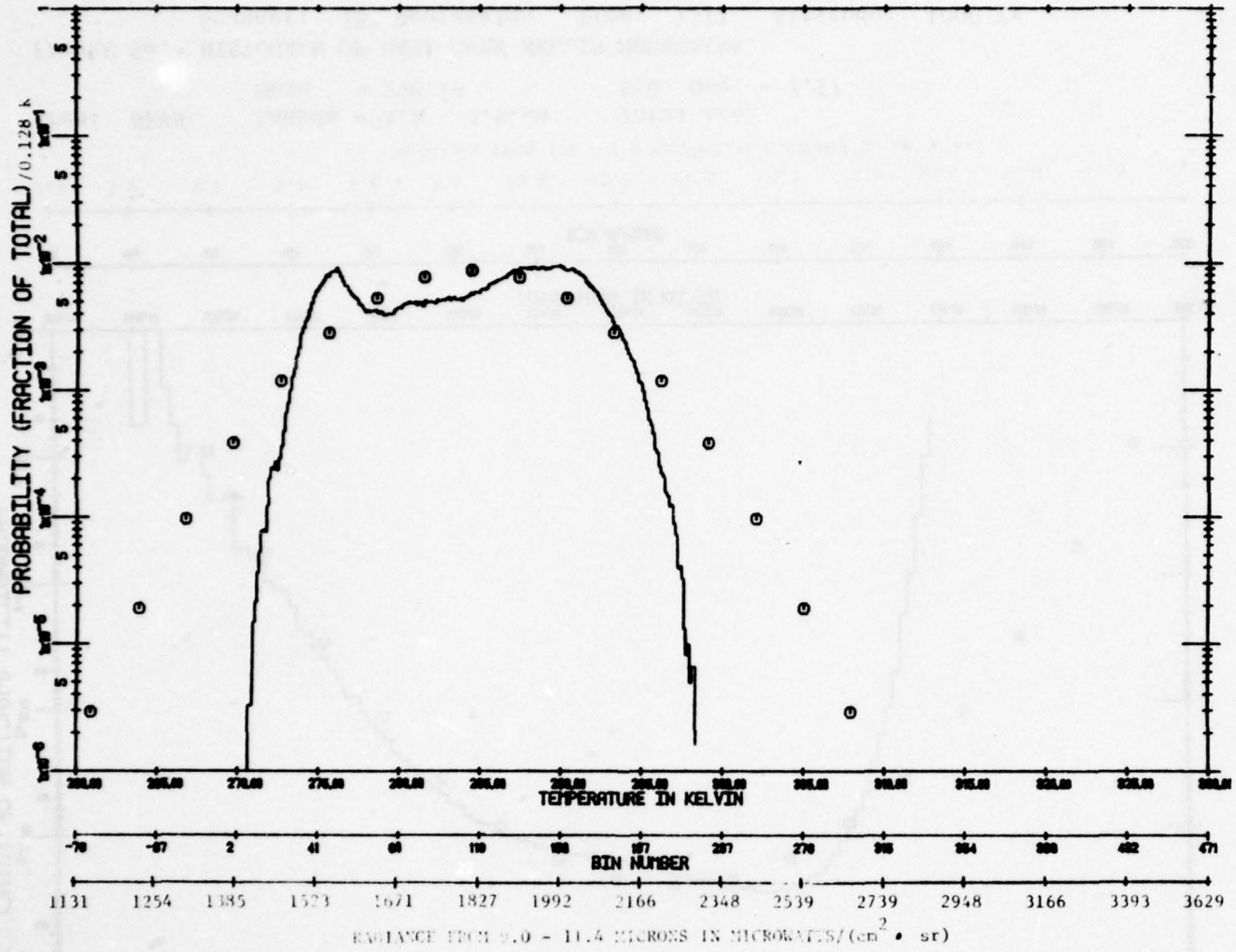

Area: NEVD Lambda = 9.0 - 11.4 μm Total Area
Mean = 284.44 Std. Dev. = 5.88

FIGURE 7c. HISTOGRAM OF DATA OVER NELLIS MOUNTAINS.
Scanner: 90° Depression Time: 0915 Altitude: 1750 Ft.

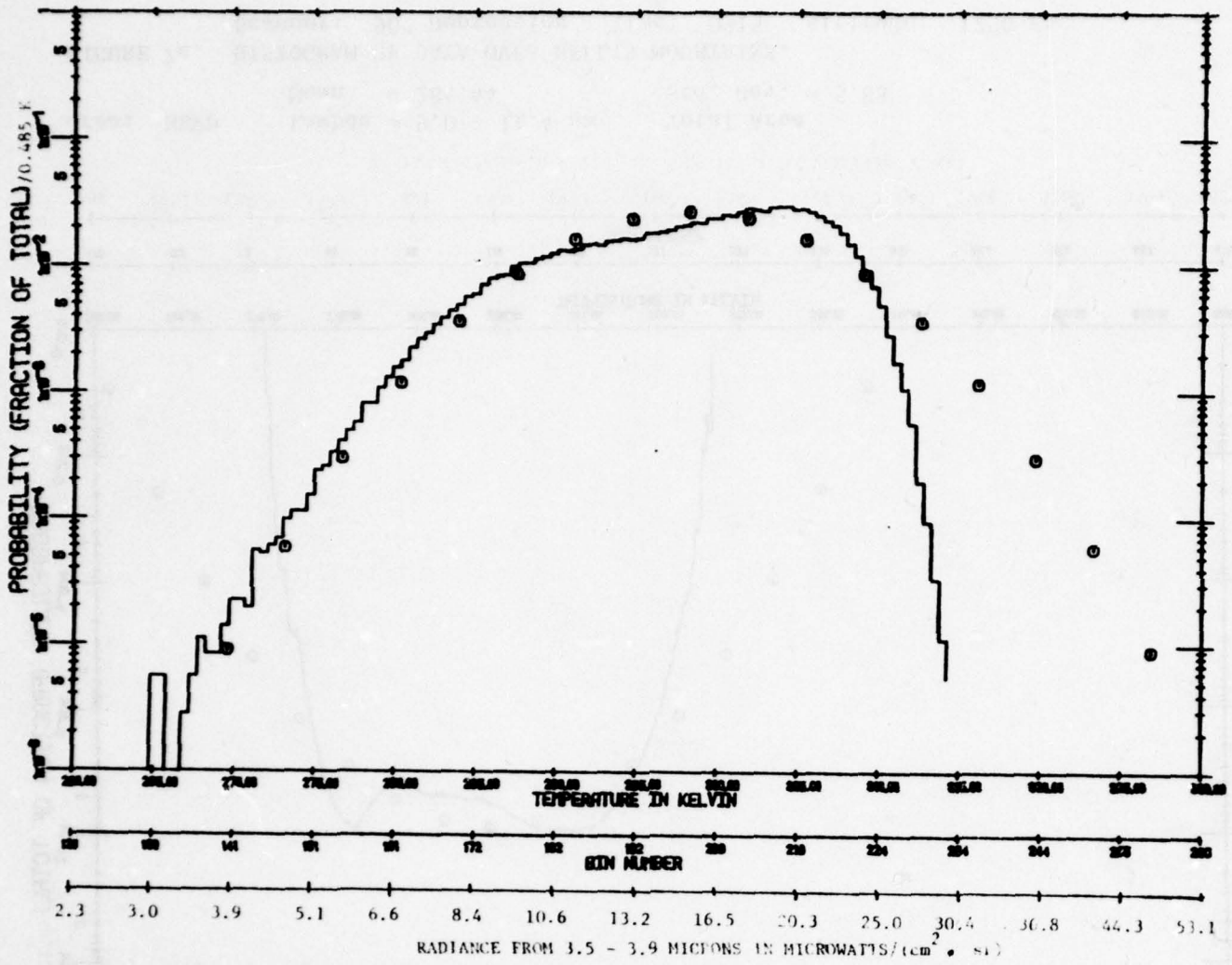

Area: NEVB Lambda = 3.5 - 3.9 μm Total Area
Mean = 298.19 Std. Dev. = 7.17

FIGURE 8a. HISTOGRAM OF DATA OVER NELLIS MOUNTAINS.
Scanner: 35° Depression Time: 1511 Altitude: 1000 Ft.

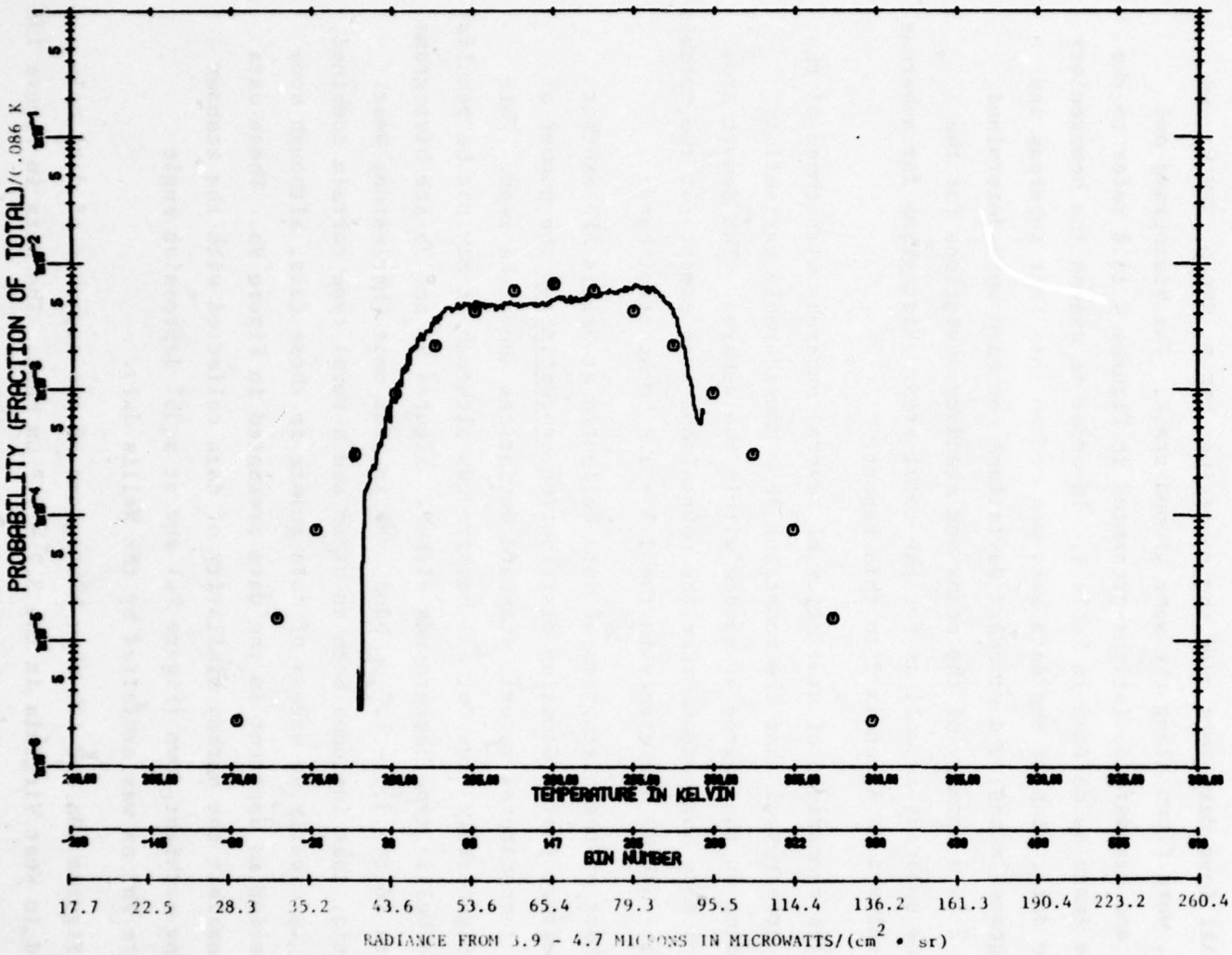

Area: NEVB Lambda = 3.9 - 4.7 μm Total Area
Mean = 290.05 Std. Dev. = 4.94

FIGURE 8b. HISTOGRAM OF DATA OVER NELLIS MOUNTAINS.
Scanner: 35° Depression Time: 1511 Altitude: 1000 Ft.

All four data sets over the mountains, NEV B, NEV D, NEV E, and NEV F, were flown along the same ground track. The histograms and means and standard deviations presented in Figures 4 to 8 refer to the entire image as defined in Table 1. In order to assess the homogeniety in the data, each of the data sets was broken into four subareas and histograms, means, and standard deviations for each were determined. Table 2 is a summary of the means and standard deviations for the various subareas as well as for the total area. Histograms for subareas are included as Appendix 2 to this report.

The comparison of statistics of several subareas with those of the total area reveal that the mountains show considerable variability depending on the degree of shadow within the subarea. The desert area is much more homogeneous than the mountainous area except for the notable NEV C1 - NEV C2 difference in the 3.5 - 3.9 μm spectral band.

Most of the histograms of data collected at Nellis AFB exhibit the feature that a Gaussian distribution overestimates the number of scene temperatures several standard deviations above the mean. This is not generally true for all backgrounds although it may not be peculiar to the Nellis type backgrounds either. Figures 9a and 9b are histograms of data in the 3.9 - 4.7 μm band over an area near Charleston, West Virginia, that includes both an urban and a rural type terrain combined. There is clearly an excess of data points in these data, although some saturation is apparent in the data presented in Figure 9b. These data also exhibit the marked similarity of data collected with the scanner viewing straight down (Figure 9a) and at a 35° depression angle (Figure 9b) as was exhibited by the Nellis data.

Figures 10a and 10b show histograms of two segments of data collected in West Virginia in the 3.9 - 4.7 μm band. The data in Figure 10a is over the urban area, the data in Figure 10b over the rural area. These data were collected between 1130 and 1215 in October with the

TABLE 2

MEANS AND STANDARD DEVIATIONS FOR SUBAREAS AND TOTAL AREA

NEVB

		3.9 - 4.7 μm	3.5 - 3.9 μm	5.1 - 5.7 μm
Subarea	1	288.46 ± 4.87	296.44 ± 7.68	282.07 ± 3.85
	2	289.38 ± 4.72	296.42 ± 7.14	282.78 ± 3.80
	3	288.42 ± 4.46	296.62 ± 6.60	282.26 ± 3.19
	4	293.90 ± 3.36	303.20 ± 4.29	284.40 ± 3.58
Total Area		290.05 ± 4.94	298.19 ± 7.17	282.88 ± 3.90

NEVC1

		3.9 - 4.7 μm	3.5 - 3.9 μm	9.0 - 11.4 μm
Subarea	1	297.48 ± 1.01	310.35 ± 2.09	298.87 ± 1.19
	2	297.24 ± 1.41	308.78 ± 2.61	298.64 ± 1.47
Total Area		297.41 ± 1.24	309.56 ± 2.49	298.75 ± 1.35

NEVC2

		3.9 - 4.7 μm	3.5 - 3.9 μm	9.0 - 11.4 μm
Subarea	1	298.76 ± 1.16	315.22 ± 2.83	298.37 ± 1.36
	2	298.94 ± 1.33	315.05 ± 3.05	298.78 ± 1.51
Total Area		298.85 ± 1.25	315.14 ± 2.95	298.58 ± 1.45

NEVD

		3.9 - 4.7 μm	3.5 - 3.9 μm	9.0 - 11.4 μm
Subarea	1	286.49 ± 3.34	296.47 ± 6.07	288.22 ± 3.75
	2	285.64 ± 3.81	296.21 ± 6.97	286.92 ± 4.43
	3	284.45 ± 4.14	293.07 ± 8.62	285.15 ± 5.05
	4	278.52 ± 3.11	281.14 ± 9.53	277.87 ± 3.76
Total Area		283.70 ± 4.80	291.58 ± 10.15	284.44 ± 5.88

NEVE

		3.9 - 4.7 μm	3.5 - 3.9 μm	5.1 - 5.7 μm
Subarea	1	290.21 ± 4.18	306.78 ± 6.60	278.04 ± 2.27
	2	291.90 ± 4.39	307.88 ± 6.81	278.47 ± 2.37
	3	290.65 ± 4.72	307.24 ± 7.18	277.99 ± 2.32
	4	293.49 ± 3.78	309.78 ± 5.73	278.12 ± 2.24
Total Area		291.58 ± 4.47	307.94 ± 6.70	278.15 ± 2.31

NEVF

		3.9 - 47 μm	3.5 - 3.9 μm	9.0 - 11.4 μm
Subarea	1	285.51 ± 4.22	296.03 ± 7.52	285.33 ± 4.91
	2	289.02 ± 5.63	301.49 ± 9.18	289.13 ± 6.35
	3	282.00 ± 4.78	288.66 ± 9.61	282.47 ± 5.70
	4	289.47 ± 4.48	300.90 ± 7.47	291.38 ± 5.16
Total Area		286.49 ± 5.68	296.76 ± 9.94	287.08 ± 6.53

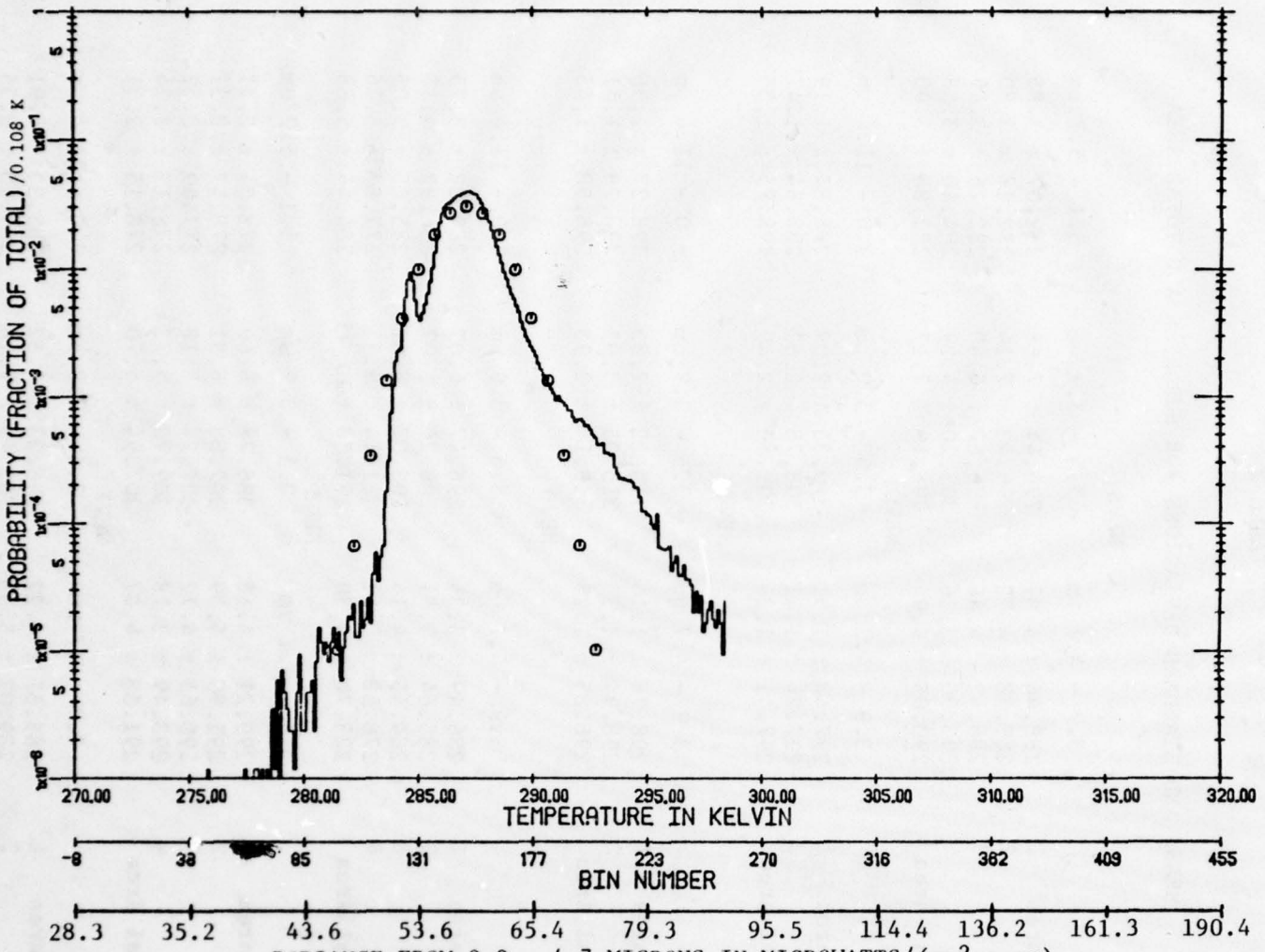

Area: WESTVA 1 Lambda = 3.9 - 4.7 μm Total Area
Mean = 287.14 St. Dev. = 1.40

FIBURE 9a. HISTOGRAM OF DATA OVER WEST VIRGINIA.
Scanner: 90° Depression Time: 1135 Altitude: 6750

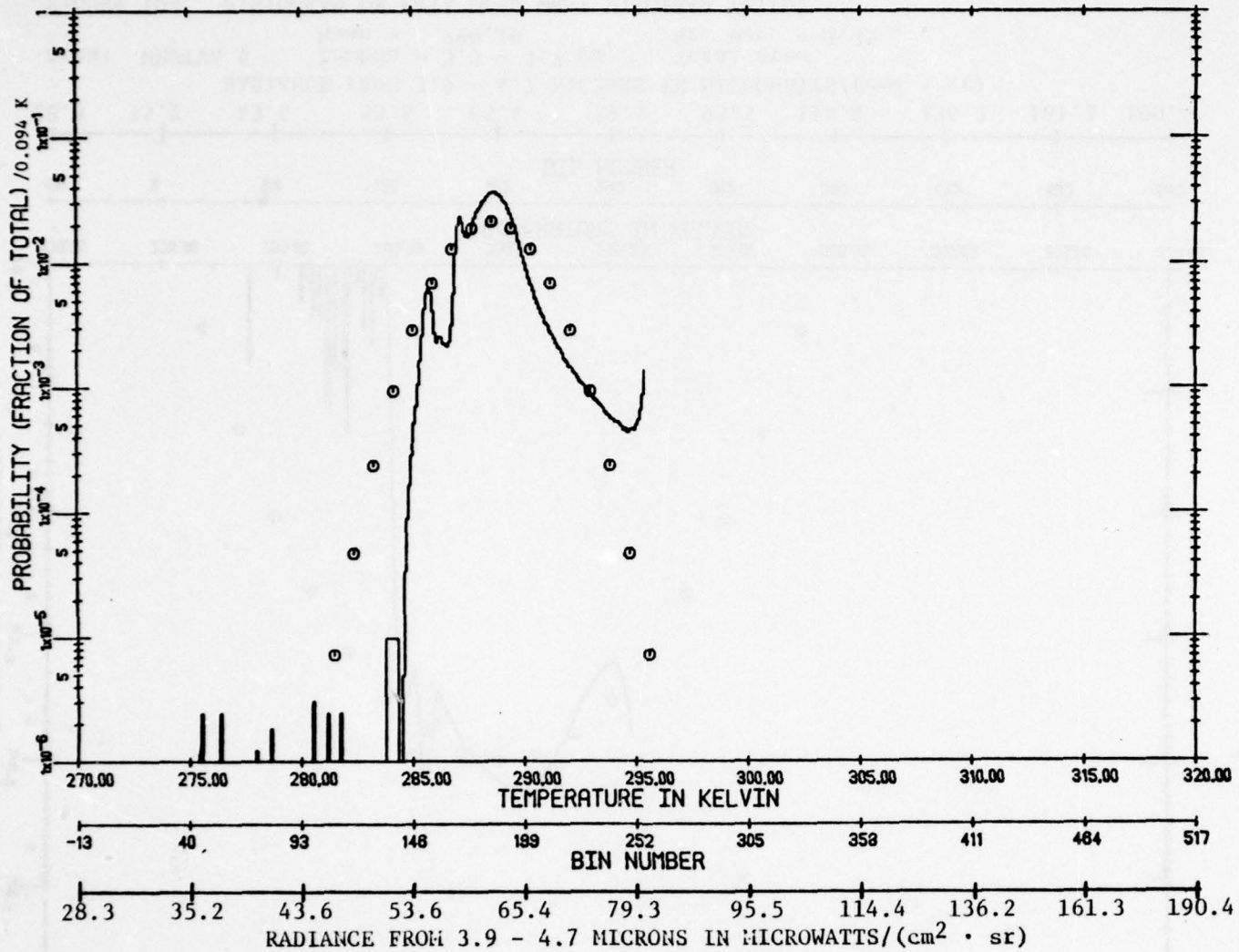

Area: WESTVA 3 Lambda = 3.9 - 4.7 μm Total Area
Mean = 288.53 St. Dev. = 1.76

FIGURE 9b. HISTOGRAM OF DATA OVER WEST VIRGINIA.
Scanner: 35° Depression Time: 1210 Altitude: 3850 Ft.

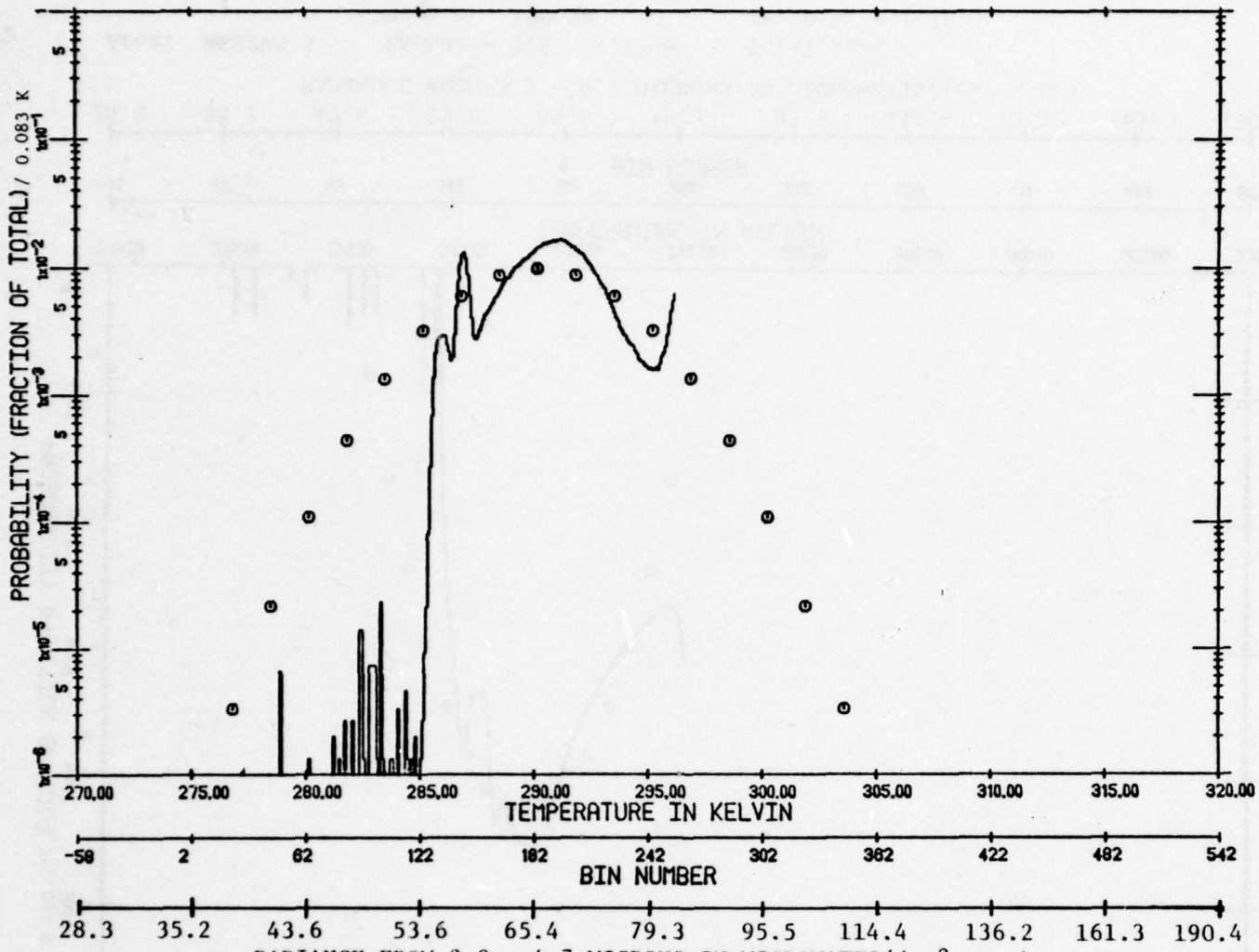

Area: WESTVA 6 Lambda = 3.9 - 4.7 μm Total Area
Mean = 290.19 St. Dev. = 3.35

FIGURE 10a. HISTOGRAM OF DATA OVER WEST VIRGINIA (City).
Scanner: 90° Depression Time: 1150 Altitude: 1750 Ft.

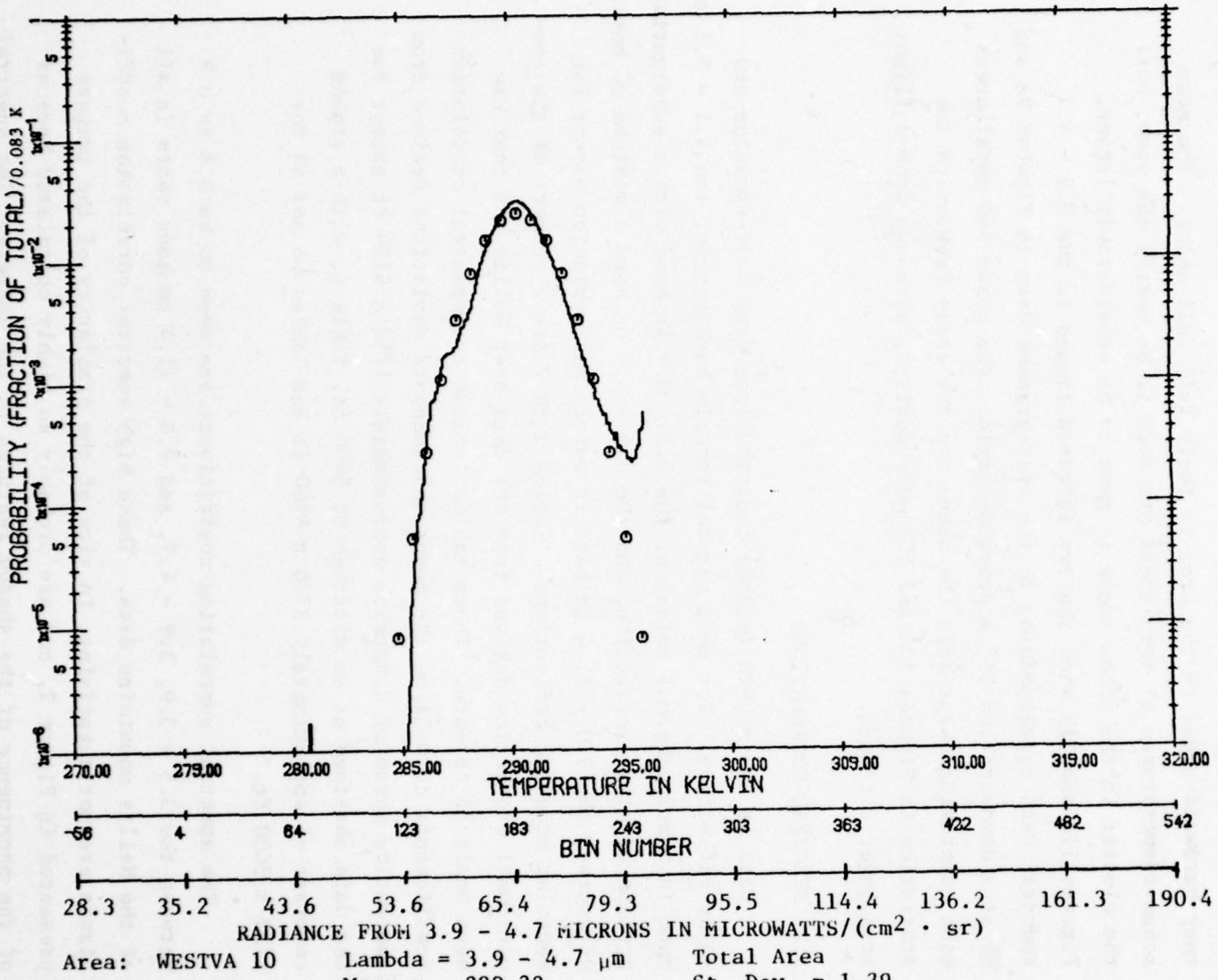

FIGURE 10b. HISTOGRAM OF DATA OVER WEST VIRGINIA (Trees).
Scanner: 90° Depression Time: 1152 Altitude: 1750 Ft.

many hardwood trees in the area in their full fall color. The mean scene temperatures of both areas are seen to be nearly the same, but the clutter in the urban scene is seen to be considerably larger. Figures 11a and 11b show the two infrared images in the 3.9 - 4.7 spectral band corresponding to the histogrammed data in Figures 9a and 9b at a downward and 35° depression angle. The urban and rural areas each comprising about half the scene are the areas from which the statistics in Figures 10a and 10b were derived, although from a flight at a lower altitude.

3.2 SPECTRAL CORRELATIONS

Data in the mid-IR include contributions from self-emission and solar reflection. For most natural terrain backgrounds, the 4.5 - 5.5 μm band is mostly thermal emission, the 3.5 - 3.9 μm band with a substantial portion of solar reflection, and the 3.9 - 4.7 μm band a mixture of both. Of course, the 9.0 - 11.4 um band is purely self-emission except for specular metallic reflections. Tables 3 to 7 are a summary of the conventional statistics derived from the data over Nellis AFB that has been analyzed to date. These tables include the spectral correlation coefficients as well as the means and standard deviations derived from the entire scene of dimension approximately 1750 x 6750 ft except for the data obtained at an altitude of 5000 ft, Table 6, with a ground coverage of approximately 8700 x 6400 ft and Tables 4A and 4B for 1750 x 3400 ft.

The spectral correlation coefficients are seen to be 0.8 to 0.9 between the 3.5 - 3.9, 3.9 - 4.7, and 9.0 - 11.4 μm band pairs in all of the Nellis mountains data. These high spectral correlation coefficients are not surprising, in view of the similarity of the imagery presented in Figure 2, and are probably so highly correlated because of the prominence of the shadow features in the imagery. The spectral correlations might not be expected to be so high where scene contrasts

(a) 3.9 - 4.7 μm, 90° Depression

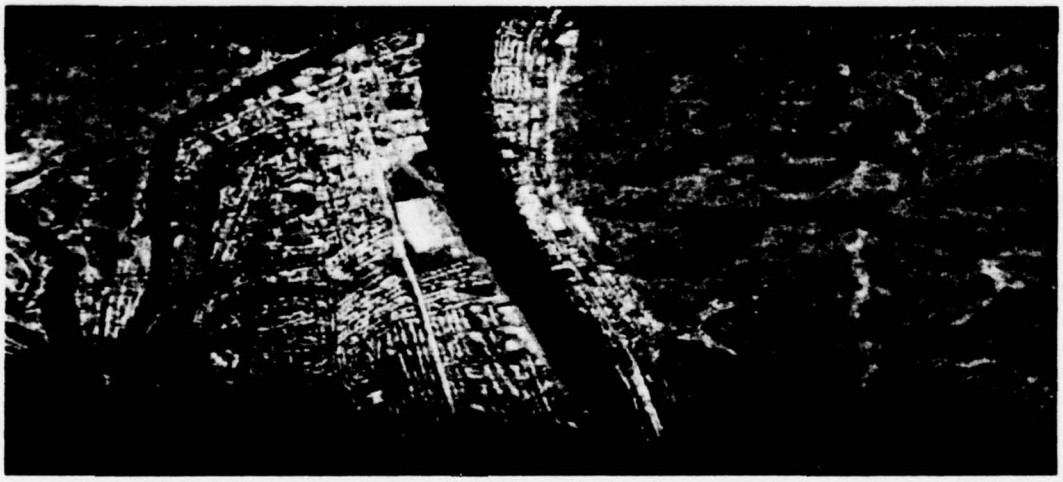

(b) 3.9 - 4.7 μm, 35° Depression

FIGURE 11. WEST VIRGINIA IMAGERY

TABLE 3

NEVB

CORRELATION MATRIX, MEANS AND STANDARD DEVIATIONS,
NELLIS MOUNTAINS, SCANNER 35° DEPRESSION, TIME 1511,
ALTITUDE 1000 FT

CORRELATION	3.9 - 4.7	3.5 - 3.9	5.1 - 5.7
3.9 - 4.7	1.000		
3.5 - 3.9	0.870	1.000	
5.1 - 5.7	0.431	0.389	1.000
CHANNELS	3.9 - 4.7	3.5 - 3.9	5.1 - 5.7
MEAN	2.9005E+02	2.9819E+02	2.8288E+02
STANDARD DEVIATION	4.9400E+00	7.1665E+00	3.8979E+00
TOTAL POINTS	355600	355600	355600

TABLE 4A

NEVC1

CORRELATION MATRIX, MEANS AND STANDARD DEVIATIONS,
NELLIS DESERT, SCANNER 35° DEPRESSION, TIME 1058,
ALTITUDE 1000 Ft.

CORRELATION	3.9 - 4.7	3.5 - 3.9	9.0 - 11.4
3.9 - 4.7	1.000		
3.5 - 3.9	0.353	1.000	
9.0 - 11.4	0.687	0.335	1.000
CHANNELS	3.9 - 4.7	3.5 - 3.9	9.0 - 11.4
MEAN	2.9741E+02	3.0956E+02	2.9875E+02
STANDARD DEVIATION	1.2421E+00	2.4920E+00	1.3479E+00
TOTAL POINTS	176400	176400	176400

TABLE 4B

NEVC2

CORRELATION MATRIX, MEANS AND STANDARD DEVIATIONS,

NELLIS DESERT, SCANNER 35° DEPRESSION, TIME 1058

ALTITUDE 1000 FT

CORRELATION	3.9 - 4.7	3.5 - 3.9	9.0 - 11.4
3.9 - 4.7	1.000		
3.5 - 3.9	0.492	1.000	
9.0 - 11.4	0.655	0.545	1.000
CHANNELS	3.9 - 4.7	3.5 - 3.9	9.0 - 11.4
MEAN	2.9885E+02	3.1514E+02	2.9858E+02
STANDARD DEVIATION	1.2536E+00	2.9485E+00	1.4528E+00
TOTAL POINTS	179200	179200	179200

TABLE 5

NEVD

CORRELATION MATRIX, MEANS AND STANDARD DEVIATIONS,

NELLIS MOUNTAINS, SCANNER 90° DEPRESSION, TIME 0915

ALTITUDE 1750 FT

CORRELATION	3.9 - 4.7	3.5 - 3.9	9.0 - 11.4
3.9 - 4.7	1.000		
3.5 - 3.9	0.813	1.000	
9.0 - 11.4	0.933	0.848	1.000
CHANNELS	3.9 - 4.7	3.5 - 3.9	9.0 - 11.4
MEAN	2.8370E+02	2.9158E+02	2.8444E+02
STANDARD DEVIATION	4.7956E+00	1.0147E+01	5.8827E+00
TOTAL POINTS	612400	612400	612400

TABLE 6

NEVE

CORRELATION MATRIX, MEANS AND STANDARD DEVIATIONS,
NELLIS MOUNTAINS, SCANNER 35° DEPRESSION, TIME 0915,
ALTITUDE 5000 FT

CORRELATION	3.9 - 4.7	3.5 - 3.9	5.1 - 5.7
3.9 - 4.7	1.000		
3.5 - 3.9	0.839	1.000	
5.1 - 5.7	0.407	0.344	1.000
CHANNELS	3.9 - 4.7	3.5 - 3.9	5.1 - 5.7
MEAN	2.9158E+02	3.0794E+02	2.7815E+02
STANDARD DEVIATION	4.4711E+00	6.7021E+00	2.3112E+00
TOTAL POINTS	67600	67600	67600

TABLE 7

NEVF

CORRELATION MATRIX, MEANS AND STANDARD DEVIATIONS,
NELLIS MOUNTAINS, SCANNER 35° DEPRESSION, TIME 1034,
ALTITUDE 1000 FT

CORRELATION	3.9 - 4.7	3.5 - 3.9	9.0 - 11.4
3.9 - 4.7	1.000		
3.5 - 3.9	0.850	1.000	
9.0 - 11.4	0.919	0.880	1.000
CHANNELS	3.9 - 4.7	3.5 - 3.9	9.0 - 11.4
MEAN	2.8649E+02	2.9676E+02	2.8708E+02
STANDARD DEVIATION	5.6758E+00	9.9428E+00	6.5334E+00
TOTAL POINTS	355600	355600	355600

result primarily from material differences (reflectances and emittances). The spectral correlation of the 5.1 - 5.7 μm band with the other IR bands is low due to the presence of a significant amount of noise in the 5.1 - 5.7 μm band imagery. The spectral correlations between the 3.5 - 3.9 μm band with the 3.9 - 4.7 and 9.0 - 11.4 μm bands in the desert data is primarily due to noise in the 3.5 - 3.9 μm band.

3.3 SUNGLINT DATA

Mid-IR band imagery have also been collected over water at Pt. Mugu, California, to assess the magnitude of solar glint in these spectral bands. With the ERIM line scanner looking straight down, the scanner scans a 90° field beneath the aircraft normal to the direction of aircraft flight. The scanner is not a framing device, so in order to scan through the sunglint and determine the magnitude of the solar reflection from water, the aircraft is flown along a very large radius turn orthogonal to the rays from the sun. The imagery so obtained in a number of mid-IR bands and in the 9.0 - 11.4 μm spectral band are shown in Figure 12. The 2.0 - 2.6, 3.0 - 4.2, 4.5 - 5.5, and 9.0 - 11.4 μm data were collected simultaneously on one pass; the 3.5 - 3.9, 3.9 - 4.7, and 5.1 - 5.7 μm data simultaneously on another pass. The sunglint from the water is seen to be very pronounced in all of the spectral bands flown from 2.0 - 2.6 to 4.5 - 5.5 μm. There may be a return in the 5.1 to 5.7 μm band but it is not apparent in the data. The only return in the 9.0 - 11.4 μm band is thermal emission, and water temperature variations in the imagery are evident. In order to quantify the solar return, video traces in the data are shown for the 2.0 - 2.6, 3.9 - 4.7, and 4.5 - 5.5 μm band in Figures 13a, 13b, and 13c. The video scan represents a 90° scan beneath the aircraft plus several calibration plate returns at the right end of the scan. As the aircraft progresses through its slow turn normal to the sun's rays, the specular peak grows and then decreases in amplitude. At its peak, the magnitude

(a) 2.0 - 2.6 µm

(b) 3.0 - 4.2 µm

(c) 3.5 - 3.9 µm

(d) 3.9 - 4.7 µm

FIGURE 12. SUNGLINT IMAGERY, PT MUGU (Continued)

(e) 4.5 - 5.5 μm

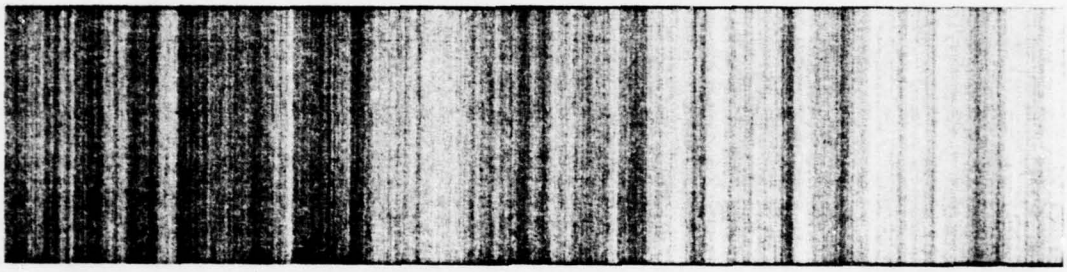

(f) 5.1 - 5.7 μm

(g) 9.0 - 11.4 μm

FIGURE 12. SUNGLINT IMAGERY, FT MUGU (Concluded)

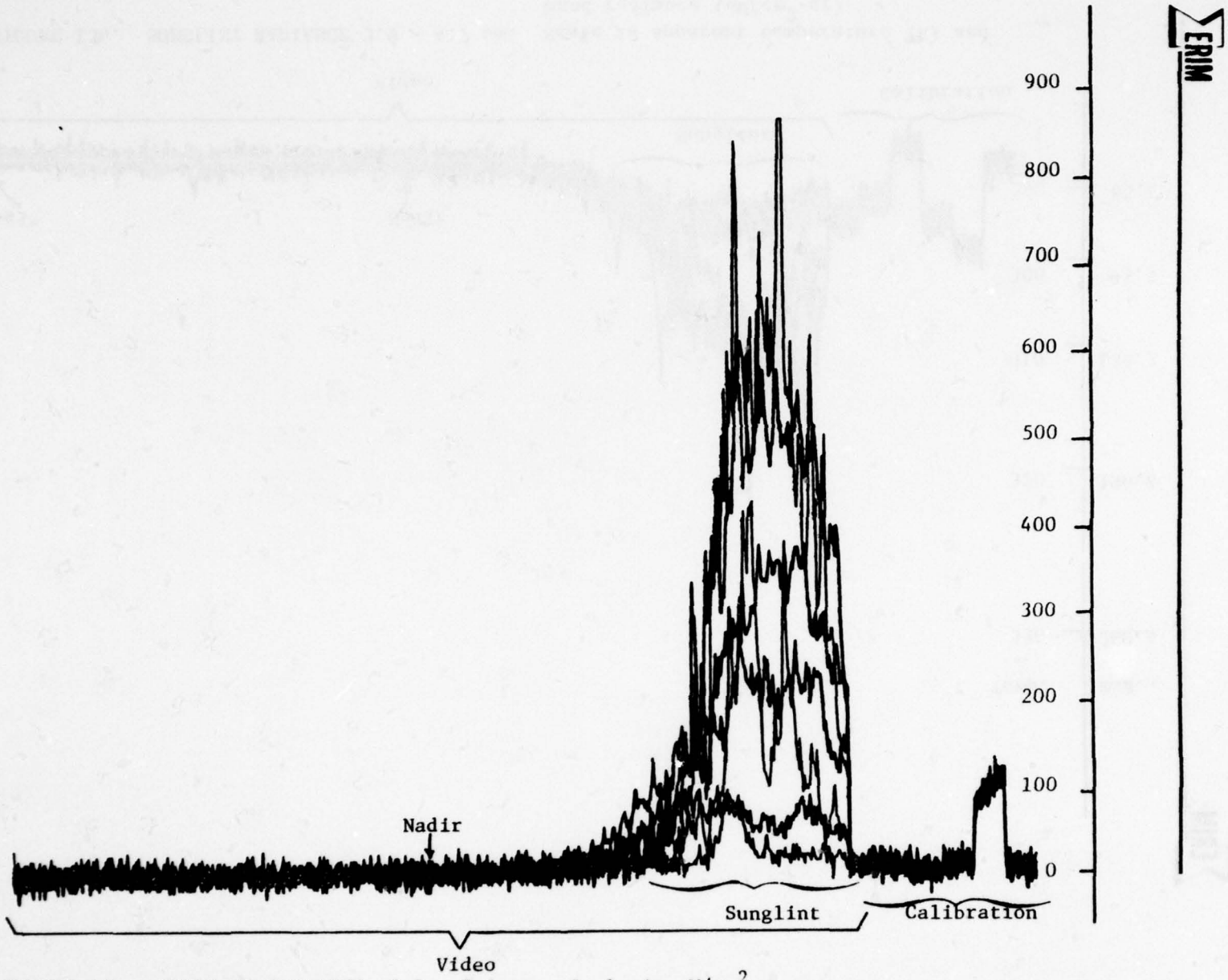

FIGURE 13a. SUNGLINT RADIANCE, 2.0 - 2.6 μm. Scale is $\mu W/cm^2 \cdot sr \cdot \mu m$

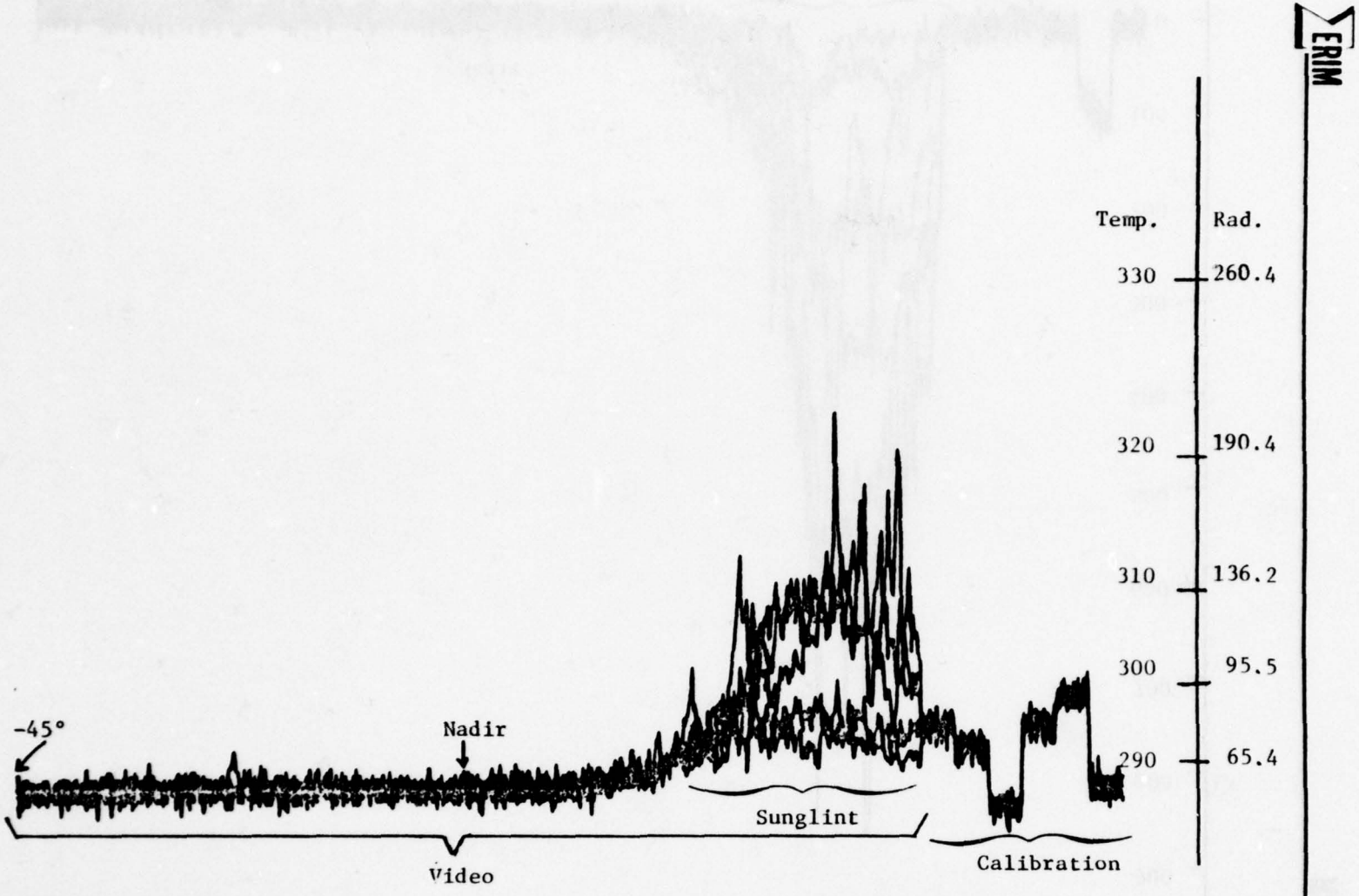

FIGURE 13b. SUNGLINT RADIANCE 3.9 - 4.7 μm. Scale is apparent temperature (K) and band radiance ($\mu W/cm^2 \cdot sr$)

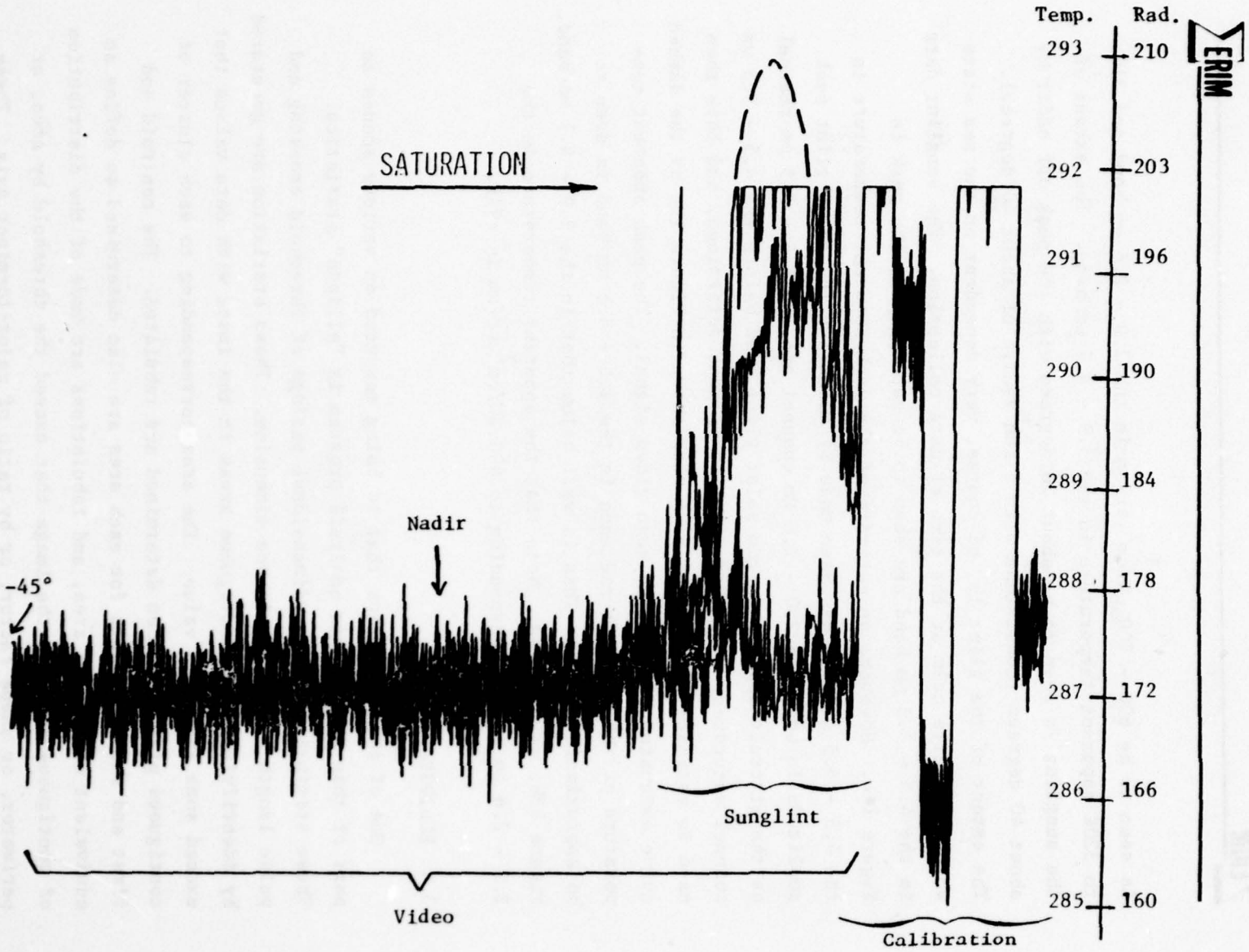

FIGURE 13. SUNGLINT RADIANCE, 4.5 - 5.5 μm. Scale is apparent temperature (K) and band radiance ($\mu W/cm^2 \cdot sr$)

is seen to be 600 - 700 $\mu W/cm^2 \cdot sr \cdot \mu m$ in the 2.0 - 2.6 μm band and 310 to 320K apparent temperature in the 3.9 - 4.7 μm band. The extent of the sunglint is seen to be about 20 degrees with the peak off nadir by about 40 degrees (consistent with a sun zenith of about 40 degrees). The extent of the glint is, of course, very dependent on the sea state which was quite calm at the time of data collection. The sunglint data in the 4.5 - 5.5 μm band are seen to be saturated at the peak in Figure 13c. However, an estimate of the peak apparent temperature in the 4.5 - 5.5 μm band has been made by measuring the solar glint peak amplitude in both the 2.0 - 2.6 μm channel and the 4.5 - 5.5 μm channel as the aircraft approaches the solar glint peak before the 4.5 - 5.5 μm channel saturates. A proportionality is thus determined, and this then used to estimate the 4.5 - 5.5 μm peak shown in Figure 13c by the dashed curve extension of the line scan video signal. The peak apparent temperature of the sunglint radiance in the 4.5 - 5.5 μm band is seen to be approximately 293K. This is well below that in the 3.9 - 4.7 μm band, Figure 13b, as expected. Note that the apparent temperature in the 2.0 - 2.6 μm band corresponding to 600 $\mu W/cm^2 \cdot sr \cdot \mu m$ is 494K.

3.4 ELLIPSES

One of the statistics that is being measured on various scenes as part of this backgrounds analysis program is "ellipse" statistics. These statistics are two-dimensional analogs of threshold crossing and pulse length statistics in one dimension. These statistics are generated by identifying those contiguous areas in the image with data values that exceed some threshold value. The area corresponding to each cluster of contiguous pixels is then determined and tabulated. The centroid and first and second moments for each area are also determined to define an equivalent elliptical area, and tabulations are made of the distribution of contiguous areas in the image that exceed the threshold by area, or perimeter, or shape factor, or by ratio of major-to-minor axis. These

"ellipse" statistics are determined for each of several threshold settings. Single pixel and contiguous two-pixel exceedances are not included in the ellipse tabulations but the number of such exceedances is noted separately.

Figures 14a and 14b show the ellipse equivalent areas which exceed thresholds of 0.8 standard deviation and 1.6 standard deviations above the mean for data collected over the desert range mountains at Nellis AFB in the 3.9 - 4.7 μm spectral band. The imagery from which these ellipses were derived is the same as that from which the histogram was developed in Figure 4b. As would be expected from the data in Figure 4b, there are no three standard deviation exceedances probably due to saturation.

Figures 15a and 15b show the ellipse for the same area as Figures 14a and 14b except in the 9.0 - 11.4 μm band. The histogram corresponding to these data is shown in Figure 4c, and although there are some scene elements with temperatures above the mean plus three standard deviation threshold, they are not clustered into groups of as many as three and so are not tabulated.

It is seen in Figures 14 and 15 that the contiguous areas that exceed the one (or two) standard deviation threshold in the 3.9 - 4.7 μm band are not exactly the same as those in the 9.0 - 11.4 μm band. The general features are the same, however, showing approximate size, shape, and location of the "bright" areas in the imagery as one would expect. The differences would appear to be due in part to the non-linear apparent temperature relationship between the two images induced in part by the solar component in the 3.9 - 4.7 μm image.

Tables 8 and 9 show how the contiguous areas that exceed several thresholds are distributed by area (square meters), by perimeter (meters) and by shape factor. The shape factor is defined to be the ratio of the perimeter/2π and the square root of the area/π,

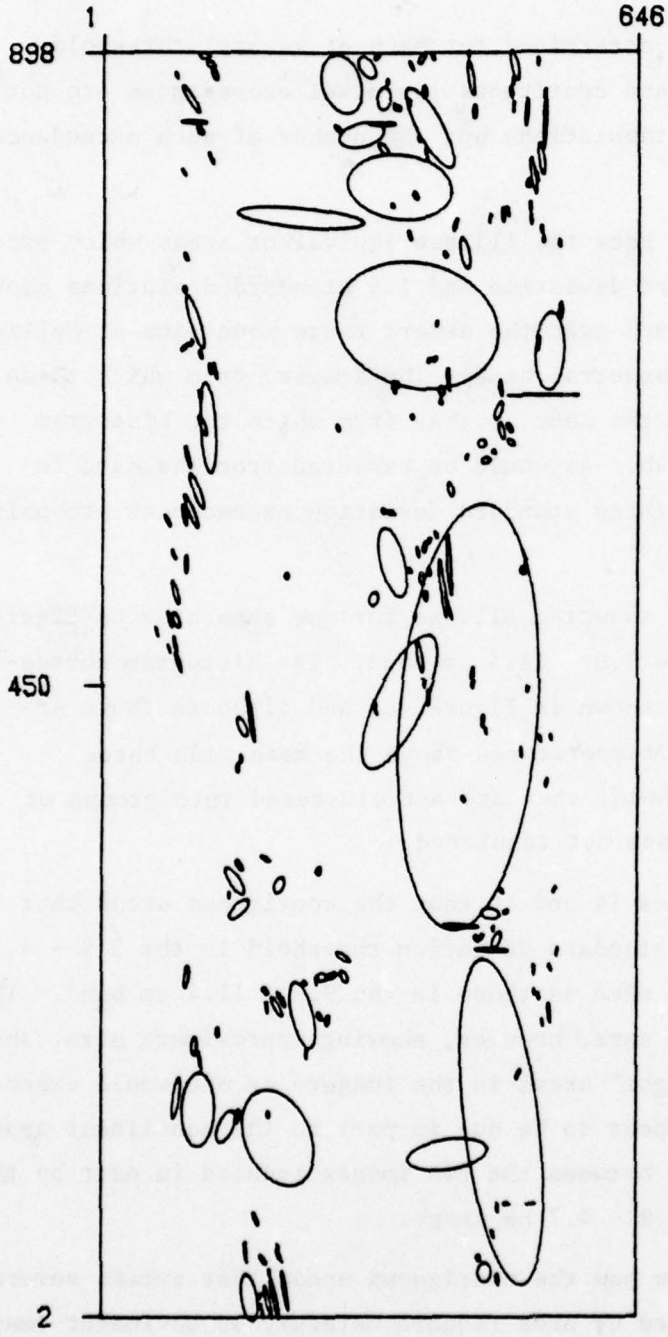

NEVF

Temperature Threshold
$= \mu + 0.8\sigma = 291.05K$

Lambda = 3.9 to 4.7 μm

FIGURE 14a. EQUIVALENT ELLIPTICAL AREAS FOR NELLIS MOUNTAINS.
Scanner: 35° Depression Time: 1034 Altitude: 1000 Ft.

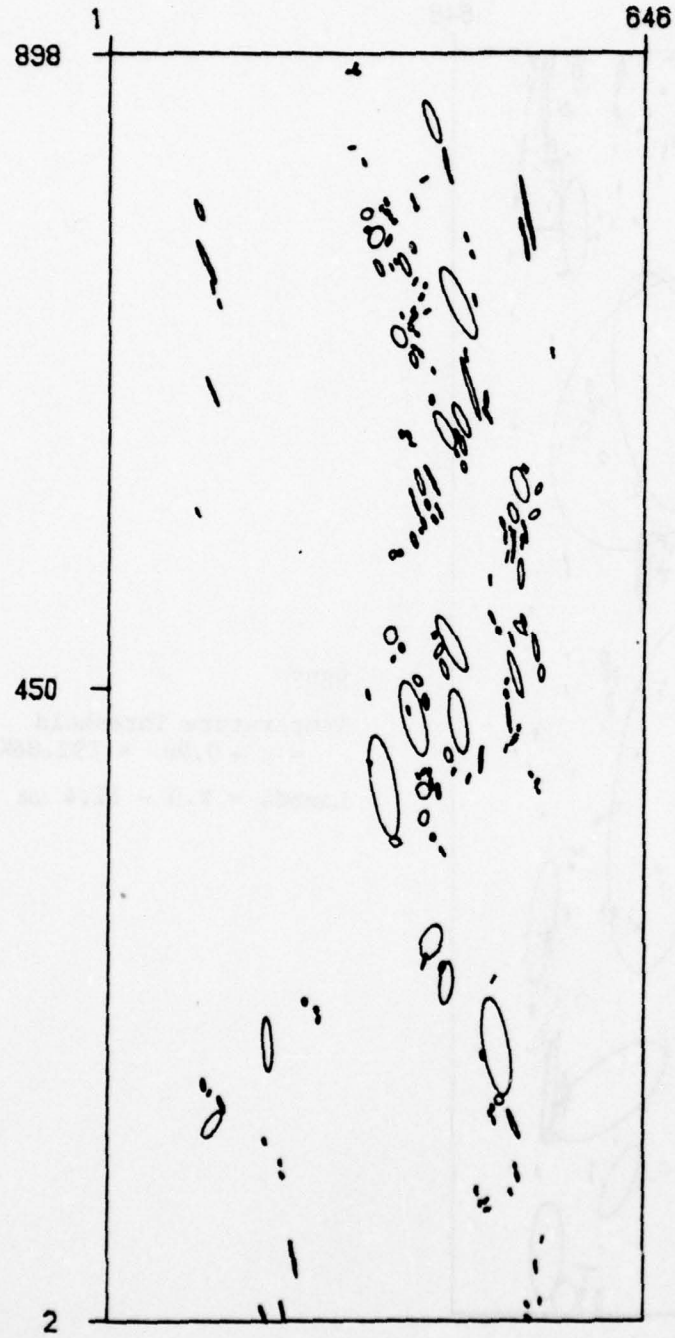

NEVF

Temperature Threshold
$= \mu + 1.6\sigma = 295.88K$

Lambda = 3.9 to 4.7 μm

FIGURE 14b. EQUIVALENT ELLIPTICAL AREAS FOR NELLIS MOUNTAINS.
Scanner: 35° Depression Time: 1034 Altitude: 1000 Ft.

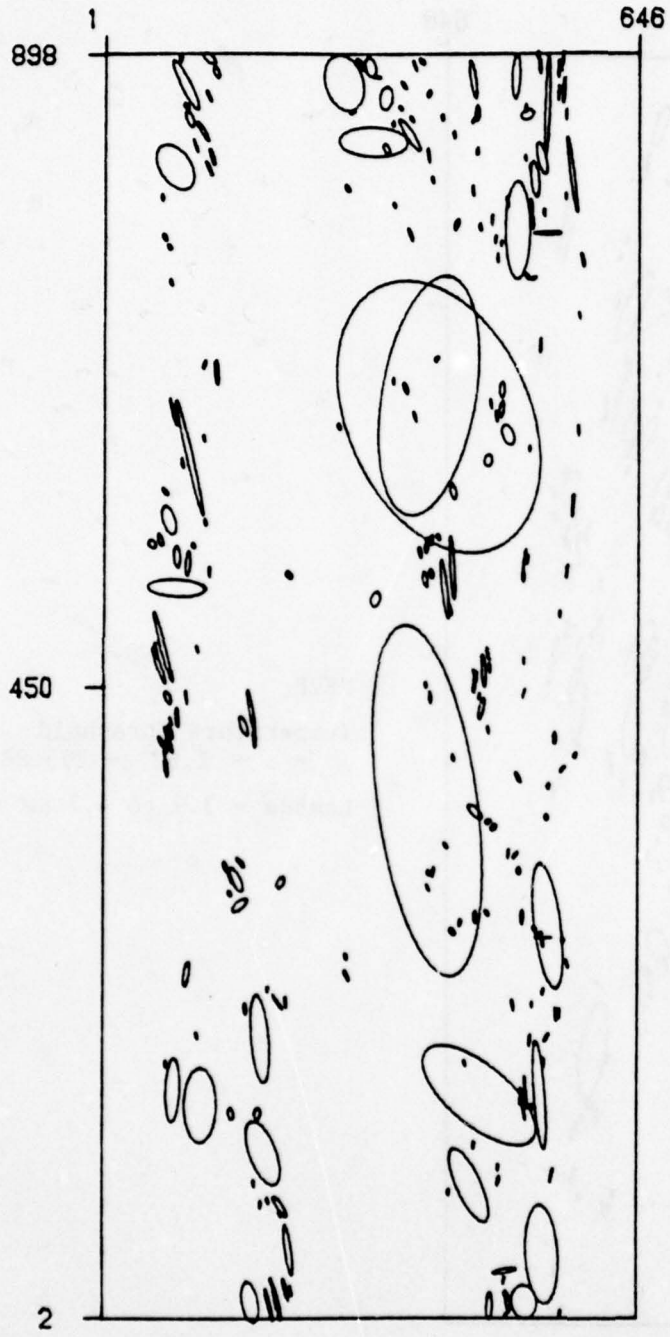

NEVF

Temperature Threshold
$= \mu + 0.9\sigma = 292.86K$

Lambda = 9.0 - 11.4 μm

FIGURE 15a. EQUIVALENT ELLIPTICAL AREAS FOR NELLIS MOUNTAINS.
Scanner: 35° Depression Time: 1034 Altitude: 1000 Ft.

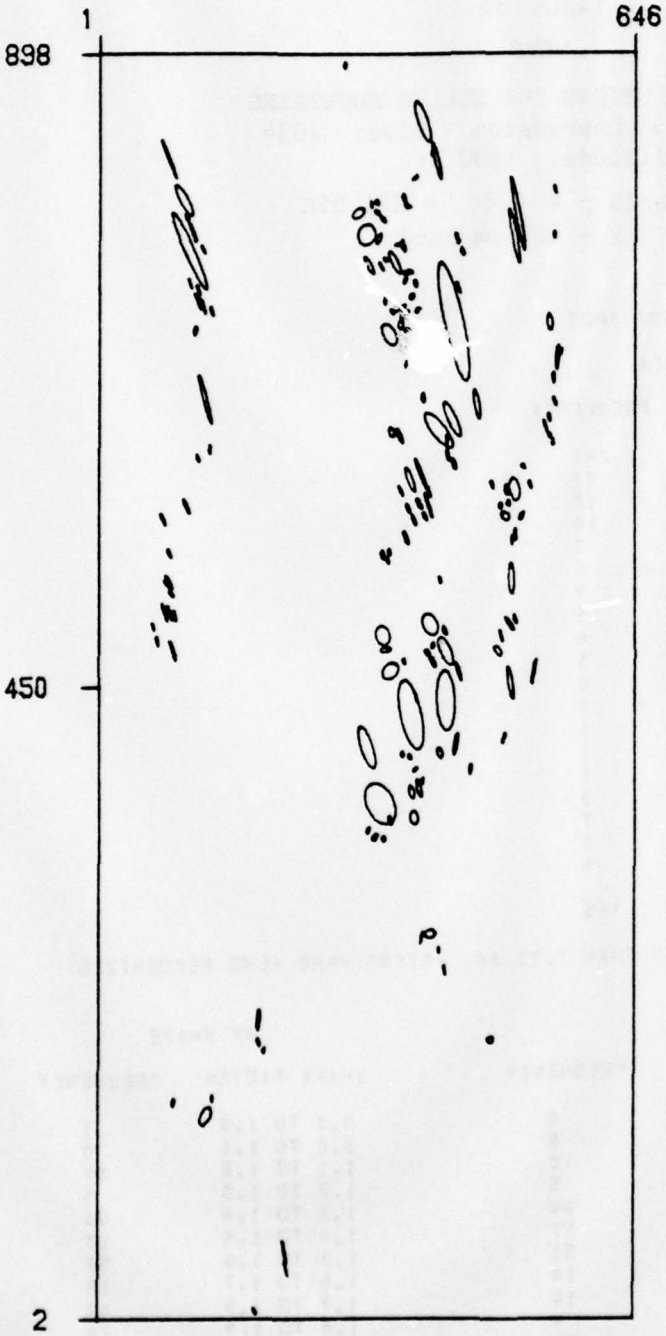

NEVF

Temperature Threshold
$= \mu + 1.8\sigma = 298.72K$

Lambda = 9.0 - 11.4 μm

FIGURE 15b. EQUIVALENT ELLIPTICAL AREAS FOR NELLIS MOUNTAINS.
Scanner: 35° Depression Time: 1034 Altitude: 1000 Ft.

TABLE 8a

NEVF

AREA DISTRIBUTIONS FOR NELLIS MOUNTAINS
Scanner: 35° Depression Time: 1034
Altitude: 1000 Ft.

Threshold $\mu + 0.8\sigma$ = 291.05K
3.9 - 4.7 μm Band

DISTRIBUTION OF RECOGNIZED HOT SPOT

BY AREA

SQUARE METERS			FREQUENCY
7.7	TO	50.0	241
50.0	TO	100.0	41
100.0	TO	150.0	18
150.0	TO	200.0	10
200.0	TO	250.0	7
250.0	TO	300.0	6
300.0	TO	400.0	9
400.0	TO	500.0	5
500.0	TO	600.0	6
600.0	TO	700.0	3
700.0	TO	800.0	0
800.0	TO	900.0	0
900.0	TO	1000.0	1
1000.0	TO	1500.0	1
1500.0	TO	2000.0	1
2000.0	TO	3000.0	3
3000.0	TO	5000.0	7
5000.0	TO	10000.0	0
OVER		10000.0	6

TOTAL NUMBER OF HOT SPOT = 365

434 FEATURES WITH AREAS LESS THAN 7.70 SQ. METERS WERE ALSO RECOGNIZED

BY PERIMETER

METERS			FEET			FREQUENCY
0	TO	7	0	TO	22	0
7	TO	10	22	TO	32	0
10	TO	12	32	TO	39	0
12	TO	14	39	TO	45	5
14	TO	16	45	TO	52	44
16	TO	17	52	TO	55	17
17	TO	20	55	TO	65	50
20	TO	22	65	TO	72	19
22	TO	24	72	TO	78	14
24	TO	26	78	TO	85	9
26	TO	28	85	TO	91	12
28	TO	30	91	TO	98	13
30	TO	32	98	TO	104	12
32	TO	39	104	TO	127	27
39	TO	45	127	TO	147	11
45	TO	55	147	TO	180	14
55	TO	71	180	TO	232	27
71	TO	100	232	TO	328	25
OVER		100	OVER		328	66

BY SHAPE

SHAPE FACTOR			FREQUENCY
0.0	TO	1.0	1
1.0	TO	1.1	0
1.1	TO	1.2	15
1.2	TO	1.3	5
1.3	TO	1.4	54
1.4	TO	1.5	17
1.5	TO	1.6	52
1.6	TO	1.7	13
1.7	TO	1.8	44
1.8	TO	1.9	20
1.9	TO	2.0	17
2.0	TO	2.4	46
2.4	TO	2.6	19
2.6	TO	2.8	14
2.8	TO	3.0	8
3.0	TO	3.5	20
3.5	TO	4.0	6
4.0	TO	4.5	3
OVER		4.5	11

TABLE 8b

NEVF
AREA DISTRIBUTIONS FOR NELLIS MOUNTAINS
Scanner: 35° Depression Time: 1034
Altitude: 1000 Ft.

Threshold $\mu + 1.6\sigma = 295.88$
3.9 - 4.7 μm Band

DISTRIBUTION OF RECOGNIZED HOT SPOT

BY AREA

SQUARE METERS		FREQUENCY
7.7 TO	50.0	184
50.0 TO	100.0	35
100.0 TO	150.0	14
150.0 TO	200.0	13
200.0 TO	250.0	4
250.0 TO	300.0	4
300.0 TO	400.0	4
400.0 TO	500.0	3
500.0 TO	600.0	1
600.0 TO	700.0	4
700.0 TO	800.0	1
800.0 TO	900.0	1
900.0 TO	1000.0	2
1000.0 TO	1500.0	3
1500.0 TO	2000.0	1
2000.0 TO	3000.0	2
3000.0 TO	5000.0	1
5000.0 TO	10000.0	2
OVER	10000.0	0

TOTAL NUMBER OF HOT SPOT = 279

284 FEATURES WITH AREAS LESS THAN 7.70 SQ. METERS WERE ALSO RECOGNIZED

BY PERIMETER

METERS		FEET		FREQUENCY
0 TO	7	0 TO	22	0
7 TO	10	22 TO	32	0
10 TO	12	32 TO	39	0
12 TO	14	39 TO	45	3
14 TO	16	45 TO	52	36
16 TO	17	52 TO	55	9
17 TO	20	55 TO	65	29
20 TO	22	65 TO	72	10
22 TO	24	72 TO	78	8
24 TO	26	78 TO	85	4
26 TO	28	85 TO	91	18
28 TO	30	91 TO	98	6
30 TO	32	98 TO	104	10
32 TO	39	104 TO	127	23
39 TO	45	127 TO	147	14
45 TO	55	147 TO	180	25
55 TO	71	180 TO	232	17
71 TO	100	232 TO	328	17
OVER	100	OVER	328	50

BY SHAPE

SHAPE FACTOR		FREQUENCY
0.0 TO	1.0	0
1.0 TO	1.1	0
1.1 TO	1.2	11
1.2 TO	1.3	9
1.3 TO	1.4	47
1.4 TO	1.5	8
1.5 TO	1.6	33
1.6 TO	1.7	11
1.7 TO	1.8	29
1.8 TO	1.9	14
1.9 TO	2.0	17
2.0 TO	2.4	49
2.4 TO	2.6	5
2.6 TO	2.8	7
2.8 TO	3.0	1
3.0 TO	3.5	12
3.5 TO	4.0	9
4.0 TO	4.5	6
OVER	4.5	11

TABLE 9a

NEVF
AREA DISTRIBUTIONS FOR NELLIS MOUNTAINS
Scanner: 35° Depression Time: 1034
Altitude: 1000 Ft.

Threshold $\mu + 0.9\sigma$ = 292.86K
9.0 - 11.4 μm Band

DISTRIBUTION OF RECOGNIZED HOT SPOT

BY AREA

SQUARE METERS			FREQUENCY
7.7	TO	50.0	305
50.0	TO	100.0	36
100.0	TO	150.0	17
150.0	TO	200.0	12
200.0	TO	250.0	6
250.0	TO	300.0	8
300.0	TO	400.0	3
400.0	TO	500.0	4
500.0	TO	600.0	4
600.0	TO	700.0	4
700.0	TO	800.0	3
800.0	TO	900.0	0
900.0	TO	1000.0	1
1000.0	TO	1500.0	3
1500.0	TO	2000.0	2
2000.0	TO	3000.0	2
3000.0	TO	5000.0	8
5000.0	TO	10000.0	2
OVER		10000.0	4

TOTAL NUMBER OF HOT SPOT = 424

419 FEATURES WITH AREAS LESS THAN 7.70 SQ. METERS WERE ALSO RECOGNIZED

BY PERIMETER

METERS			FEET			FREQUENCY
0	TO	7	0	TO	22	0
7	TO	10	22	TO	32	0
10	TO	12	32	TO	39	0
12	TO	14	39	TO	45	2
14	TO	16	45	TO	52	53
16	TO	17	52	TO	55	31
17	TO	20	55	TO	65	58
20	TO	22	65	TO	72	23
22	TO	24	72	TO	78	23
24	TO	26	78	TO	85	12
26	TO	28	85	TO	91	17
28	TO	30	91	TO	98	11
30	TO	32	98	TO	104	15
32	TO	39	104	TO	127	28
39	TO	45	127	TO	147	12
45	TO	55	147	TO	180	29
55	TO	71	180	TO	232	19
71	TO	100	232	TO	328	25
OVER		100	OVER		328	66

BY SHAPE

SHAPE FACTOR			FREQUENCY
0.0	TO	1.0	1
1.0	TO	1.1	1
1.1	TO	1.2	17
1.2	TO	1.3	9
1.3	TO	1.4	60
1.4	TO	1.5	19
1.5	TO	1.6	63
1.6	TO	1.7	25
1.7	TO	1.8	46
1.8	TO	1.9	25
1.9	TO	2.0	24
2.0	TO	2.4	54
2.4	TO	2.6	13
2.6	TO	2.8	18
2.8	TO	3.0	4
3.0	TO	3.5	16
3.5	TO	4.0	11
4.0	TO	4.5	3
OVER		4.5	15

TABLE 9b

NEVF

AREA DISTIRBUTIONS FOR NELLIS MOUNTAINS
Scanner: 35° Depression Time: 1034
Altitude: 1000 Ft.

Threshold $\mu + 1.8\sigma$ = 298.72K

9.0 - 11.4 μm Band

DISTRIBUTION OF RECOGNIZED HOT SPOT

BY AREA

SQUARE METERS			FREQUENCY
7.7	TO	50.0	179
50.0	TO	100.0	31
100.0	TO	150.0	13
150.0	TO	200.0	7
200.0	TO	250.0	2
250.0	TO	300.0	2
300.0	TO	400.0	5
400.0	TO	500.0	2
500.0	TO	600.0	5
600.0	TO	700.0	4
700.0	TO	800.0	1
800.0	TO	900.0	1
900.0	TO	1000.0	0
1000.0	TO	1500.0	2
1500.0	TO	2000.0	1
2000.0	TO	3000.0	3
3000.0	TO	5000.0	1
5000.0	TO	10000.0	0
OVER		10000.0	0

TOTAL NUMBER OF HOT SPOT = 259

234 FEATURES WITH AREAS LESS THAN 7.70 SQ. METERS WERE ALSO RECOGNIZED

BY PERIMETER

METERS		FEET		FREQUENCY
0 TO	7	0 TO	22	0
7 TO	10	22 TO	32	0
10 TO	12	32 TO	39	0
12 TO	14	39 TO	45	2
14 TO	16	45 TO	52	24
16 TO	17	52 TO	55	7
17 TO	20	55 TO	65	40
20 TO	22	65 TO	72	17
22 TO	24	72 TO	78	11
24 TO	26	78 TO	85	5
26 TO	28	85 TO	91	4
28 TO	30	91 TO	98	14
30 TO	32	98 TO	104	9
32 TO	39	104 TO	127	19
39 TO	45	127 TO	147	17
45 TO	55	147 TO	180	16
55 TO	71	180 TO	232	16
71 TO	100	232 TO	328	18
OVER	100	OVER	328	40

BY SHAPE

SHAPE FACTOR			FREQUENCY
0.0	TO	1.0	0
1.0	TO	1.1	0
1.1	TO	1.2	7
1.2	TO	1.3	7
1.3	TO	1.4	36
1.4	TO	1.5	15
1.5	TO	1.6	34
1.6	TO	1.7	14
1.7	TO	1.8	27
1.8	TO	1.9	14
1.9	TO	2.0	9
2.0	TO	2.4	40
2.4	TO	2.6	14
2.6	TO	2.8	6
2.8	TO	3.0	7
3.0	TO	3.5	11
3.5	TO	4.0	9
4.0	TO	4.5	4
OVER		4.5	5

$$\text{i.e.,} \quad \text{shape factor} = \frac{\text{perimeter}/2\pi}{\sqrt{\text{area}/\pi}}$$

For a circular area, the shape factor so defined is equal to unity.

It is seen in Tables 8 and 9 that most of the exceedances at the one standard deviation threshold are due to pixels clustered together forming areas of 50 to 100 m^2 with only a few clustering together in areas larger than 200 m^2.

The ellipse data together with the histogram data could be important in determining the threshold required for a sensor. At a range where a 50 - 100 m^2 area on the ground appears as a point target, there are numerous equivalent point targets in the background 1 to 2 standard deviations, i.e., in this data 5 to 10K, above the mean background temperature. If such sources generate enough radiant intensity at the collecting aperture to pass the sensor threshold, then they will trigger the sensor. It must be remembered that although 5 to 10K is not a very large ΔT, the radiant intensity must be scaled by the area in deriving the equivalent point target.

The ellipse data in Tables 8 and 9, and even more notably in Figures 14 and 15, also show the presence of a number of larger areas of brightness that are obvious in the imagery of Figure 2. The presence of these large areas at 1 to 2 standard deviations above the mean is attributable to the mountainous terrain relief and the large sunlit and shadowed regions in the scene. These could also be significant for sensors having some sensitivity to edges.

In order to show how the ellipse statistics vary from one type of terrain background to another, ellipses have also been generated from imagery over a combined NEV C1 and NEV C2 flat desert-type terrain at Nellis AFB. Figures 16 and 17 show the equivalent elliptical areas

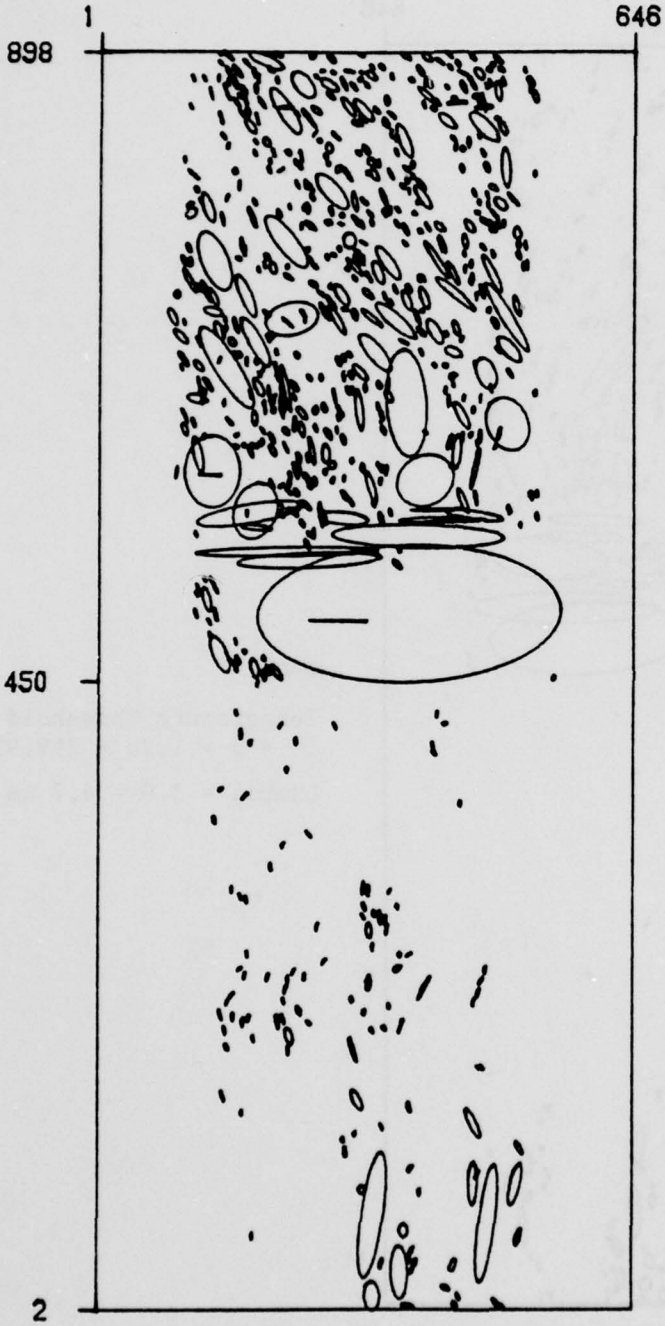

NEVC

Temperature Threshold
= μ + 1σ = 299.38K

Lambda = 3.9 to 4.7 μm

FIGURE 16a. EQUIVALENT ELLIPTICAL AREAS FOR NELLIS DESERT.
Scanner: 35° Depression Time: 1058 Altitude: 1000 Ft.

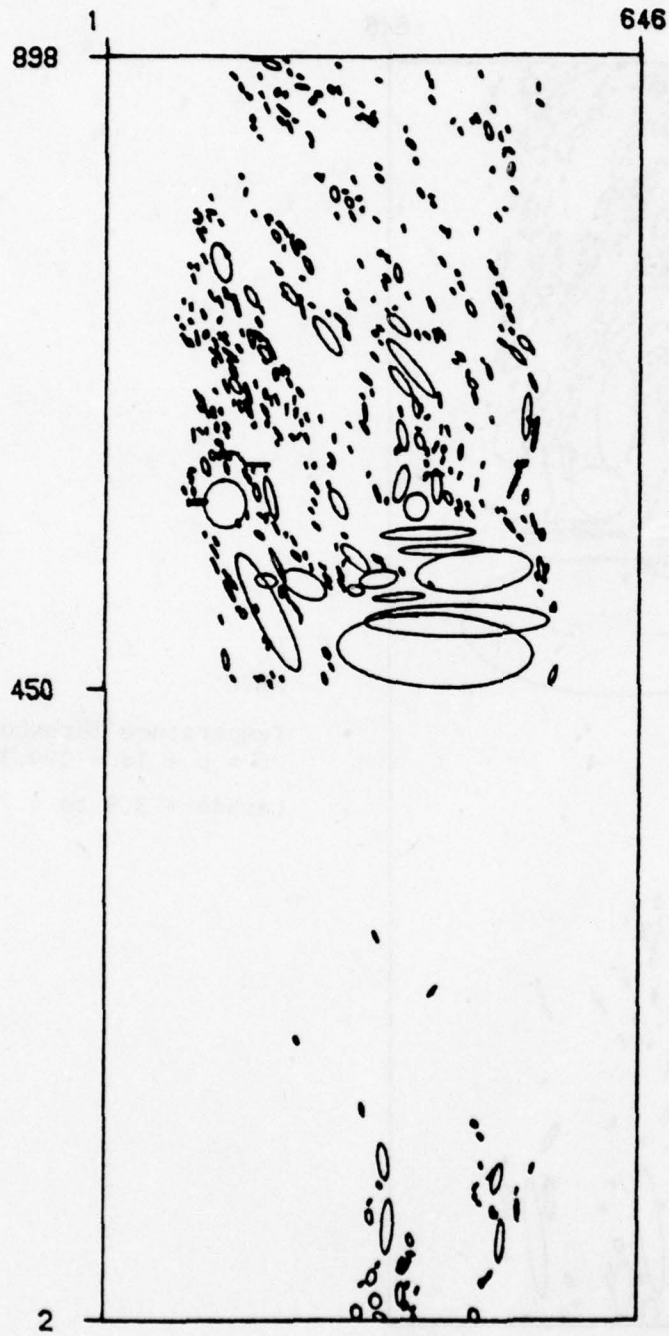

FIGURE 16b. EQUIVALENT ELLIPTICAL AREAS FOR NELLIS DESERT.
Scanner: 35° Depression Time: 1058 Altitude: 1000 Ft.

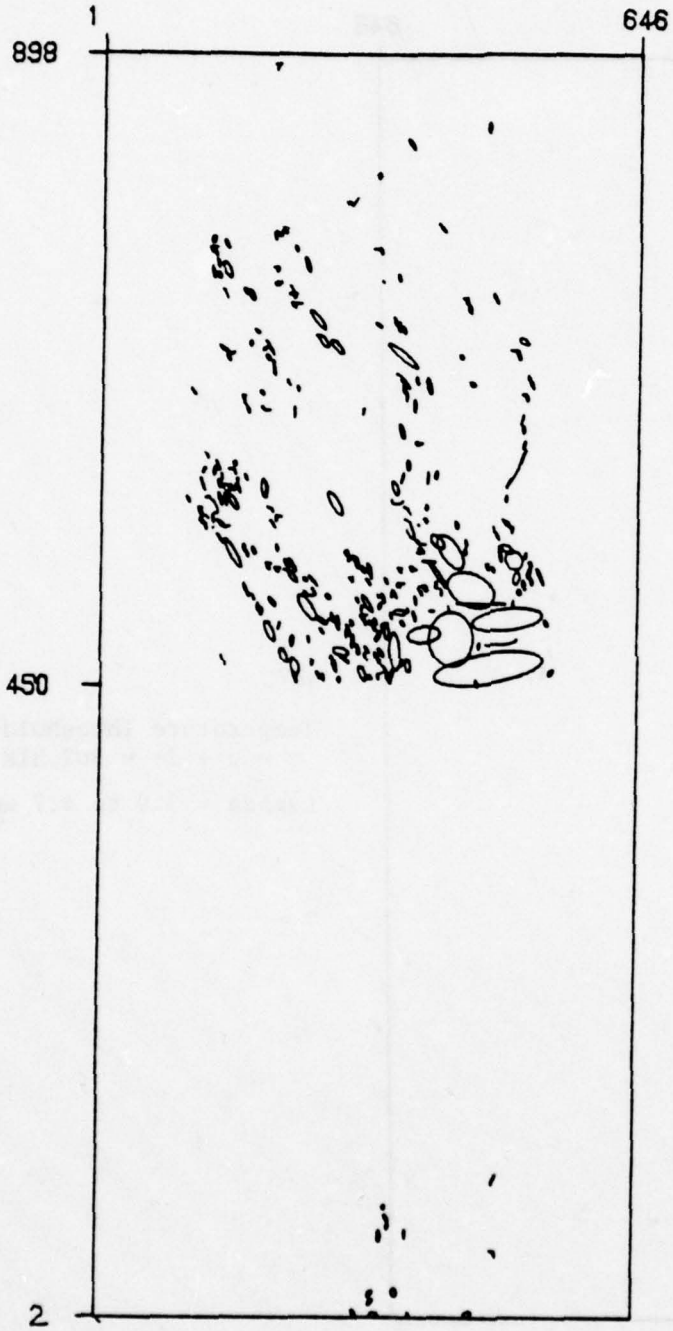

NEVC

Temperature Threshold
$= \mu + 1.4\sigma = 300.45K$

Lambda = 3.9 to 4.7 μm

FIGURE 16c. EQUIVALENT ELLIPTICAL AREAS FOR NELLIS DESERT.
Scanner: 35° Depression Time: 1058 Altitude: 1000 Ft.

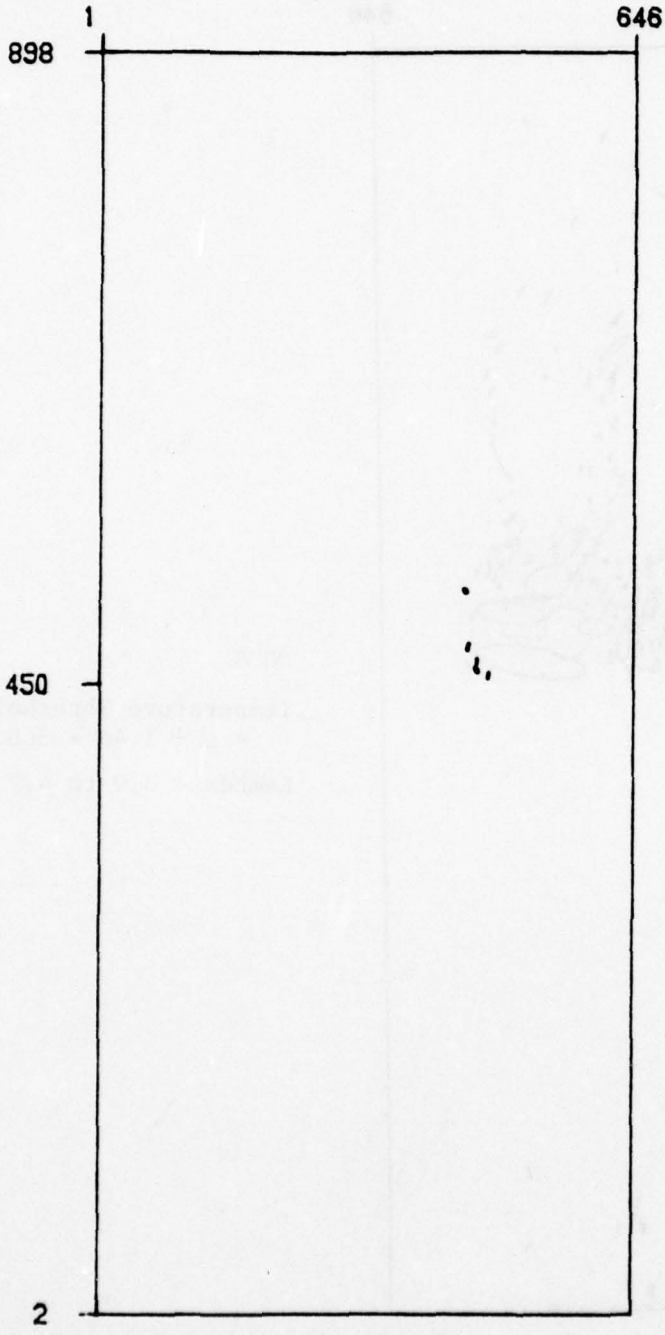

FIGURE 16d. EQUIVALENT ELLIPTICAL AREAS FOR NELLIS DESERT.
Scanner: 35° Depression Time: 1058 Altitude: 1000 Ft.

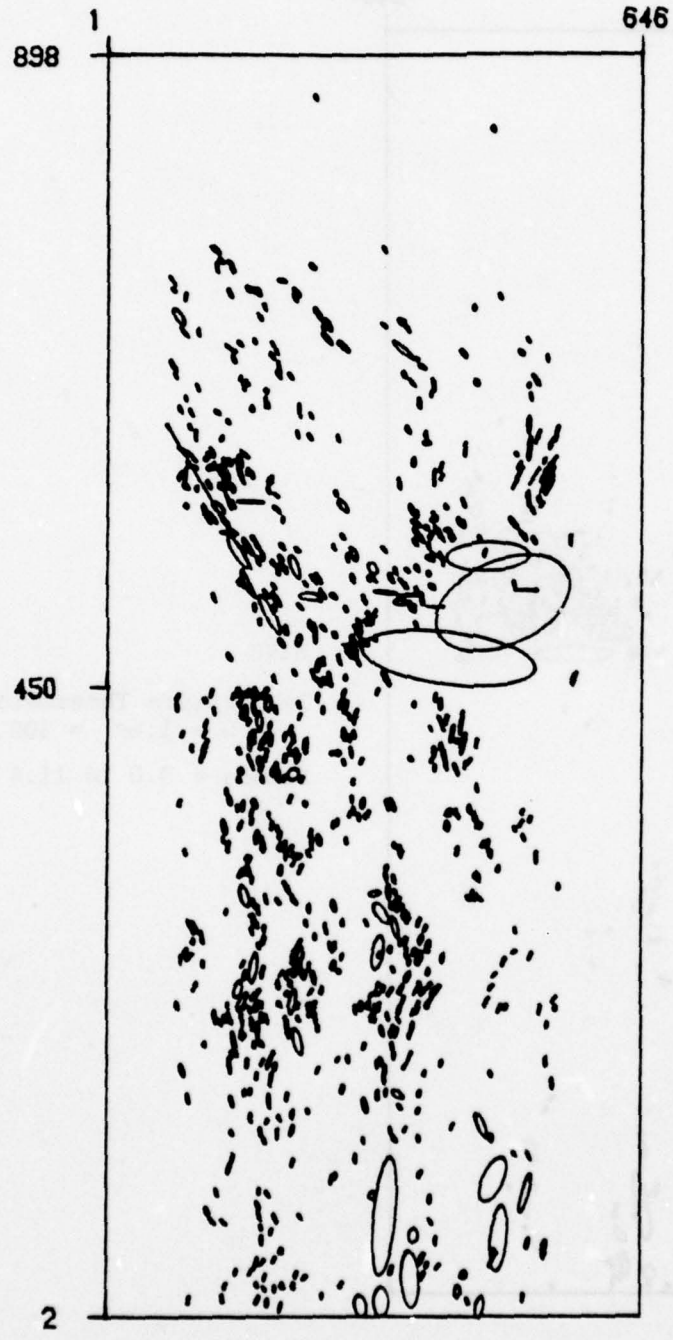

NEVC

Temperature Threshold
$= \mu + 1.2\sigma = 300.33K$

Lambda = 9.0 to 11.4 μm

FIGURE 17a. EQUIVALENT ELLIPTICAL AREAS FOR NELLIS DESERT.
Scanner: 35° Depression Time: 1058 Altitude: 1000 Ft.

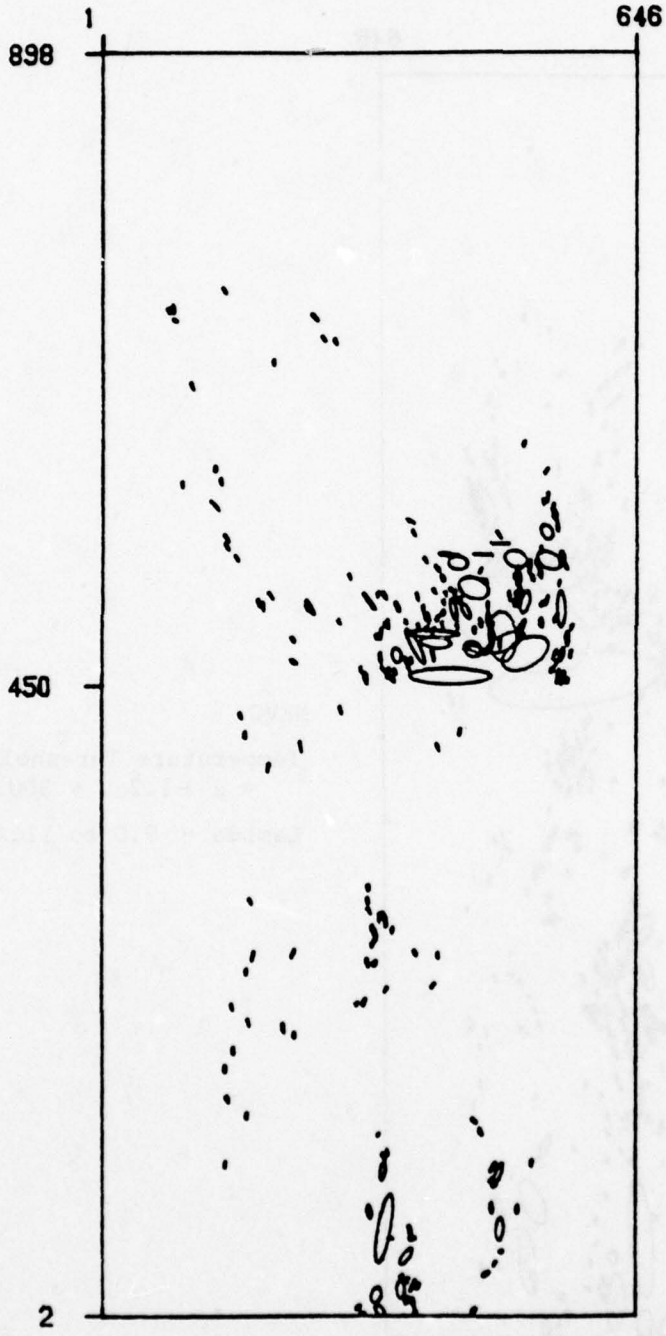

NEVC

Temperature Threshold
$= \mu + 1.6\sigma = 300.97$

Lambda = 9.0 to 11.4 μm

FIGURE 17b. EQUIVALENT ELLIPTICAL AREAS FOR NELLIS DESERT.
Scanner: 35° Depression Time: 1058 Altitude: 1000 Ft.

at several threshold settings for the 3.9 - 4.7 and 9.0 - 11.4 μm data. The corresponding ellipse tabulations are given in Tables 10 and 11. As in the data over the mountains, there are many areas less than 200 m^2 that exceed the one standard deviation threshold. However, it should also be noted that the standard deviation is smaller over the desert-type terrain than over the mountainous-type terrain. It should also be noted in comparing Figures 14 and 15 that there are significantly fewer large areas that exceed the one standard deviation threshold.

The imagery from which Figures 16 and 17 were generated actually consisted of two segments of a single image over desert-type terrain at Nellis AFB obtained on one flight that has been linked together for economy in computing. The first 450 lines of the imagery, NEV C1, are over a portion of the desert that appears from the actual imagery to be quieter with fewer plants and shadows than the segment made up of the last 450 lines of imagery, NEV C2. It is clear that as the threshold is raised in either the 3.9 - 4.7 μm or 9.0 - 11.4 μm bands, more ellipses remain in the NEV C2 segment.

As a final example of the processing performed on the data to date, equivalent elliptical areas and ellipse tabulations for the urban and rural areas in West Virginia are shown for the 3.9 - 4.7 μm band in Figures 18 and 19 and in Tables 12 and 13. Apparent again in the mountainous data is the more frequent occurrence of areas larger than 200 m^2 than in the relatively flat urban area. The equivalent ellipse data over the West Virginia terrain is unlike the Nellis AFB data, however, in that there tends to be many more data points several standard deviations above the mean. This is apparent both in the histogram data, Figures 9 and 10, and in the ellipse data, Figures 18 and 19.

TABLE 10a

NEVC
AREA DISTRIBUTIONS FOR NELLIS DESERT
Scanner: 35° Depression Time: 1058
Altitude: 1000 Ft.

Threshold $\mu + 1\sigma$ = 299.38K
3.9 - 4.7 μm Band

DISTRIBUTION OF RECOGNIZED HOT SPOT

BY AREA

SQUARE METERS			FREQUENCY
7.7	TO	50.0	874
50.0	TO	100.0	121
100.0	TO	150.0	42
150.0	TO	200.0	28
200.0	TO	250.0	12
250.0	TO	300.0	11
300.0	TO	400.0	12
400.0	TO	500.0	12
500.0	TO	600.0	3
600.0	TO	700.0	4
700.0	TO	800.0	2
800.0	TO	900.0	6
900.0	TO	1000.0	2
1000.0	TO	1500.0	8
1500.0	TO	2000.0	5
2000.0	TO	3000.0	1
3000.0	TO	5000.0	8
5000.0	TO	10000.0	6
OVER		10000.0	1

TOTAL NUMBER OF HOT SPOT = 1158

1923 FEATURES WITH AREAS LESS THAN 7.70 SQ. METERS WERE ALSO RECOGNIZED

BY PERIMETER

METERS			FEET			FREQUENCY
0	TO	7	0	TO	22	1
7	TO	10	22	TO	32	1
10	TO	12	32	TO	39	0
12	TO	14	39	TO	45	10
14	TO	16	45	TO	52	127
16	TO	17	52	TO	55	39
17	TO	20	55	TO	65	178
20	TO	22	65	TO	72	95
22	TO	24	72	TO	78	36
24	TO	26	78	TO	85	40
26	TO	28	85	TO	91	63
28	TO	30	91	TO	98	44
30	TO	32	98	TO	104	32
32	TO	39	104	TO	127	93
39	TO	45	127	TO	147	48
45	TO	55	147	TO	180	62
55	TO	71	180	TO	232	74
71	TO	100	232	TO	328	62
OVER		100	OVER		328	153

BY SHAPE

SHAPE FACTOR			FREQUENCY
0.0	TO	1.0	2
1.0	TO	1.1	0
1.1	TO	1.2	32
1.2	TO	1.3	15
1.3	TO	1.4	171
1.4	TO	1.5	44
1.5	TO	1.6	134
1.6	TO	1.7	68
1.7	TO	1.8	148
1.8	TO	1.9	51
1.9	TO	2.0	53
2.0	TO	2.4	207
2.4	TO	2.6	43
2.6	TO	2.8	44
2.8	TO	3.0	21
3.0	TO	3.5	45
3.5	TO	4.0	25
4.0	TO	4.5	11
OVER		4.5	44

TABLE 10b

NEVC
AREA DISTRIBUTIONS FOR NELLIS DESERT
Scanner: 35° Depression Time: 1058
Altitude: 1000 Ft.

Threshold $\mu + 1.2\sigma$ = 299.97K
3.9 - 4.7 μm Band

DISTRIBUTION OF RECOGNIZED HOT SPOT

BY AREA

SQUARE METERS		FREQUENCY
7.7 TO	50.0	695
50.0 TO	100.0	87
100.0 TO	150.0	28
150.0 TO	200.0	14
200.0 TO	250.0	10
250.0 TO	300.0	11
300.0 TO	400.0	8
400.0 TO	500.0	1
500.0 TO	600.0	3
600.0 TO	700.0	5
700.0 TO	800.0	4
800.0 TO	900.0	0
900.0 TO	1000.0	2
1000.0 TO	1500.0	5
1500.0 TO	2000.0	2
2000.0 TO	3000.0	2
3000.0 TO	5000.0	1
5000.0 TO	10000.0	2
OVER	10000.0	2

TOTAL NUMBER OF HOT SPOT = 882

1427 FEATURES WITH AREAS LESS THAN 7.70 SQ. METERS WERE ALSO RECOGNIZED

BY PERIMETER

METERS		FEET		FREQUENCY
0 TO	7	0 TO	22	0
7 TO	10	22 TO	32	0
10 TO	12	32 TO	39	0
12 TO	14	39 TO	45	8
14 TO	16	45 TO	52	103
16 TO	17	52 TO	55	26
17 TO	20	55 TO	65	136
20 TO	22	65 TO	72	78
22 TO	24	72 TO	78	26
24 TO	26	78 TO	85	31
26 TO	28	85 TO	91	49
28 TO	30	91 TO	98	54
30 TO	32	98 TO	104	34
32 TO	39	104 TO	127	57
39 TO	45	127 TO	147	41
45 TO	55	147 TO	180	53
55 TO	71	180 TO	232	43
71 TO	100	232 TO	328	43
OVER	100	OVER	328	100

BY SHAPE

SHAPE FACTOR		FREQUENCY
0.0 TO	1.0	1
1.0 TO	1.1	0
1.1 TO	1.2	29
1.2 TO	1.3	7
1.3 TO	1.4	132
1.4 TO	1.5	32
1.5 TO	1.6	109
1.6 TO	1.7	45
1.7 TO	1.8	114
1.8 TO	1.9	48
1.9 TO	2.0	55
2.0 TO	2.4	137
2.4 TO	2.6	38
2.6 TO	2.8	31
2.8 TO	3.0	18
3.0 TO	3.5	31
3.5 TO	4.0	19
4.0 TO	4.5	9
OVER	4.5	27

TABLE 10c

NEVC

AREA DISTRIBUTIONS FOR NELLIS DESERT
Scanner: 35° Depression Time: 1058
Altitude: 1000 Ft.

Threshold $\mu + 1.4\sigma \approx 300.45K$
3.9 - 4.7 μm Band

DISTRIBUTION OF RECOGNIZED HOT SPOT

BY AREA

SQUARE METERS			FREQUENCY
7.7	TO	50.0	480
50.0	TO	100.0	48
100.0	TO	150.0	12
150.0	TO	200.0	11
200.0	TO	250.0	2
250.0	TO	300.0	5
300.0	TO	400.0	3
400.0	TO	500.0	2
500.0	TO	600.0	2
600.0	TO	700.0	2
700.0	TO	800.0	1
800.0	TO	900.0	0
900.0	TO	1000.0	0
1000.0	TO	1500.0	2
1500.0	TO	2000.0	0
2000.0	TO	3000.0	0
3000.0	TO	5000.0	3
5000.0	TO	10000.0	1
OVER		10000.0	0

TOTAL NUMBER OF HOT SPOT = 574

1008 FEATURES WITH AREAS LESS THAN 7.70 SQ. METERS WERE ALSO RECOGNIZED

BY PERIMETER

METERS			FEET			FREQUENCY
0	TO	7	0	TO	22	0
7	TO	10	22	TO	32	0
10	TO	12	32	TO	39	0
12	TO	14	39	TO	45	6
14	TO	16	45	TO	52	79
16	TO	17	52	TO	55	16
17	TO	20	55	TO	65	106
20	TO	22	65	TO	72	63
22	TO	24	72	TO	78	17
24	TO	26	78	TO	85	22
26	TO	28	85	TO	91	31
28	TO	30	91	TO	98	18
30	TO	32	98	TO	104	17
32	TO	39	104	TO	127	36
39	TO	45	127	TO	147	23
45	TO	55	147	TO	180	33
55	TO	71	180	TO	232	33
71	TO	100	232	TO	328	22
OVER		100	OVER		328	52

BY SHAPE

SHAPE FACTOR			FREQUENCY
0.0	TO	1.0	0
1.0	TO	1.1	0
1.1	TO	1.2	23
1.2	TO	1.3	9
1.3	TO	1.4	100
1.4	TO	1.5	14
1.5	TO	1.6	70
1.6	TO	1.7	26
1.7	TO	1.8	42
1.8	TO	1.9	25
1.9	TO	2.0	36
2.0	TO	2.4	79
2.4	TO	2.6	26
2.6	TO	2.8	15
2.8	TO	3.0	15
3.0	TO	3.5	22
3.5	TO	4.0	9
4.0	TO	4.5	7
OVER		4.5	16

TABLE 10d

NEVC
AREA DISTRIBUTIONS FOR NELLIS DESERT
Scanner: 35° Depression Time: 1058
Altitude: 1000 Ft.

Threshold $\mu + 2\sigma$ = 302.31K
3.9 - 4.7 μm Band

DISTRIBUTION OF RECOGNIZED HOT SPOT

BY AREA

SQUARE METERS			FREQUENCY
7.7	TO	50.0	17
50.0	TO	100.0	0
100.0	TO	150.0	0
150.0	TO	200.0	0
200.0	TO	250.0	0
250.0	TO	300.0	0
300.0	TO	400.0	0
400.0	TO	500.0	0
500.0	TO	600.0	0
600.0	TO	700.0	0
700.0	TO	800.0	0
800.0	TO	900.0	0
900.0	TO	1000.0	0
1000.0	TO	1500.0	0
1500.0	TO	2000.0	0
2000.0	TO	3000.0	0
3000.0	TO	5000.0	0
5000.0	TO	10000.0	0
OVER		10000.0	0

TOTAL NUMBER OF HOT SPOT = 17

64 FEATURES WITH AREAS LESS THAN 7.70 SQ. METERS WERE ALSO RECOGNIZED

BY PERIMETER

METERS		FEET		FREQUENCY
0 TO	7	0 TO	22	0
7 TO	10	22 TO	32	0
10 TO	12	32 TO	39	0
12 TO	14	39 TO	45	1
14 TO	16	45 TO	52	6
16 TO	17	52 TO	55	0
17 TO	20	55 TO	65	2
20 TO	22	65 TO	72	3
22 TO	24	72 TO	78	2
24 TO	26	78 TO	85	0
26 TO	28	85 TO	91	0
28 TO	30	91 TO	98	0
30 TO	32	98 TO	104	1
32 TO	39	104 TO	127	1
39 TO	45	127 TO	147	1
45 TO	55	147 TO	180	0
55 TO	71	180 TO	232	0
71 TO	100	232 TO	328	0
OVER	100	OVER	328	0

BY SHAPE

SHAPE FACTOR			FREQUENCY
0.0	TO	1.0	0
1.0	TO	1.1	0
1.1	TO	1.2	2
1.2	TO	1.3	0
1.3	TO	1.4	6
1.4	TO	1.5	0
1.5	TO	1.6	3
1.6	TO	1.7	1
1.7	TO	1.8	3
1.8	TO	1.9	0
1.9	TO	2.0	1
2.0	TO	2.4	0
2.4	TO	2.6	1
2.6	TO	2.8	0
2.8	TO	3.0	0
3.0	TO	3.5	0
3.5	TO	4.0	0
4.0	TO	4.5	0
OVER		4.5	0

TABLE 11a
NEVC
AREA DISTRIBUTION FOR NELLIS DESERT
Scanner: 35° Depression Time: 1058
Altitude: 1000 Ft.

Threshold $\mu + 1.2\sigma$ = 300.33K
9.0 - 11.4 μm Band

DISTRIBUTION OF RECOGNIZED HOT SPOT

BY AREA

SQUARE METERS			FREQUENCY
7.7	TO	50.0	1269
50.0	TO	100.0	116
100.0	TO	150.0	39
150.0	TO	200.0	18
200.0	TO	250.0	6
250.0	TO	300.0	6
300.0	TO	400.0	6
400.0	TO	500.0	3
500.0	TO	600.0	2
600.0	TO	700.0	1
700.0	TO	800.0	2
800.0	TO	900.0	1
900.0	TO	1000.0	0
1000.0	TO	1500.0	0
1500.0	TO	2000.0	0
2000.0	TO	3000.0	3
3000.0	TO	5000.0	1
5000.0	TO	10000.0	1
OVER		10000.0	2

TOTAL NUMBER OF HOT SPOT = 1476

2357 FEATURES WITH AREAS LESS THAN 7.70 SQ. METERS WERE ALSO RECOGNIZED

BY PERIMETER

METERS		FEET		FREQUENCY
0 TO	7	0 TO	22	0
7 TO	10	22 TO	32	0
10 TO	12	32 TO	39	0
12 TO	14	39 TO	45	11
14 TO	16	45 TO	52	188
16 TO	17	52 TO	55	65
17 TO	20	55 TO	65	269
20 TO	22	65 TO	72	126
22 TO	24	72 TO	78	39
24 TO	26	78 TO	85	38
26 TO	28	85 TO	91	102
28 TO	30	91 TO	98	77
30 TO	32	98 TO	104	54
32 TO	39	104 TO	127	136
39 TO	45	127 TO	147	56
45 TO	55	147 TO	180	87
55 TO	71	180 TO	232	71
71 TO	100	232 TO	328	60
OVER	100	OVER	328	97

BY SHAPE

SHAPE FACTOR			FREQUENCY
0.0	TO	1.0	0
1.0	TO	1.1	0
1.1	TO	1.2	32
1.2	TO	1.3	15
1.3	TO	1.4	237
1.4	TO	1.5	35
1.5	TO	1.6	234
1.6	TO	1.7	52
1.7	TO	1.8	206
1.8	TO	1.9	102
1.9	TO	2.0	94
2.0	TO	2.4	254
2.4	TO	2.6	52
2.6	TO	2.8	35
2.8	TO	3.0	28
3.0	TO	3.5	55
3.5	TO	4.0	16
4.0	TO	4.5	10
OVER		4.5	19

TABLE 11b

NEVC

AREA DISTRIBUTION FOR NELLIS DESERT
Scanner: 35° Depression Time: 1058
Altitude: 1000 Ft.

Threshold $\mu + 1.6\sigma$ = 300.97K
9.0 - 11.4 μm Band

DISTRIBUTION OF RECOGNIZED HOT SPOT

BY AREA

SQUARE METERS			FREQUENCY
7.7	TO	50.0	352
50.0	TO	100.0	28
100.0	TO	150.0	9
150.0	TO	200.0	1
200.0	TO	250.0	3
250.0	TO	300.0	3
300.0	TO	400.0	6
400.0	TO	500.0	1
500.0	TO	600.0	2
600.0	TO	700.0	4
700.0	TO	800.0	0
800.0	TO	900.0	2
900.0	TO	1000.0	0
1000.0	TO	1500.0	2
1500.0	TO	2000.0	1
2000.0	TO	3000.0	3
3000.0	TO	5000.0	0
5000.0	TO	10000.0	0
OVER		10000.0	0

TOTAL NUMBER OF HOT SPOT = 417

981 FEATURES WITH AREAS LESS THAN 7.70 SQ. METERS WERE ALSO RECOGNIZED

BY PERIMETER

METERS		FEET		FREQUENCY
0 TO	7	0 TO	22	0
7 TO	10	22 TO	32	0
10 TO	12	32 TO	39	0
12 TO	14	39 TO	45	2
14 TO	16	45 TO	52	53
16 TO	17	52 TO	55	18
17 TO	20	55 TO	65	88
20 TO	22	65 TO	72	34
22 TO	24	72 TO	78	16
24 TO	26	78 TO	85	8
26 TO	28	85 TO	91	29
28 TO	30	91 TO	98	21
30 TO	32	98 TO	104	12
32 TO	39	104 TO	127	36
39 TO	45	127 TO	147	17
45 TO	55	147 TO	180	14
55 TO	71	180 TO	232	19
71 TO	100	232 TO	328	11
OVER	100	OVER	328	39

BY SHAPE

SHAPE FACTOR			FREQUENCY
0.0	TO	1.0	0
1.0	TO	1.1	0
1.1	TO	1.2	8
1.2	TO	1.3	10
1.3	TO	1.4	67
1.4	TO	1.5	8
1.5	TO	1.6	64
1.6	TO	1.7	19
1.7	TO	1.8	74
1.8	TO	1.9	24
1.9	TO	2.0	21
2.0	TO	2.4	59
2.4	TO	2.6	15
2.6	TO	2.8	10
2.8	TO	3.0	4
3.0	TO	3.5	8
3.5	TO	4.0	6
4.0	TO	4.5	1
OVER		4.5	19

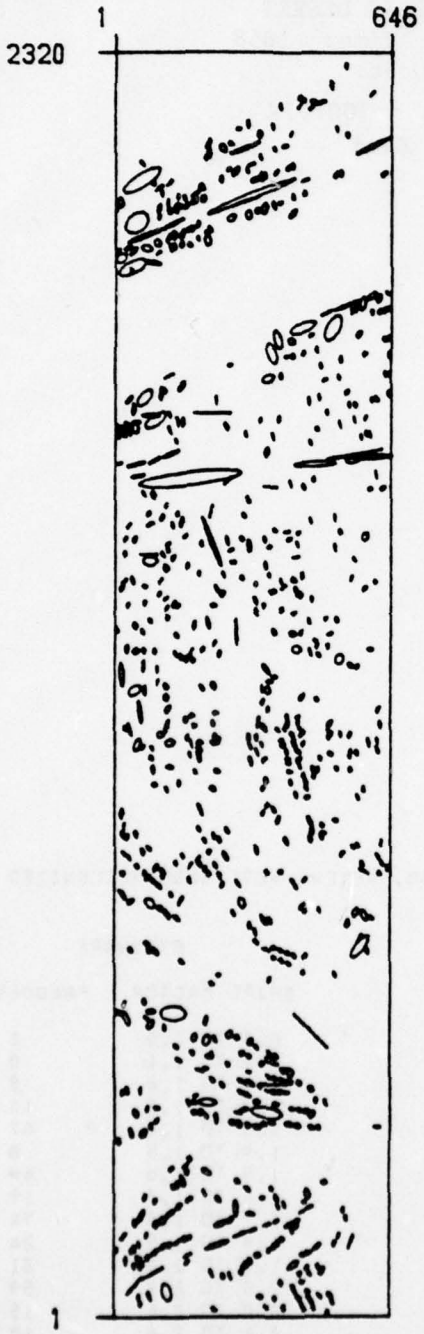

WVA6

Temperature Threshold
= μ + 1σ = 293.54K

Lambda = 3.9 to 4.7 μm

FIGURE 18a. EQUIVALENT ELLIPTICAL AREAS FOR URBAN WEST VIRGINIA.
Scanner: 90° Depression Time: 1150 Altitude: 1750 Ft.

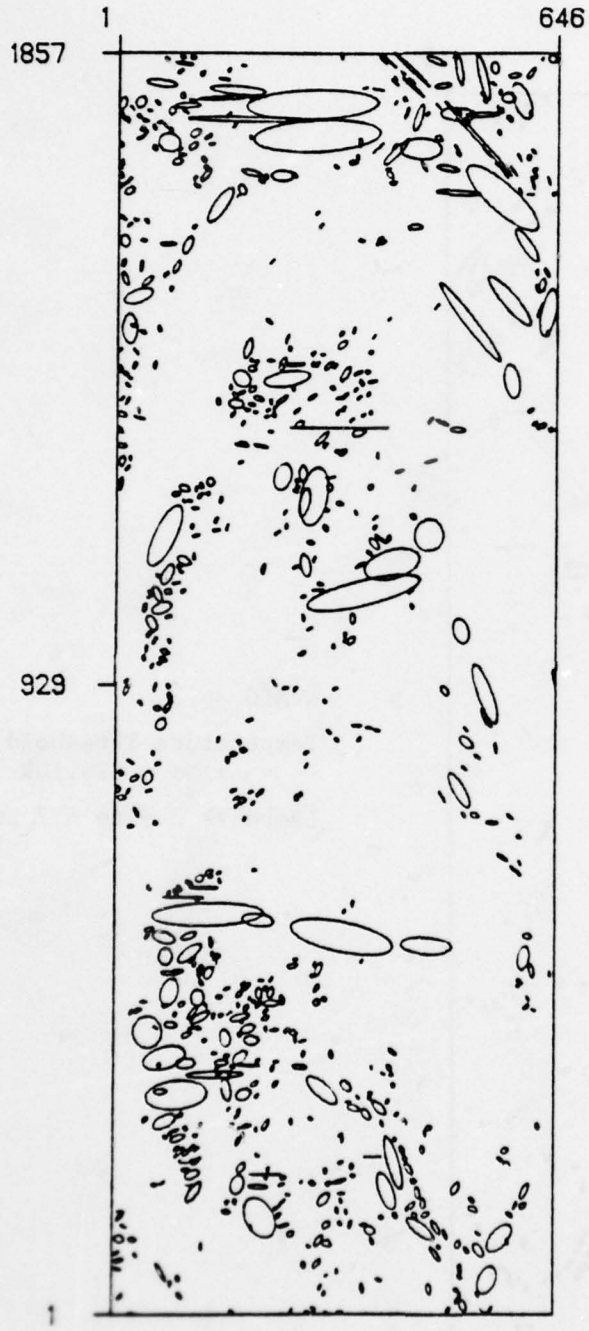

WVA10

Temperature Threshold
= μ + 1σ = 291.71K

Lambda = 3.9 to 4.7 μm

FIGURE 19a. EQUIVALENT ELLIPTICAL AREAS FOR RURAL WEST VIRGINIA.
Scanner: 90° Depression Time: 1152 Altitude: 1750 Ft.

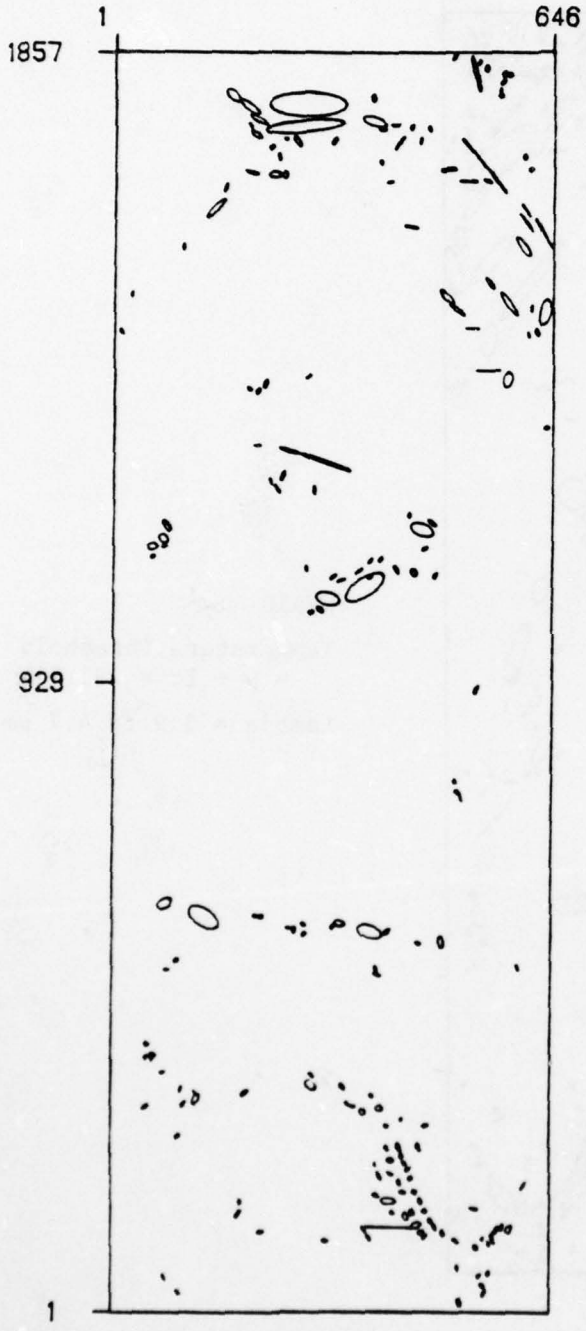

WVA10

Temperature Threshold
$= \mu + 2\sigma = 293.10K$

Lambda = 3.9 to 4.7 μm

FIGURE 19b. EQUIVALENT ELLIPTICAL AREAS FOR RURAL WEST VIRGINIA.
Scanner: 90° Depression Time: 1152 Altitude: 1750 Ft.

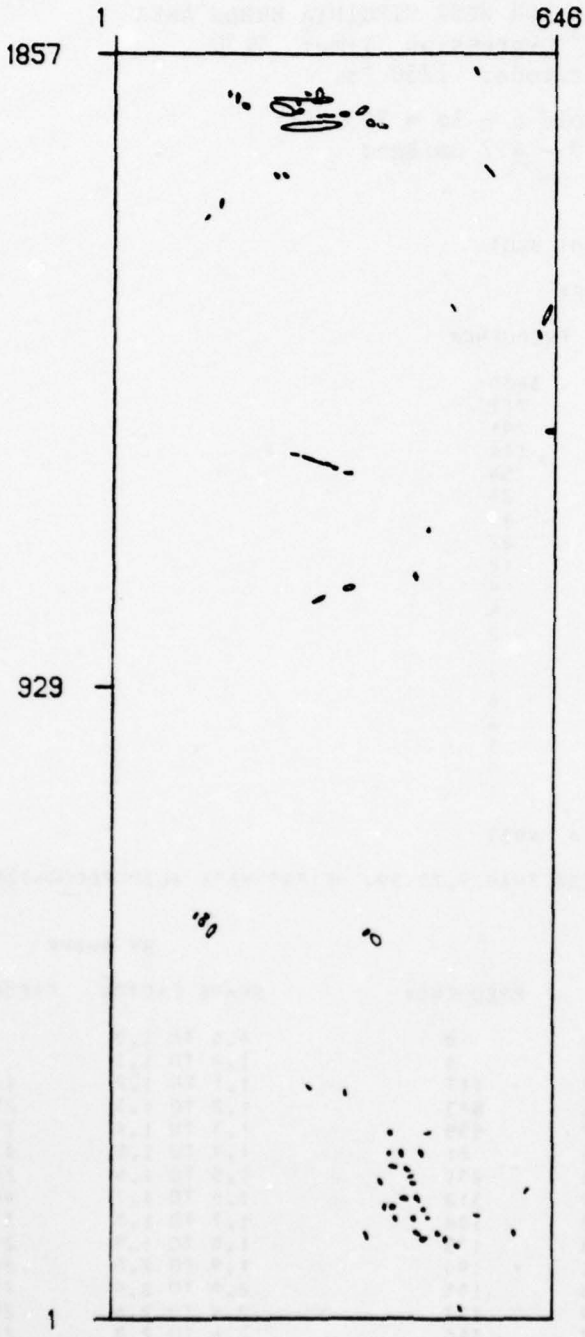

WVA10

Temperature Threshold
$= \mu + 3\sigma = 294.49K$

Lambda = 3.9 to 4.7 μm

FIGURE 19c. EQUIVALENT ELLIPTICAL AREAS FOR RURAL WEST VIRGINIA.
Scanner: 90° Depression Time: 1152 Altitude: 1750 Ft.

TABLE 12

WVA6
AREA DISTRIBUTION FOR WEST VIRGINIA URBAN AREA
Scanner: 90° Depression Time: 1150
Altitude: 1750 Ft.

Threshold $\mu + 1\sigma$ = 293.54K
3.9 - 4.7 μm Band

DISTRIBUTION OF RECOGNIZED HOT SPOT

BY AREA

SQUARE METERS			FREQUENCY
5.7	TO	50.0	3680
50.0	TO	100.0	712
100.0	TO	150.0	246
150.0	TO	200.0	104
200.0	TO	250.0	54
250.0	TO	300.0	28
300.0	TO	400.0	41
400.0	TO	500.0	22
500.0	TO	600.0	12
600.0	TO	700.0	4
700.0	TO	800.0	6
800.0	TO	900.0	2
900.0	TO	1000.0	1
1000.0	TO	1500.0	7
1500.0	TO	2000.0	6
2000.0	TO	3000.0	4
3000.0	TO	5000.0	3
5000.0	TO	10000.0	0
OVER		10000.0	1

TOTAL NUMBER OF HOT SPOT = 4933

3169 FEATURES WITH AREAS LESS THAN 5.70 SQ. METERS WERE ALSO RECOGNIZED

BY PERIMETER

METERS			FEET			FREQUENCY
0	TO	7	0	TO	22	0
7	TO	10	22	TO	32	0
10	TO	12	32	TO	39	117
12	TO	14	39	TO	45	503
14	TO	16	45	TO	52	535
16	TO	17	52	TO	55	21
17	TO	20	55	TO	65	431
20	TO	22	65	TO	72	312
22	TO	24	72	TO	78	104
24	TO	26	78	TO	85	173
26	TO	28	85	TO	91	190
28	TO	30	91	TO	98	105
30	TO	32	98	TO	104	137
32	TO	39	104	TO	127	360
39	TO	45	127	TO	147	293
45	TO	55	147	TO	180	382
55	TO	71	180	TO	232	433
71	TO	100	232	TO	328	389
OVER		100	OVER		328	448

BY SHAPE

SHAPE FACTOR			FREQUENCY
0.0	TO	1.0	0
1.0	TO	1.1	0
1.1	TO	1.2	146
1.2	TO	1.3	256
1.3	TO	1.4	787
1.4	TO	1.5	316
1.5	TO	1.6	268
1.6	TO	1.7	461
1.7	TO	1.8	335
1.8	TO	1.9	244
1.9	TO	2.0	285
2.0	TO	2.4	784
2.4	TO	2.6	259
2.6	TO	2.8	219
2.8	TO	3.0	168
3.0	TO	3.5	230
3.5	TO	4.0	123
4.0	TO	4.5	48
OVER		4.5	44

TABLE 13a.
WVA10

AREA DISTRIBUTIONS FOR WEST VIRGINIA RURAL AREA
Scanner: 90° Depression Time: 1152
Altitude: 1750 Ft.

Threshold $\mu + 1\sigma$ = 291.71K
3.9 - 4.7 μm Band

DISTRIBUTION OF RECOGNIZED HOT SPOT

BY AREA

SQUARE METERS			FREQUENCY
6.0	TO	50.0	2502
50.0	TO	100.0	308
100.0	TO	150.0	96
150.0	TO	200.0	50
200.0	TO	250.0	26
250.0	TO	300.0	29
300.0	TO	400.0	25
400.0	TO	500.0	16
500.0	TO	600.0	13
600.0	TO	700.0	4
700.0	TO	800.0	5
800.0	TO	900.0	6
900.0	TO	1000.0	4
1000.0	TO	1500.0	11
1500.0	TO	2000.0	13
2000.0	TO	3000.0	10
3000.0	TO	5000.0	9
5000.0	TO	10000.0	4
OVER		10000.0	6

TOTAL NUMBER OF HOT SPOT = 3137

3167 FEATURES WITH AREAS LESS THAN 6.00 SQ. METERS WERE ALSO RECOGNIZED

BY PERIMETER

METERS			FEET			FREQUENCY
0	TO	7	0	TO	22	0
7	TO	10	22	TO	32	1
10	TO	12	32	TO	39	0
12	TO	14	39	TO	45	576
14	TO	16	45	TO	52	453
16	TO	17	52	TO	55	0
17	TO	20	55	TO	65	360
20	TO	22	65	TO	72	252
22	TO	24	72	TO	78	0
24	TO	26	78	TO	85	208
26	TO	28	85	TO	91	171
28	TO	30	91	TO	98	3
30	TO	32	98	TO	104	113
32	TO	39	104	TO	127	193
39	TO	45	127	TO	147	153
45	TO	55	147	TO	180	144
55	TO	71	180	TO	232	134
71	TO	100	232	TO	328	118
OVER		100	OVER		328	258

BY SHAPE

SHAPE FACTOR			FREQUENCY
0.0	TO	1.0	2
1.0	TO	1.1	0
1.1	TO	1.2	172
1.2	TO	1.3	236
1.3	TO	1.4	701
1.4	TO	1.5	347
1.5	TO	1.6	272
1.6	TO	1.7	332
1.7	TO	1.8	206
1.8	TO	1.9	140
1.9	TO	2.0	138
2.0	TO	2.4	277
2.4	TO	2.6	66
2.6	TO	2.8	42
2.8	TO	3.0	29
3.0	TO	3.5	59
3.5	TO	4.0	34
4.0	TO	4.5	28
OVER		4.5	56

TABLE 13b

WVA10

AREA DISTRIBUTIONS FOR WEST VIRGINIA RURAL AREA
Scanner: 90° Depression Time: 1152
Altitude: 1750 Ft.

Threshold $\mu + 2\sigma$ = 293.10K
3.9 - 4.7 μm Band

DISTRIBUTION OF RECOGNIZED HOT SPOT

BY AREA

SQUARE METERS			FREQUENCY
6.0	TO	50.0	677
50.0	TO	100.0	80
100.0	TO	150.0	34
150.0	TO	200.0	11
200.0	TO	250.0	6
250.0	TO	300.0	5
300.0	TO	400.0	6
400.0	TO	500.0	0
500.0	TO	600.0	6
600.0	TO	700.0	3
700.0	TO	800.0	0
800.0	TO	900.0	1
900.0	TO	1000.0	0
1000.0	TO	1500.0	4
1500.0	TO	2000.0	0
2000.0	TO	3000.0	1
3000.0	TO	5000.0	2
5000.0	TO	10000.0	1
OVER		10000.0	0

TOTAL NUMBER OF HOT SPOT = 837

833 FEATURES WITH AREAS LESS THAN 6.00 SQ. METERS WERE ALSO RECOGNIZED

BY PERIMETER

METERS		FEET		FREQUENCY
0 TO	7	0 TO	22	0
7 TO	10	22 TO	32	1
10 TO	12	32 TO	39	0
12 TO	14	39 TO	45	153
14 TO	16	45 TO	52	145
16 TO	17	52 TO	55	0
17 TO	20	55 TO	65	87
20 TO	22	65 TO	72	66
22 TO	24	72 TO	78	1
24 TO	26	78 TO	85	42
26 TO	28	85 TO	91	40
28 TO	30	91 TO	98	0
30 TO	32	98 TO	104	38
32 TO	39	104 TO	127	50
39 TO	45	127 TO	147	31
45 TO	55	147 TO	180	43
55 TO	71	180 TO	232	31
71 TO	100	232 TO	328	46
OVER	100	OVER	328	63

BY SHAPE

SHAPE FACTOR			FREQUENCY
0.0	TO	1.0	1
1.0	TO	1.1	0
1.1	TO	1.2	36
1.2	TO	1.3	63
1.3	TO	1.4	193
1.4	TO	1.5	93
1.5	TO	1.6	48
1.6	TO	1.7	112
1.7	TO	1.8	51
1.8	TO	1.9	30
1.9	TO	2.0	46
2.0	TO	2.4	59
2.4	TO	2.6	21
2.6	TO	2.8	15
2.8	TO	3.0	17
3.0	TO	3.5	24
3.5	TO	4.0	12
4.0	TO	4.5	6
OVER		4.5	10

TABLE 13c

WVA10

AREA DISTRIBUTIONS FOR WEST VIRGINIA RURAL AREA

Scanner: 90° Depression Time: 1152

Altitude: 1750 Ft.

Threshold $\mu + 3\sigma$ = 294.49K

3.9 - 4.7 μm Band

DISTRIBUTION OF RECOGNIZED HOT SPOT

BY AREA

SQUARE METERS			FREQUENCY
6.0	TO	50.0	238
50.0	TO	100.0	30
100.0	TO	150.0	10
150.0	TO	200.0	4
200.0	TO	250.0	2
250.0	TO	300.0	2
300.0	TO	400.0	4
400.0	TO	500.0	0
500.0	TO	600.0	0
600.0	TO	700.0	0
700.0	TO	800.0	0
800.0	TO	900.0	0
900.0	TO	1000.0	0
1000.0	TO	1500.0	1
1500.0	TO	2000.0	1
2000.0	TO	3000.0	0
3000.0	TO	5000.0	0
5000.0	TO	10000.0	0
OVER		10000.0	0

TOTAL NUMBER OF HOT SPOT = 292

359 FEATURES WITH AREAS LESS THAN 6.00 SQ. METERS WERE ALSO RECOGNIZED

BY PERIMETER

METERS		FEET		FREQUENCY
0 TO	7	0 TO	22	0
7 TO	10	22 TO	32	0
10 TO	12	32 TO	39	0
12 TO	14	39 TO	45	46
14 TO	16	45 TO	52	31
16 TO	17	52 TO	55	0
17 TO	20	55 TO	65	35
20 TO	22	65 TO	72	23
22 TO	24	72 TO	78	0
24 TO	26	78 TO	85	19
26 TO	28	85 TO	91	24
28 TO	30	91 TO	98	0
30 TO	32	98 TO	104	11
32 TO	39	104 TO	127	25
39 TO	45	127 TO	147	13
45 TO	55	147 TO	180	17
55 TO	71	180 TO	232	17
71 TO	100	232 TO	328	10
OVER	100	OVER	328	21

BY SHAPE

SHAPE FACTOR			FREQUENCY
0.0	TO	1.0	0
1.0	TO	1.1	0
1.1	TO	1.2	10
1.2	TO	1.3	13
1.3	TO	1.4	51
1.4	TO	1.5	25
1.5	TO	1.6	25
1.6	TO	1.7	27
1.7	TO	1.8	12
1.8	TO	1.9	16
1.9	TO	2.0	29
2.0	TO	2.4	43
2.4	TO	2.6	9
2.6	TO	2.8	5
2.8	TO	3.0	9
3.0	TO	3.5	8
3.5	TO	4.0	3
4.0	TO	4.5	2
OVER		4.5	5

3.5 POWER SPECTRA

One dimensional power spectra have been measured for each of the data sets obtained at Nellis AFB that have been analyzed in this report. The power spectra have not been analyzed further and so are included in Appendix 3.

4.0

CONCLUSIONS

Terrain and water backgrounds measurement data in the mid-IR have been collected and analyzed in support of the Navy Optical Signatures Program. This is a continuing program to provide representative backgrounds data for various system performance studies. Calibrated digital data tapes of the backgrounds data are maintained as part of the program. Statistical analyses are performed on the data in order to characterize different background types and to develop statistical parameters useful to the systems designer.

Selected data over desert and mountainous terrain at Nellis AFB, along with data over a rural and urban terrain in West Virginia were analyzed for several specific purposes in this report, namely depression angle, time of day, altitude (5.1 - 5.7 μm band) and terrain type (desert vs mountains and rural vs urban). The results of a number of specific comparisons were summarized in Section 1 and discussed in detail in Section 3. In addition, sunglint data over the water at Pt. Mugu were analyzed in a number of IR spectral bands. As a result of the analyses presented in this report several general conclusions can be drawn.

First, the terrain clutter is significantly smaller in the 5.1 - 5.7 μm band than in the window IR bands at altitudes of 1000 ft, and is smaller at higher altitudes. This is evident in the Nellis data and is most likely true elsewhere.

Second, shadows are an important parameter for the mountains at Nellis. These shadows tend to increase terrain clutter and lower mean temperatures over what would be observed on an otherwise flat terrain such as the desert. Spectral correlations measured over large areas of sunlit and shadowed terrain tend to be high between the various band pairs 3.5 - 3.9, 3.9 - 4.7, and 9.0 - 11.4 μm.

Third, the magnitudes of the sunglint from water for relatively calm seas as were present at Pt. Mugu in several mid-IR spectral bands were measured. The sunglint was very apparent in the 4.5 - 5.5 μm spectral band but not observed in the 9.0 - 11.4 μm band.

Although the effects of depression angle were investigated in this study to some degree, it was not possible to clearly identify effects purely due to changes in depression angle because of the accompanying difference in time between data collections.

Additional data collected at Nellis are available for further investigation of the effects of shadows on the terrain data as a function of flight direction. In addition data are available in the 2.0 - 2.6 and 4.5 - 5.5 μm spectral band. These data will be analyzed and reported in the future.

REFERENCES

1. Beard, J., Braithwaite, J., and Turner, R., Infrared Background Survey and Analysis, ERIM Report No. 118000-1-F, Environmental Research Institute of Michigan, Ann Arbor, June 1976.

2. Beard, J., Maxwell, J. R., and Spellicy, R., Statistical Analysis of Terrain Background Measurements Data, ERIM Report No. 120500-12-F, Environmental Research Institute of Michigan, Ann Arbor, March 1977.

3. Maxwell, J. R., Statistical Analysis of Terrain Backgrounds, Volume 22, Proceedings of IRIS, ERIM Report No. 127200-7-X, Environmental Research Institute of Michigan, Ann Arbor, February 1978, pp. 101-129.

APPENDIX 1

APPENDIX 1

Tables 1.1, 1.2, 1.3, and 1.4 are contained in this appendix which relate apparent temperature to radiance in the 3.5 - 3.9, 3.9 - 4.7, 5.1 - 5.7, and 9.0 - 11.4 μm spectral bands.

TABLE 1.1

RADIANCE FROM 3.5 - 3.9 MICRONS IN MICROWATTS/(cm^2 · sr)

Radiance	Apparent Temperature K
0.21479E+01	259
0.24074E+01	261
0.26937E+01	263
0.30089E+01	265
0.33555E+01	267
0.37360E+01	269
0.41531E+01	271
0.46096E+01	273
0.51087E+01	275
0.56534E+01	277
0.62472E+01	279
0.68935E+01	281
0.75963E+01	283
0.83594E+01	285
0.91869E+01	287
0.10083E+02	289
0.11053E+02	291
0.12101E+02	293
0.13232E+02	295
0.14452E+02	297
0.15765E+02	299
0.17178E+02	301
0.18697E+02	303
0.20327E+02	305
0.22076E+02	307
0.23950E+02	309
0.25955E+02	311
0.28100E+02	313
0.30392E+02	315
0.32838E+02	317
0.35448E+02	319
0.38228E+02	321
0.41187E+02	323
0.44336E+02	325
0.47682E+02	327
0.51236E+02	329
0.55007E+02	331

AD-A060 153 ENVIRONMENTAL RESEARCH INST OF MICHIGAN ANN ARBOR IN--ETC F/G 17/5
STATISTICAL ANALYSES OF SELECTED TERRAIN AND WATER BACKGROUND M--ETC(U)
JUL 78 J R MAXWELL N00123-77-C-0682
UNCLASSIFIED ERIM-132300-1-F NL

2 OF 2
ADA
060153

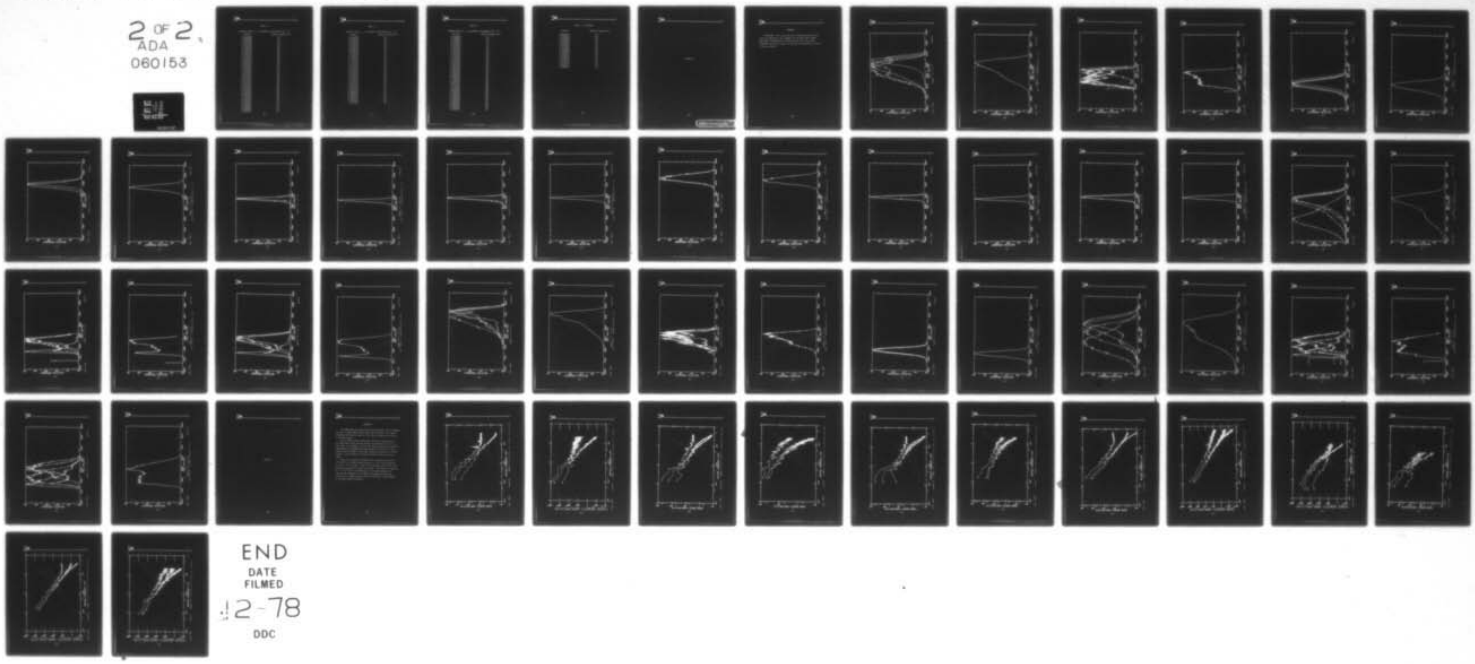

END
DATE
FILMED
12-78
DDC

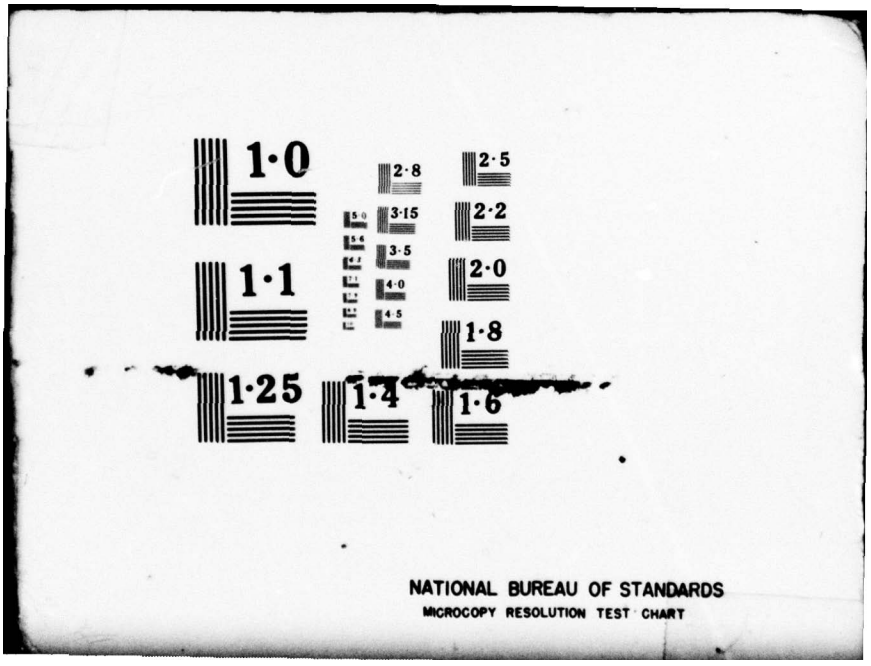
1·0
1·1
1·25
2·8
3·15
3·5
4·0
4·5
1·4
2·5
2·2
2·0
1·8
1·6
NATIONAL BUREAU OF STANDARDS
MICROCOPY RESOLUTION TEST CHART

TABLE 1.2

RADIANCE FROM 3.9 - 4.7 MICRONS IN MICROWATTS/(cm^2 · sr)

Radiance	Apparent Temperature K
0.35222E+02	275
0.36783E+02	276
0.38400E+02	277
0.40077E+02	278
0.41813E+02	279
0.43613E+02	280
0.45476E+02	281
0.47405E+02	282
0.49401E+02	283
0.51467E+02	284
0.53604E+02	285
0.55815E+02	286
0.58100E+02	287
0.60462E+02	288
0.62903E+02	289
0.65425E+02	290
0.68030E+02	291
0.70721E+02	292
0.73498E+02	293
0.76365E+02	294
0.79323E+02	295
0.82375E+02	296
0.85523E+02	297
0.88770E+02	298
0.92117E+02	299
0.95567E+02	300
0.99122E+02	301
0.10279E+03	302
0.10656E+03	303
0.11044E+03	304
0.11445E+03	305
0.11856E+03	306
0.12280E+03	307
0.12717E+03	308
0.13165E+03	309
0.13627E+03	310
0.14102E+03	311
0.14590E+03	312
0.15092E+03	313
0.15608E+03	314
0.16138E+03	315
0.16682E+03	316

TABLE 1.3

RADIANCE FROM 5.1 - 5.7 MICRONS IN MICROWATTS/(cm^2 · sr)

Radiance	Apparent Temperature K
0.53339E+02	259
0.57695E+02	261
0.62332E+02	263
0.67263E+02	265
0.72503E+02	267
0.78064E+02	269
0.83960E+02	271
0.90206E+02	273
0.96816E+02	275
0.10380E+03	277
0.11119E+03	279
0.11898E+03	281
0.12720E+03	283
0.13585E+03	285
0.14497E+03	287
0.15456E+03	289
0.16463E+03	291
0.17522E+03	293
0.18632E+03	295
0.19797E+03	297
0.21018E+03	299
0.22296E+03	301
0.23634E+03	303
0.25033E+03	305
0.26495E+03	307
0.28022E+03	309
0.29616E+03	311
0.31278E+03	313
0.33011E+03	315
0.34817E+03	317
0.36696E+03	319
0.38652E+03	321
0.40687E+03	323
0.42801E+03	325
0.44997E+03	327
0.47278E+03	329
0.49645E+03	331

TABLE 1.4

RADIANCE FROM 9.0 - 11.4 MICRONS IN MICROWATTS/(cm^2 · sr)

Radiance	Apparent Temperature K
0.14113E+04	271
0.14388E+04	272
0.14667E+04	273
0.14949E+04	274
0.15234E+04	275
0.15522E+04	276
0.15815E+04	277
0.16110E+04	278
0.16409E+04	279
0.16711E+04	280
0.17017E+04	281
0.17326E+04	282
0.17638E+04	283
0.17954E+04	284
0.18273E+04	285
0.18596E+04	286
0.18922E+04	287
0.19252E+04	288
0.19585E+04	289
0.19922E+04	290
0.20262E+04	291
0.20606E+04	292
0.20953E+04	293
0.21304E+04	294
0.21658E+04	295
0.22016E+04	296
0.22377E+04	297
0.22742E+04	298
0.23110E+04	299
0.23482E+04	300
0.23857E+04	301
0.24236E+04	302
0.24618E+04	303
0.25004E+04	304
0.25393E+04	305
0.25786E+04	306
0.26183E+04	307
0.26583E+04	308
0.26987E+04	309
0.27394E+04	310
0.27804E+04	311

TABLE 1.4 (CONTINUED)

Radiance	Apparent Temperature K
0.28219E+04	312
0.28637E+04	313
0.29058E+04	314
0.29483E+04	315
0.29912E+04	316
0.30344E+04	317
0.30779E+04	318
0.31219E+04	319
0.31661E+04	320
0.32108E+04	321
0.32558E+04	322
0.33011E+04	323
0.33468E+04	324
0.33929E+04	325
0.34393E+04	326
0.34861E+04	327
0.35332E+04	328
0.35807E+04	329
0.36286E+04	330

APPENDIX 2

APPENDIX 2

Histograms of the total area and of subareas within the total area are presented in this appendix for the NEVB, NEVC1, NEVC2, NEVD, NEVE, and NEVF data for each spectral band. The flight parameters and terrain types for each area are identified in Table 1 in the main report.

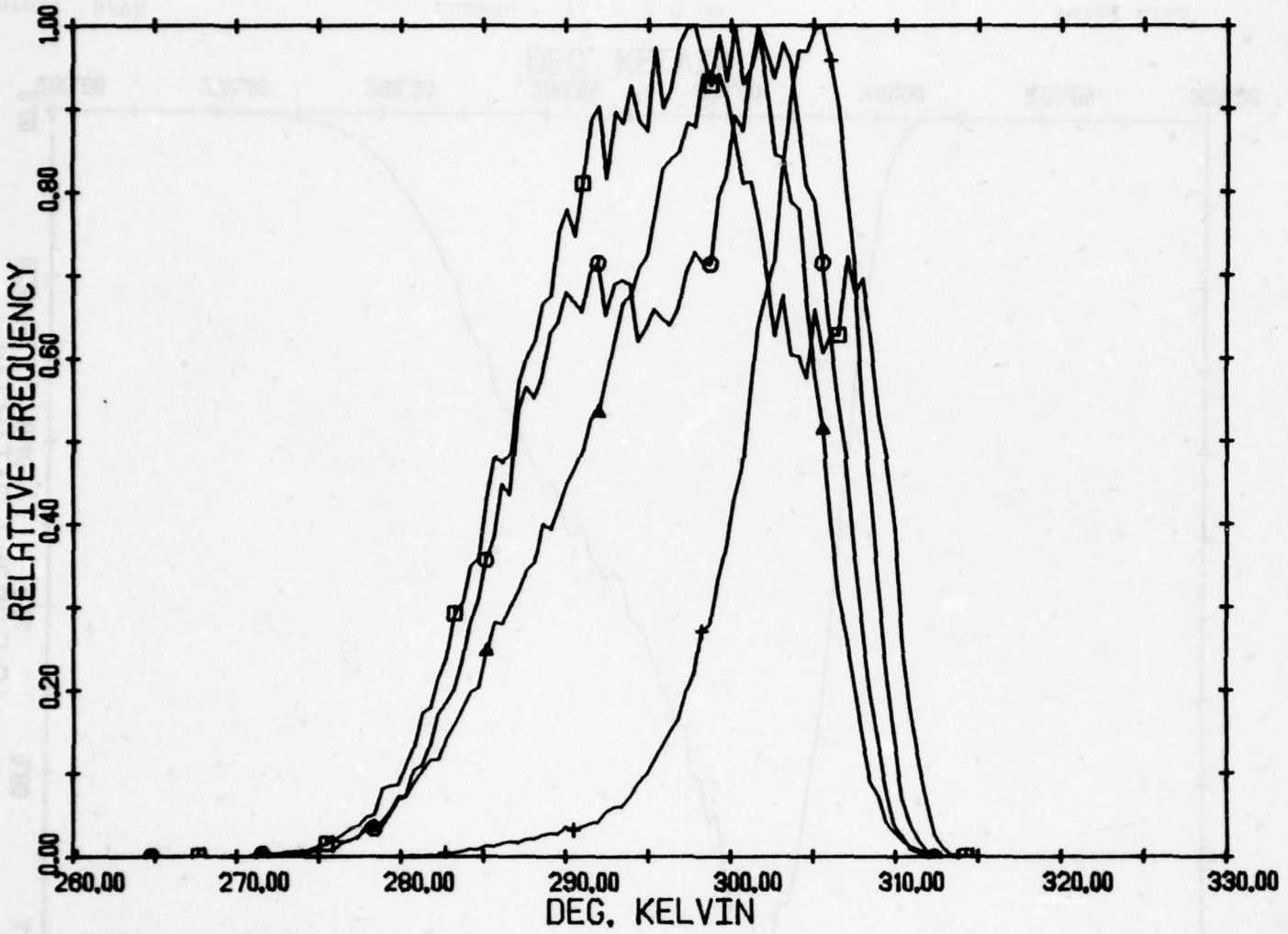

Area: NEVB

Lambda = 3.5 - 3.9 μm

Subareas

ERIM

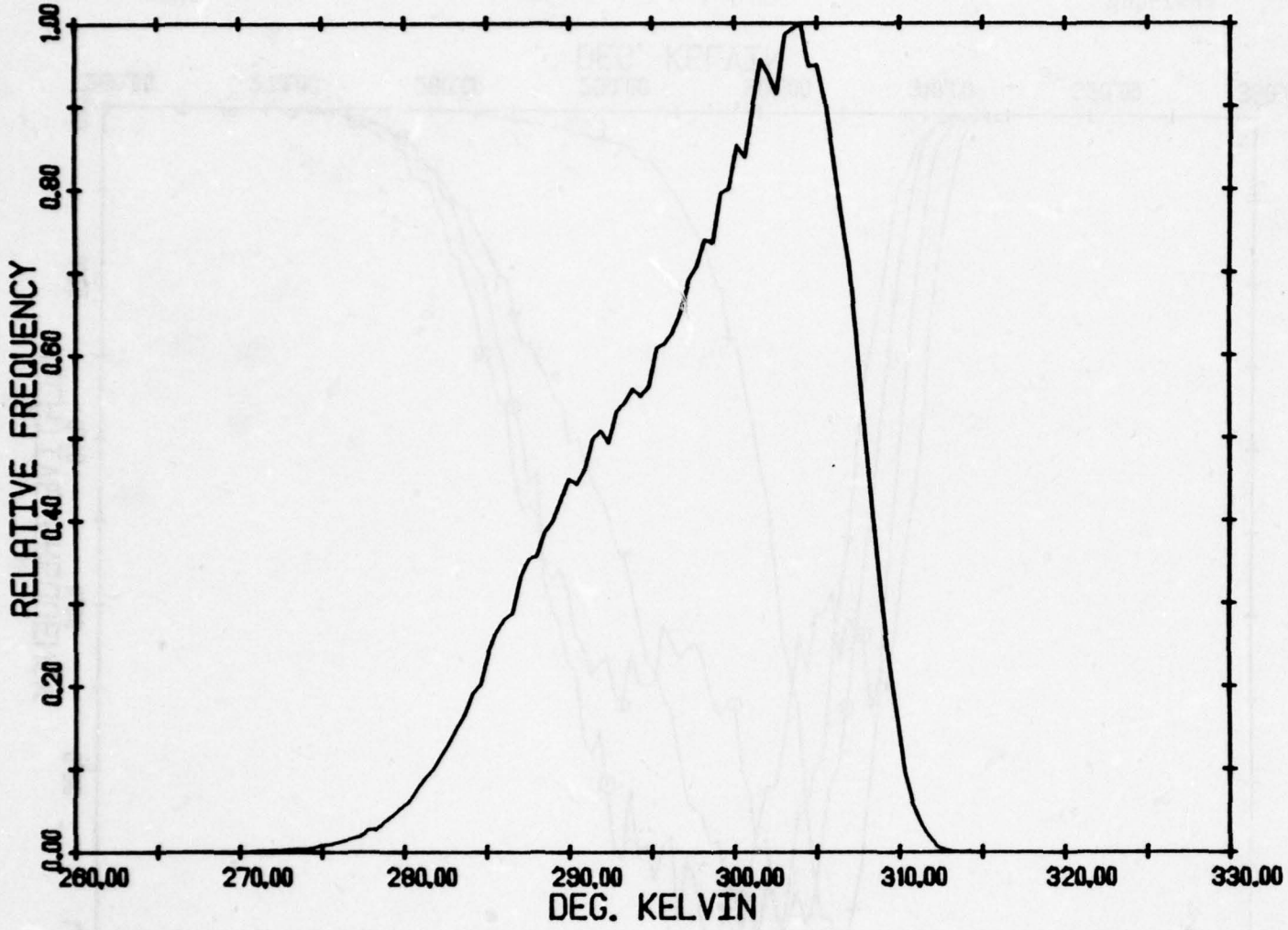

Area: NEVB Lambda = 3.5 - 3.9 μm Total Area

Mean = 298.19 Standard Deviation = 7.17

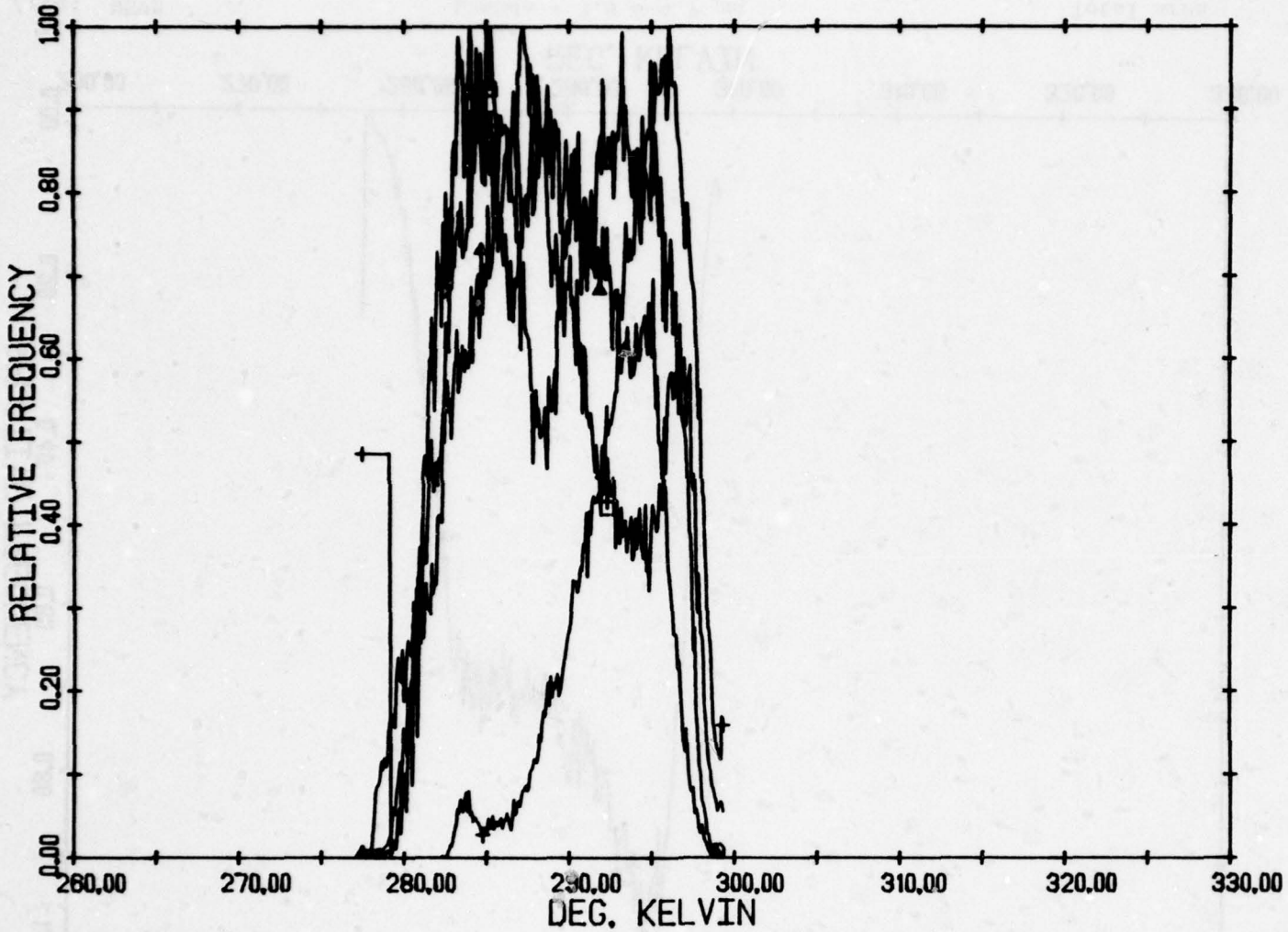

Area: NEVB

Lambda = 3.9 - 4.7 μm

Subareas

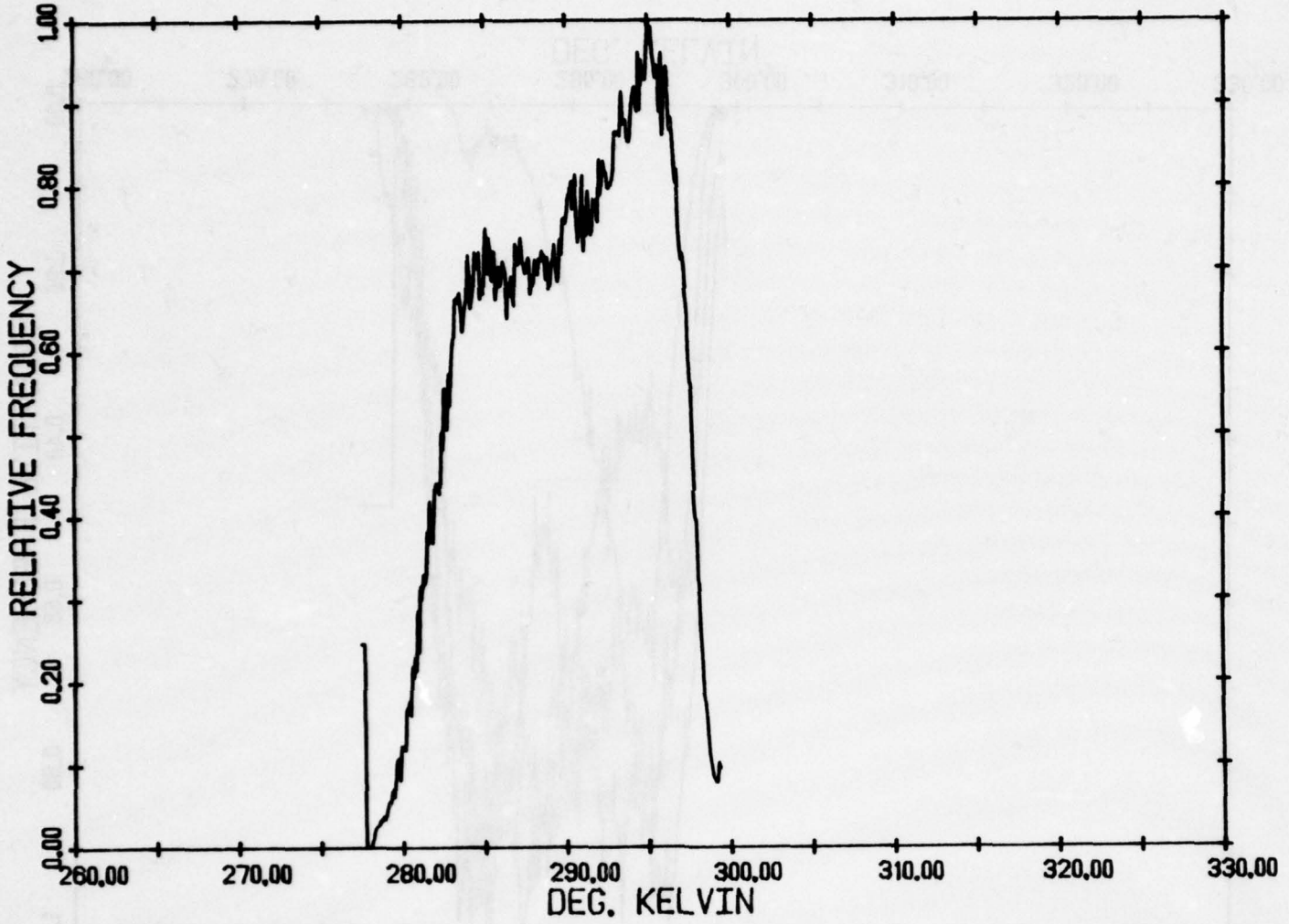

Area: NEVB Lambda = 3.9 - 4.7 μm Total Area

Mean = 290.05 Standard Deviation = 4.94

ERIM

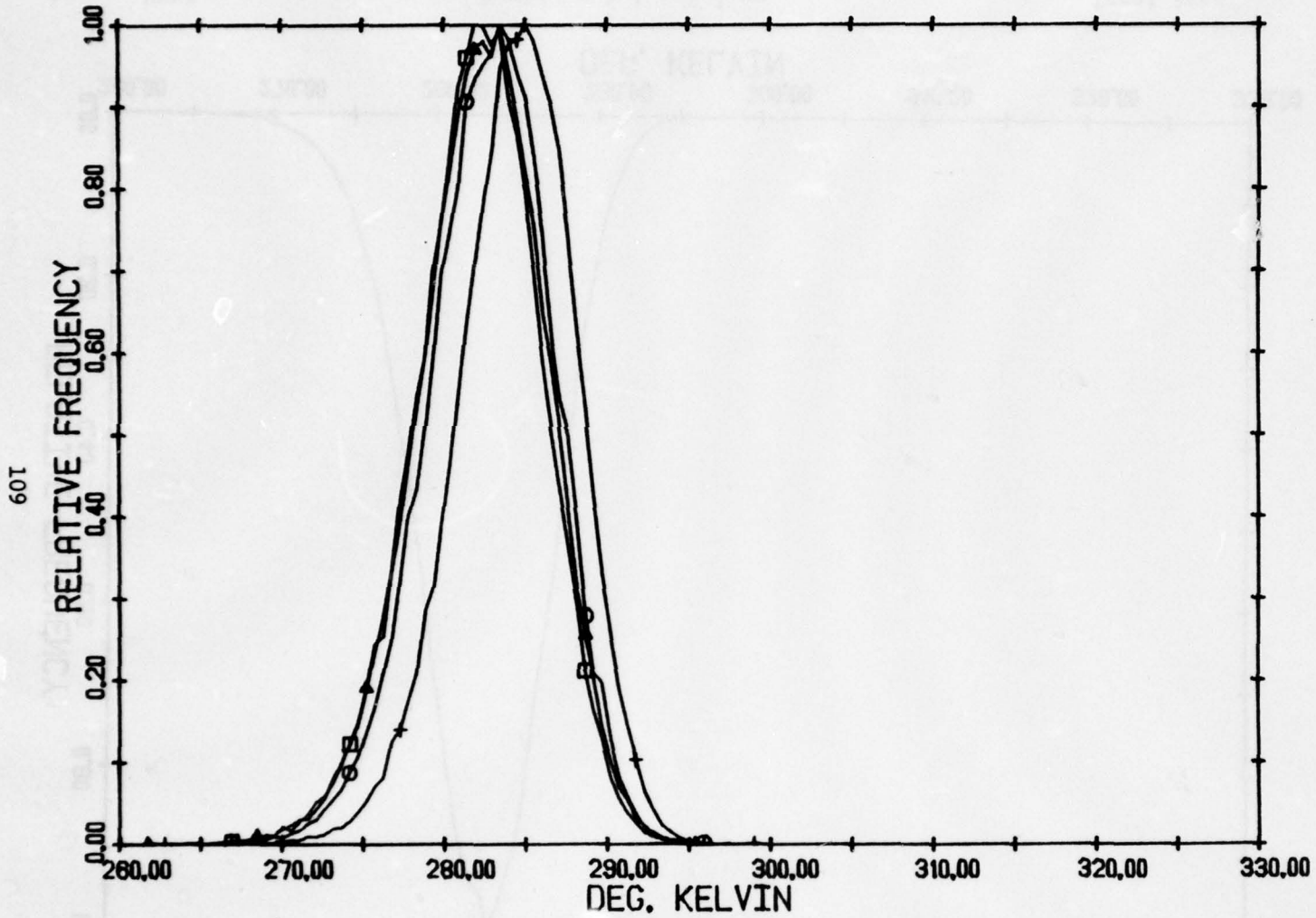

Area: NEVB

Lambda = 5.1 - 5.7 μm

Subareas

ERIM

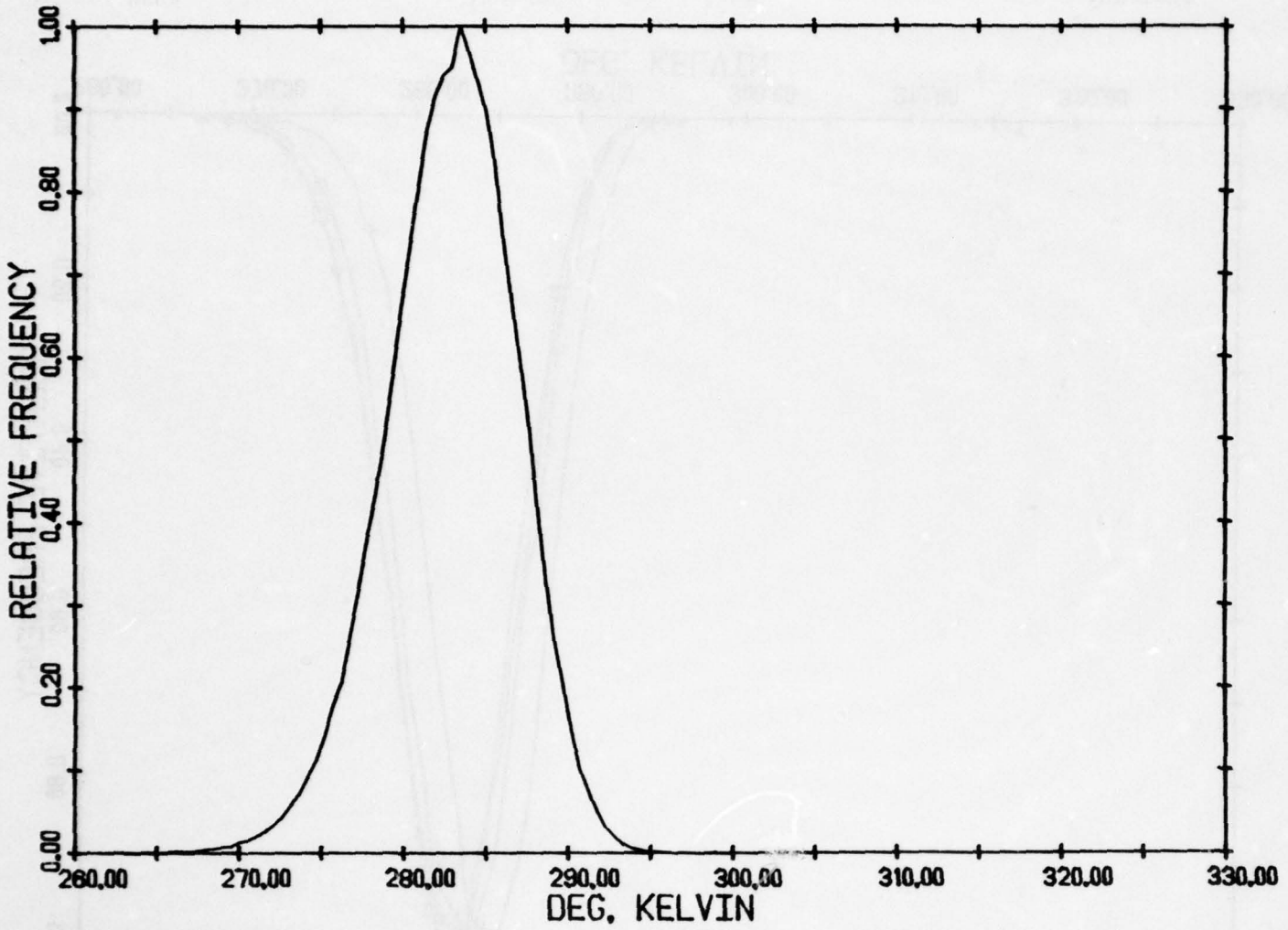

Area: NEVB Lambda = 5.1 - 5.7 μm Total Area

Mean = 282.88 Standard Deviation = 3.90

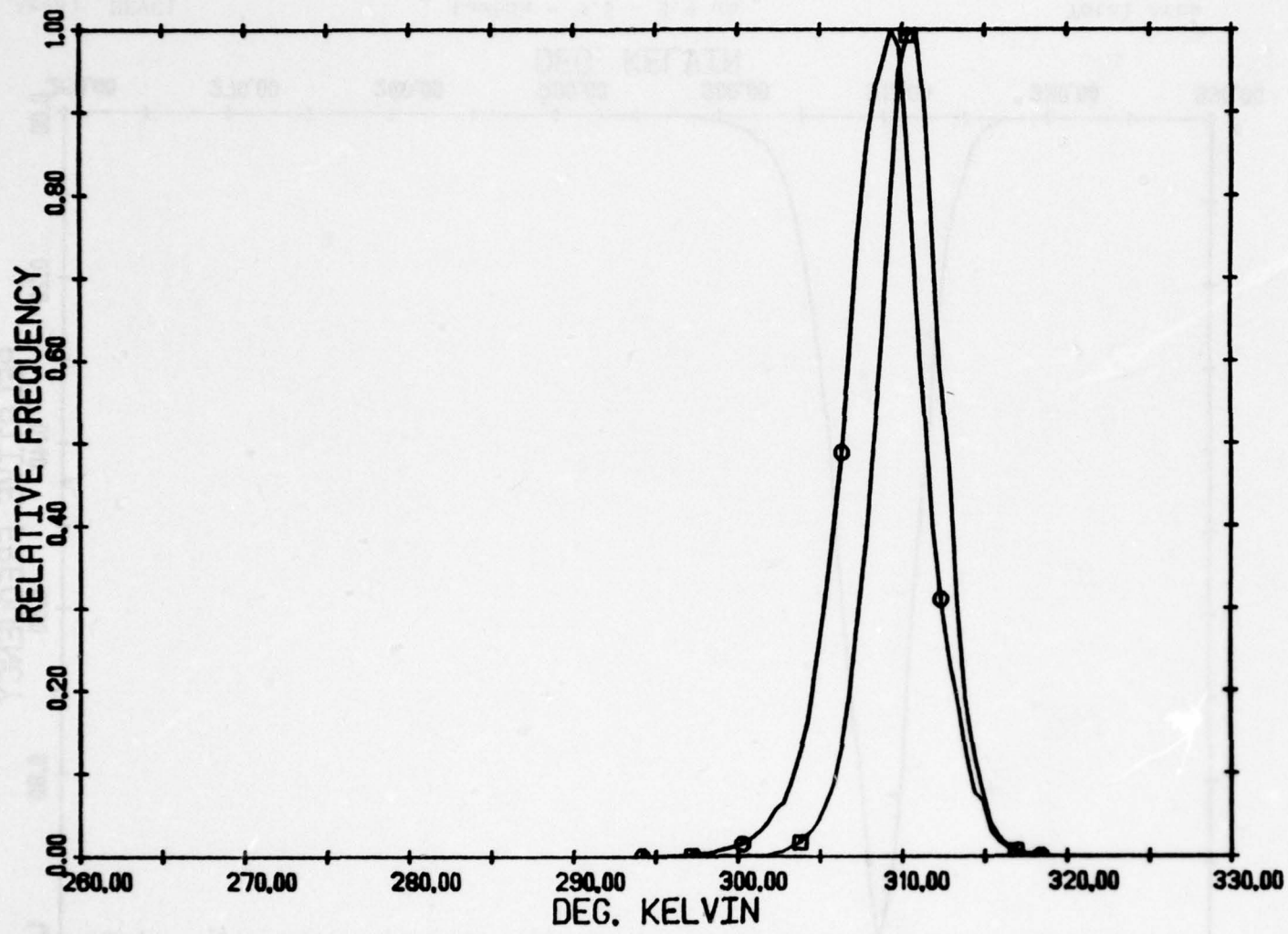

Area: NEVC1 Lambda = 3.5 - 3.9 μm Subareas

ERIM

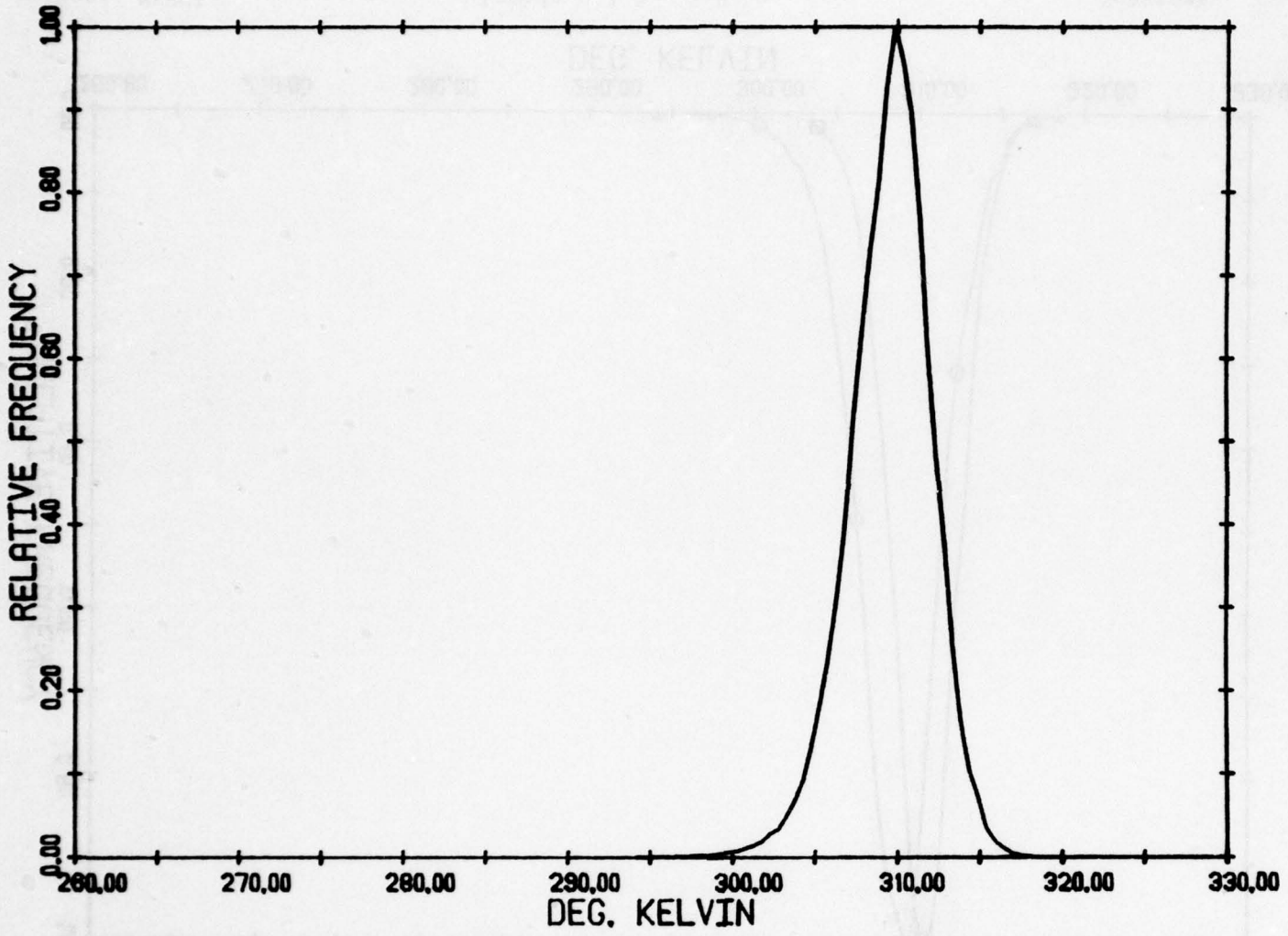

Area: NEVC1 Lambda = 3.5 - 3.9 μm Total Area

Mean = 309.56 Standard Deviation = 2.49

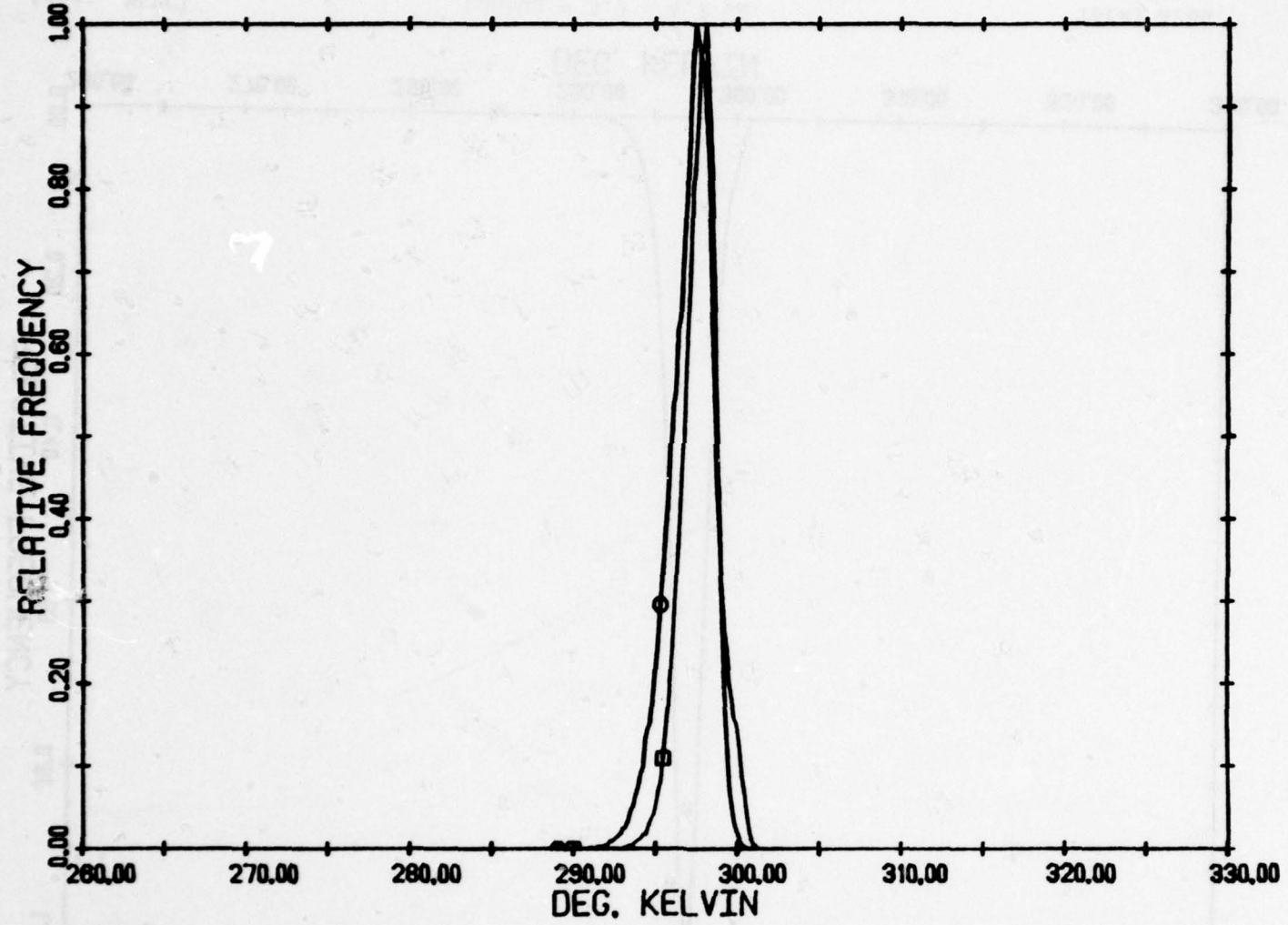

Area: NEVC1

Lambda = 3.9 - 4.7 μm

Subareas

ERIM

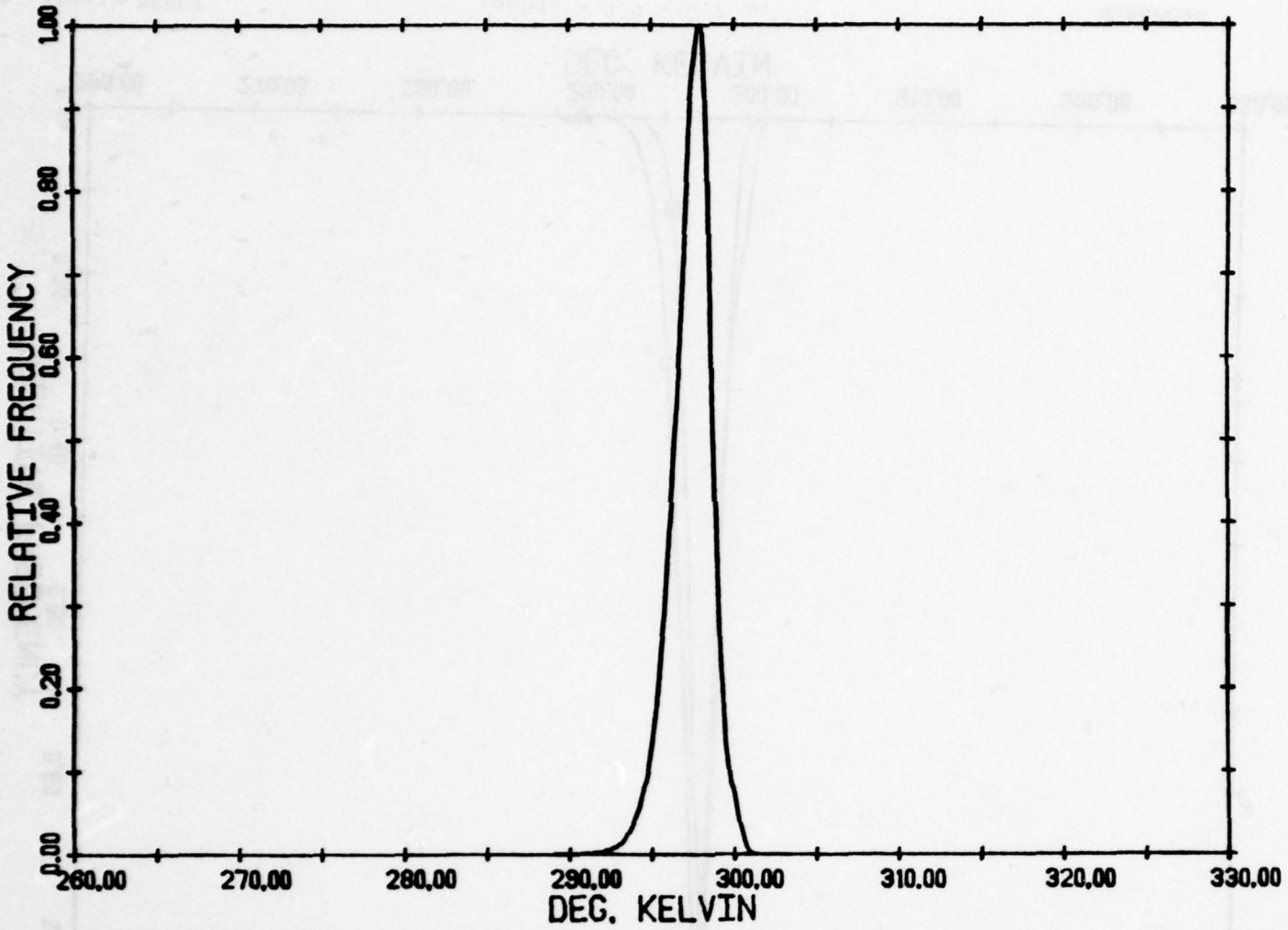

Area: NEVC1 Lambda = 3.9 - 4.7 μm Total Area

Mean = 297.41 Standard Deviation = 1.24

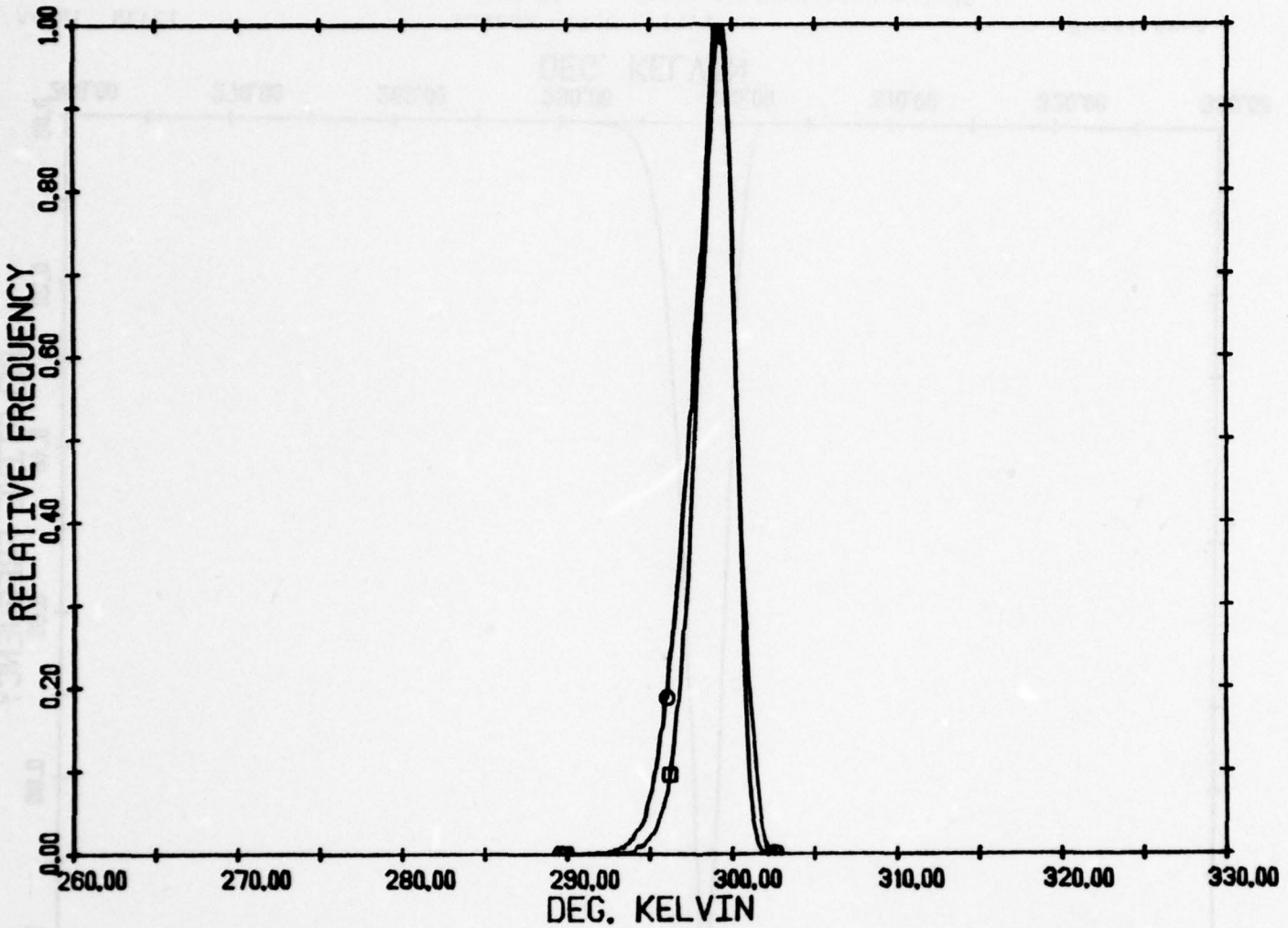

Area: NEVC1 Lambda = 9.0 - 11.4 μm Subareas

ERIM

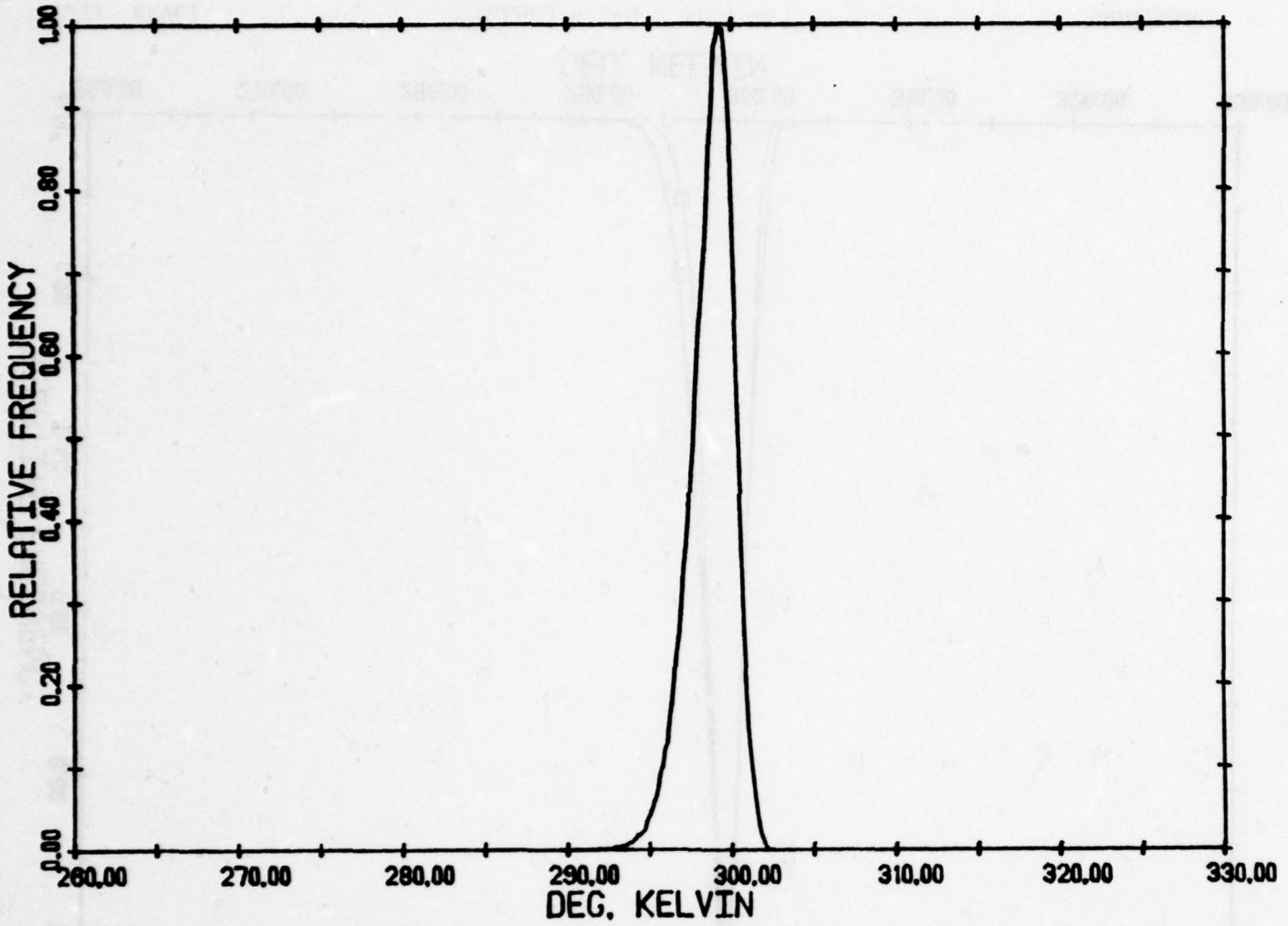

Area: NEVC1 Lambda = 9.0 - 11.4 μm Total Area

Mean = 298.75 Standard Deviation = 1.35

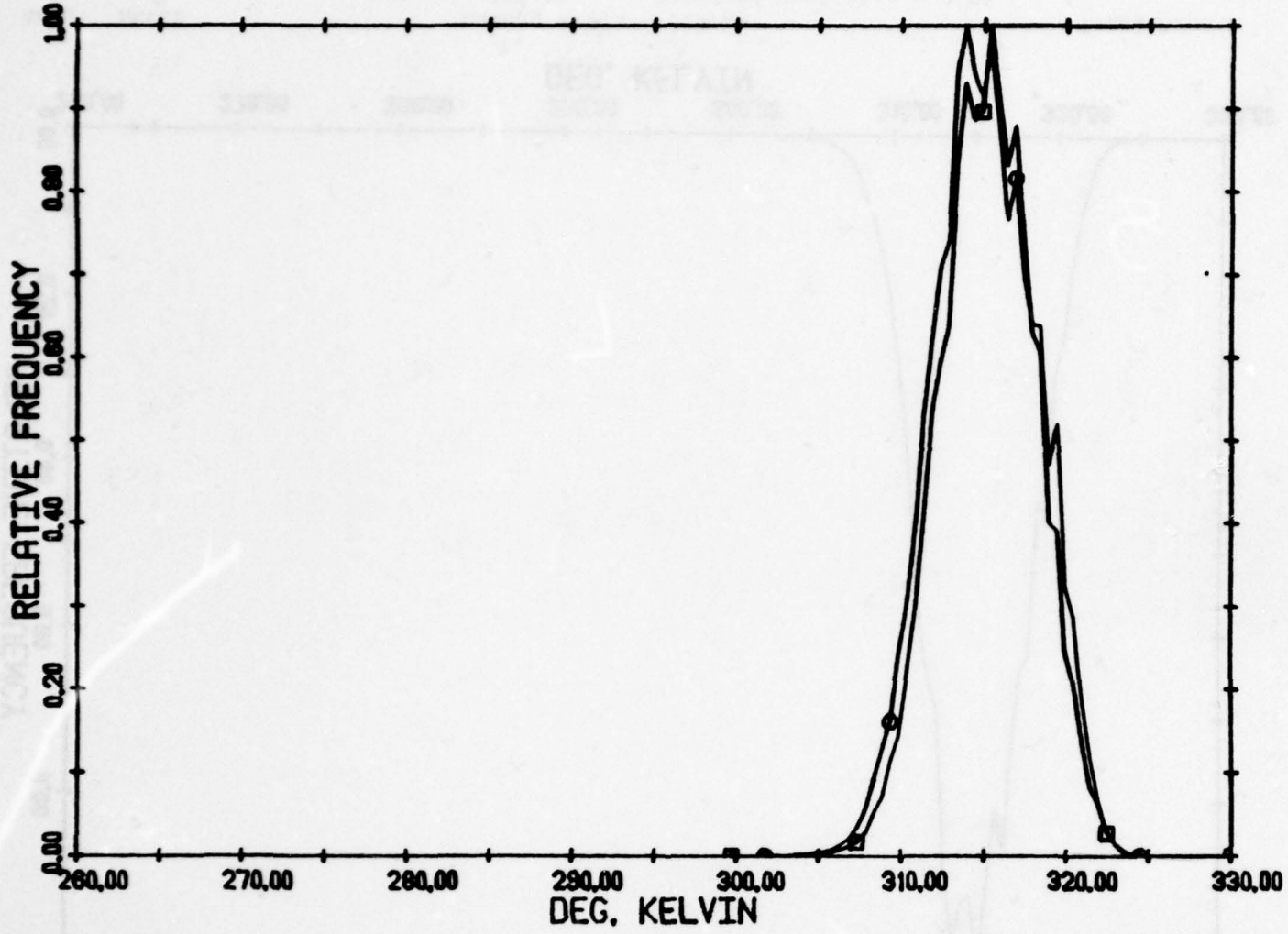

Area: NEVC2 Lambda = 3.5 - 3.9 μm Subareas

ERIM

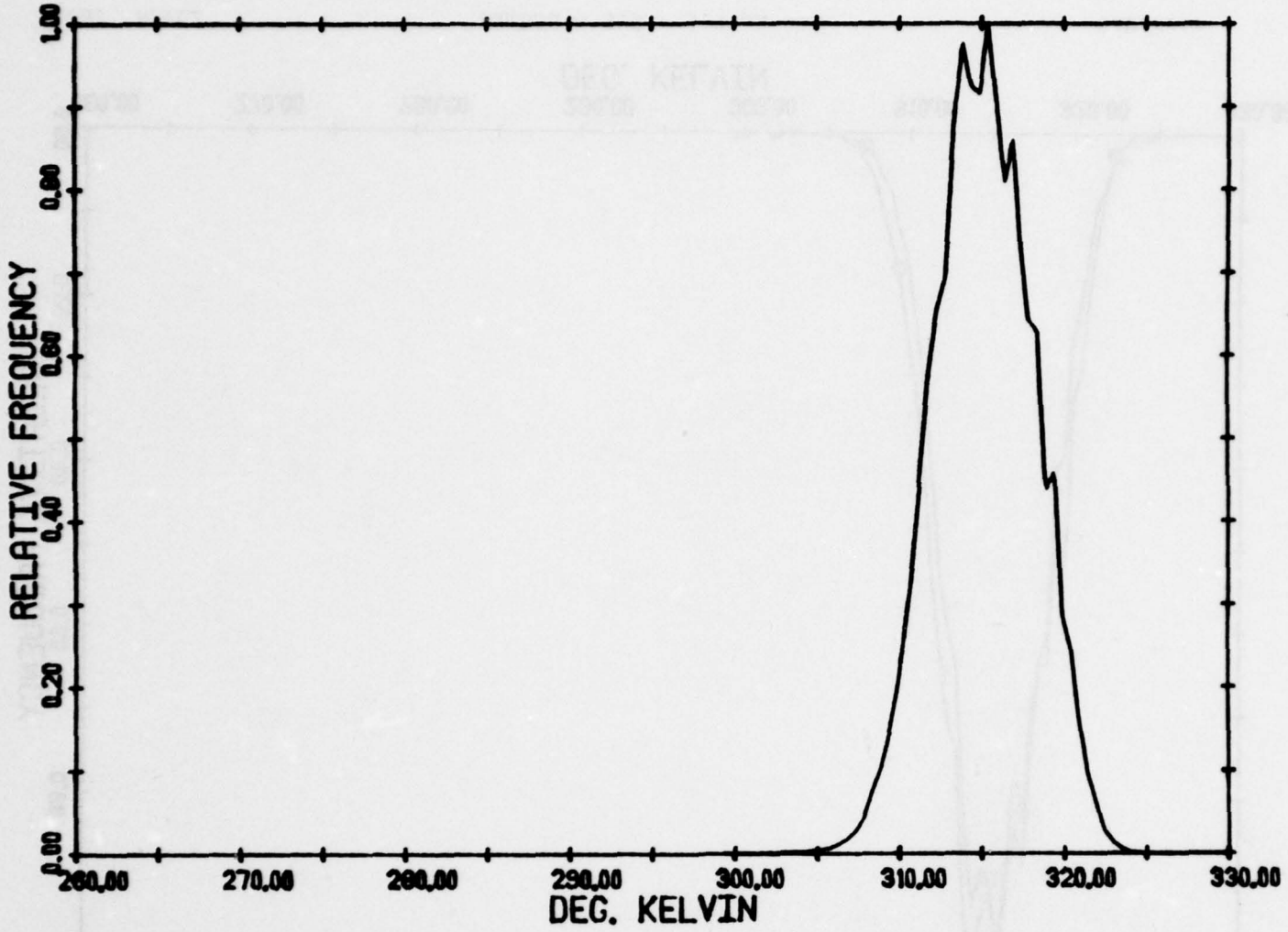

Area: NEVC2 Lambda = 3.5 - 3.9 μm Total Area

Mean = 315.14 Standard Deviation = 2.95

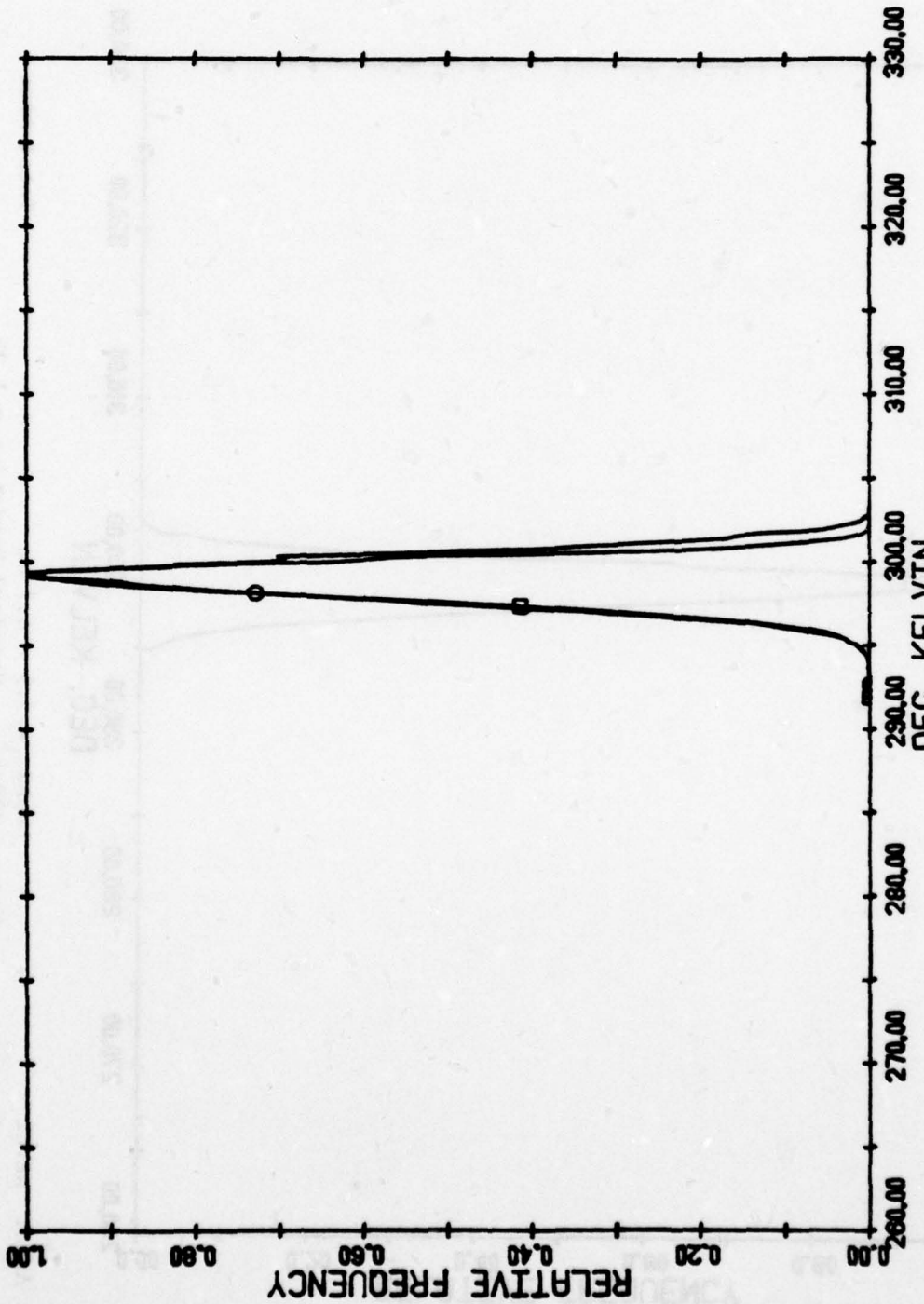

Area: NEVC2 Lambda = 3.9 - 4.7 μm Subareas

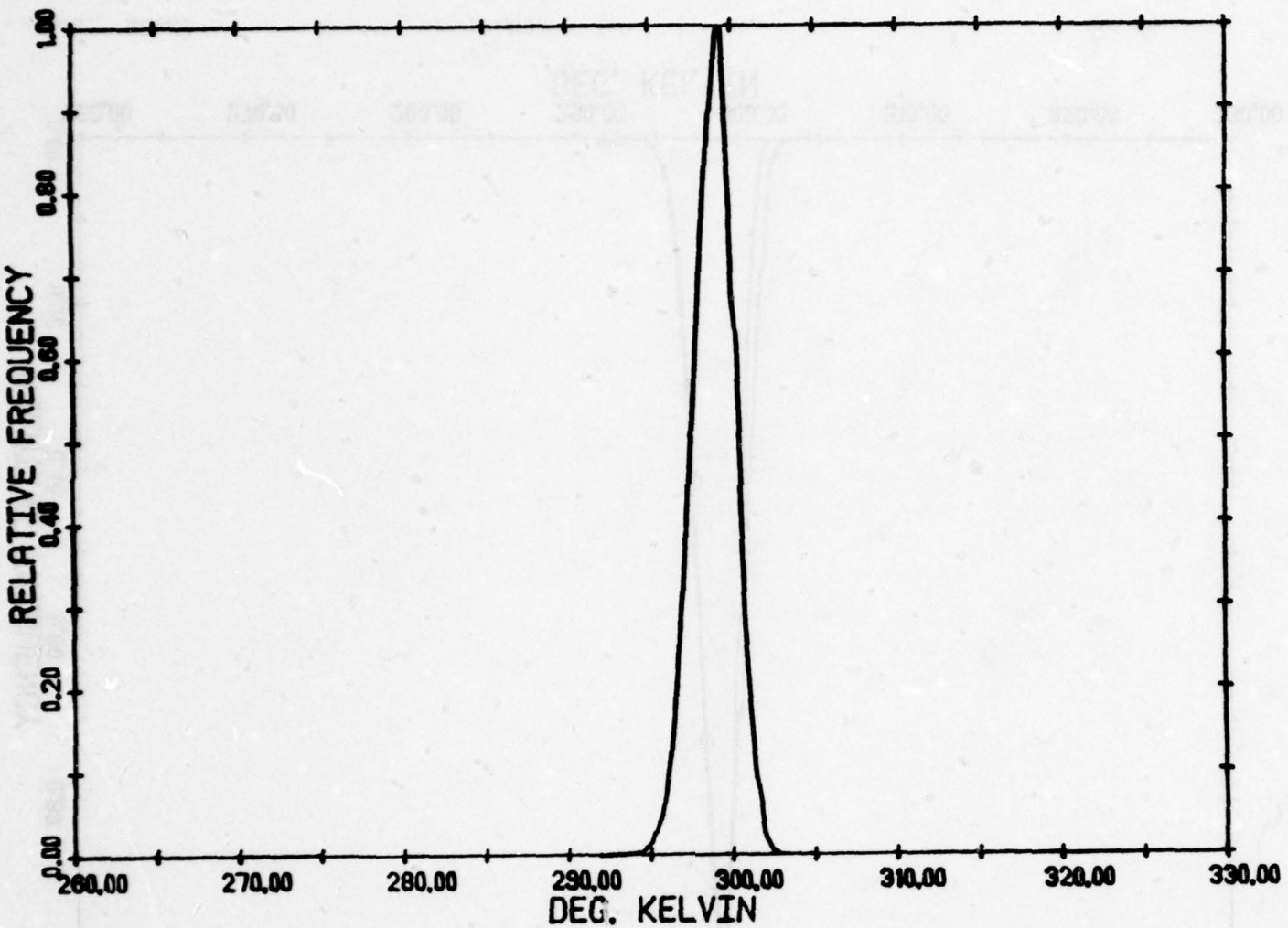

Area: NEVC2 Lambda = 3.9 - 4.7 μm Total Area

Mean = 298.85 Standard Deviation = 1.25

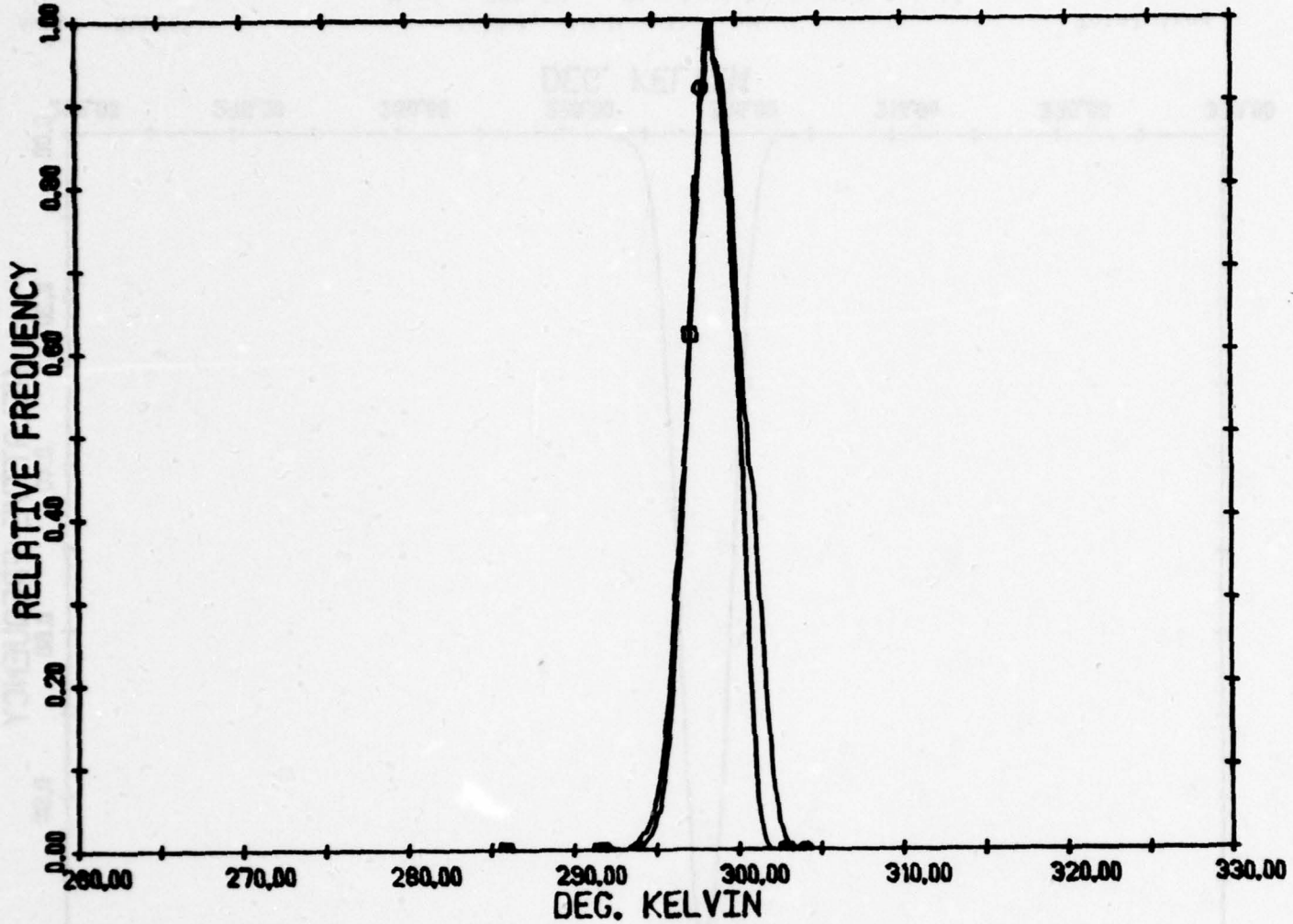

Area: NEVC2 Lambda = 9.0 - 11.4 μm Subareas

ERIM

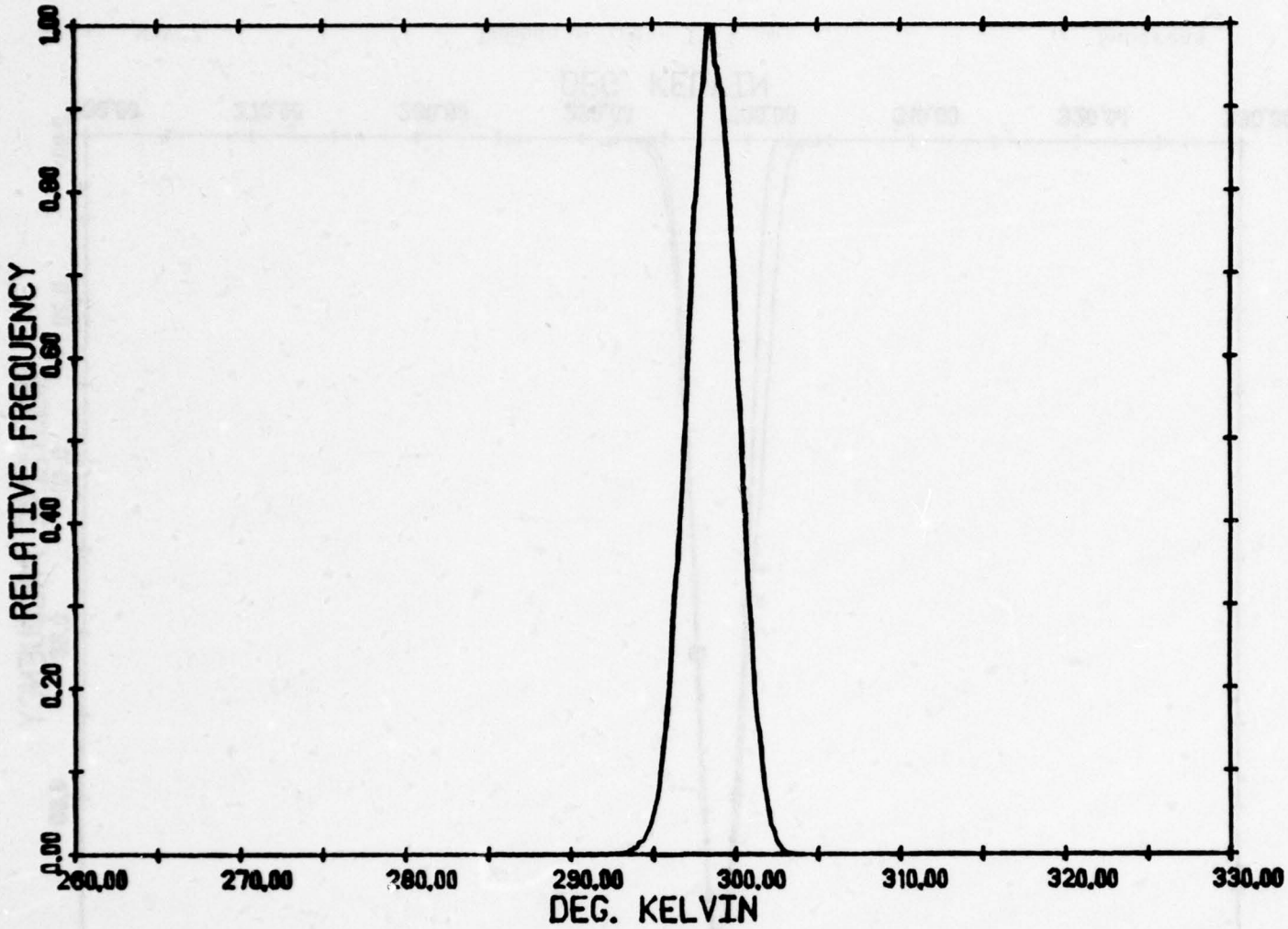

Area: NEVC2 Lambda = 9.0 - 11.4 μm Total Area

Mean = 298.58 Standard Deviation = 1.45

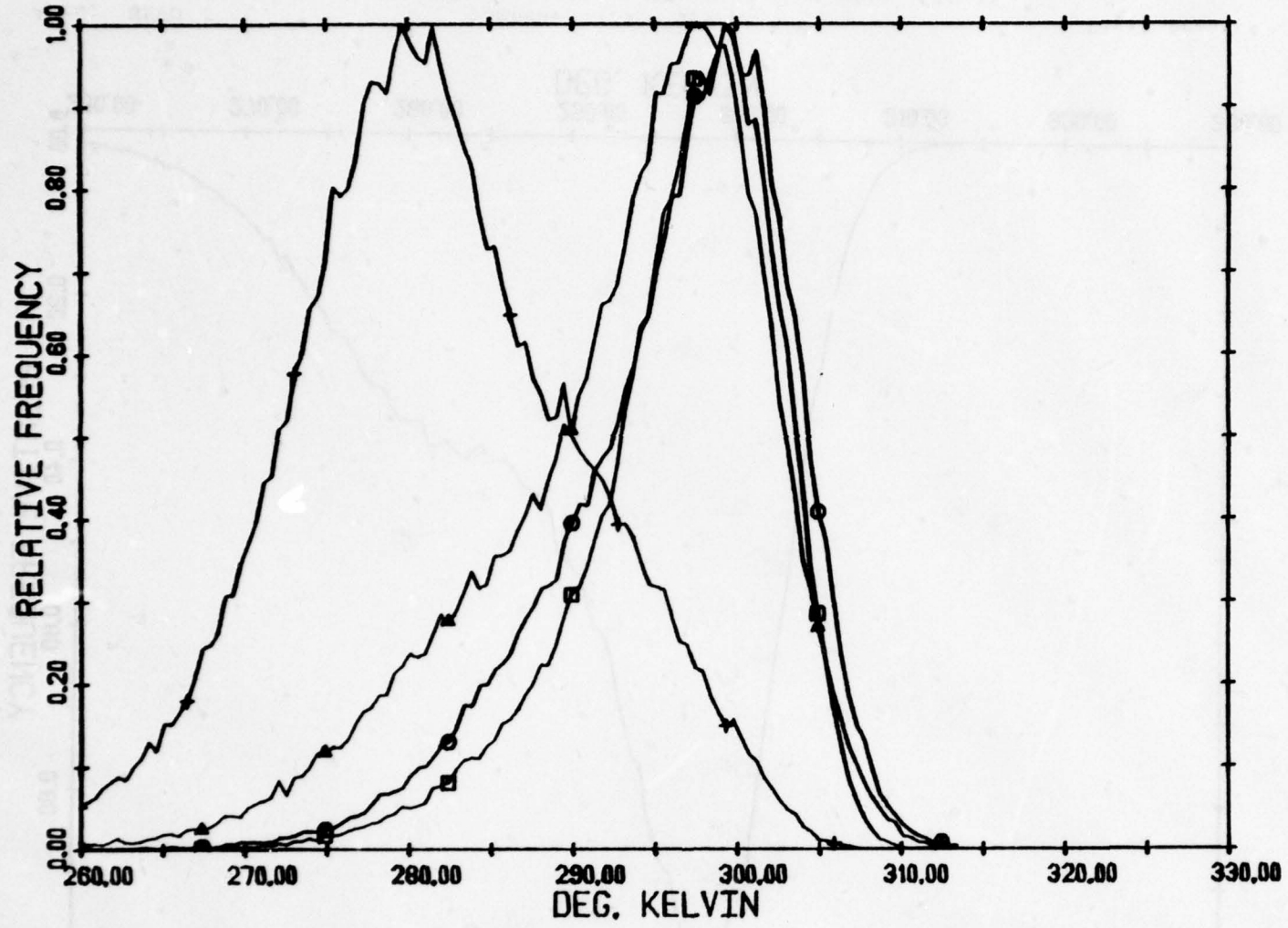

Area: NEVD Lambda = 3.5 - 3.9 μm Subareas

ERIM

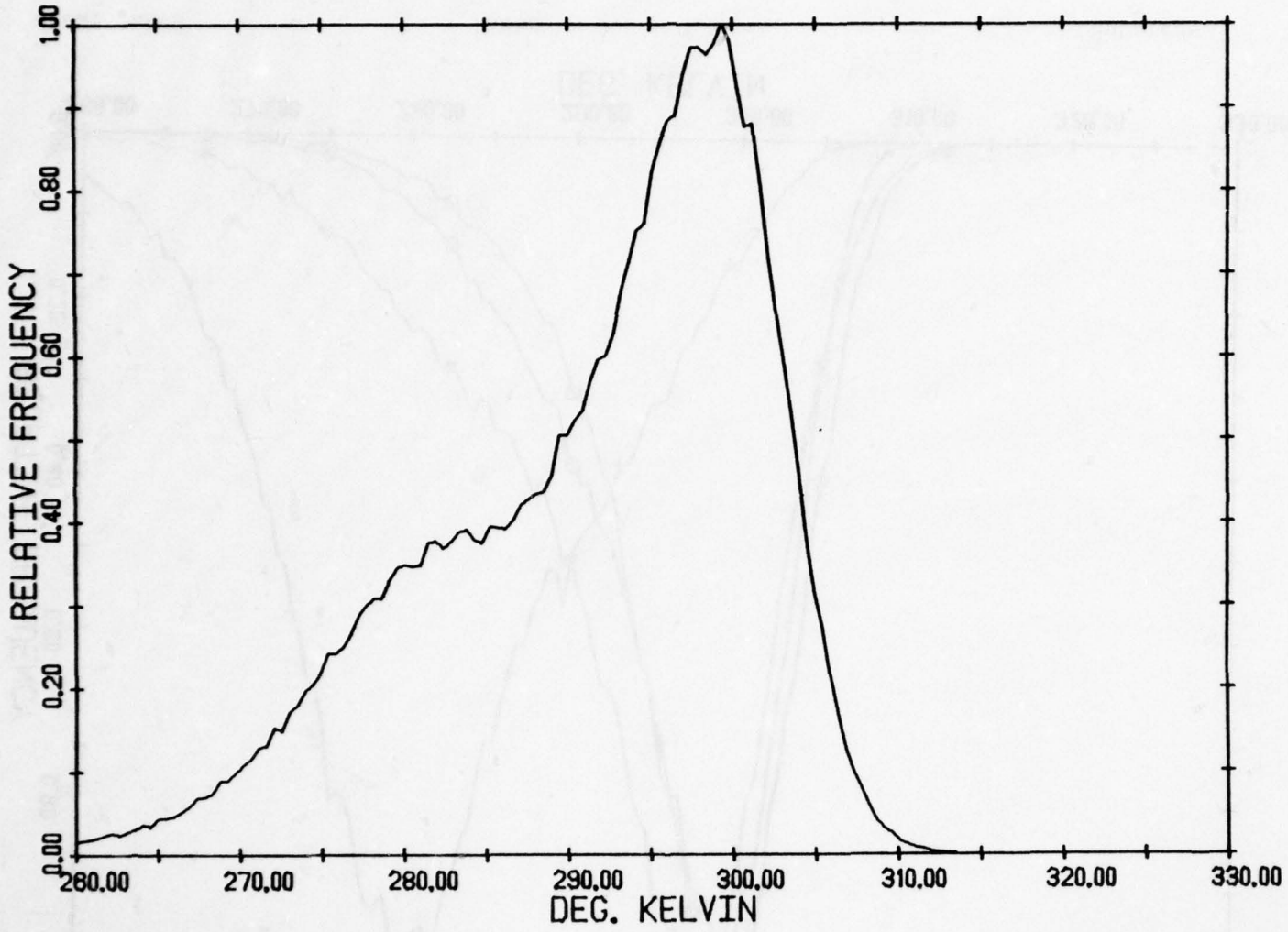

Area: NEVD Lambda = 3.5 - 3.9 μm Total Area

Mean = 291.58 Standard Deviation = 10.15

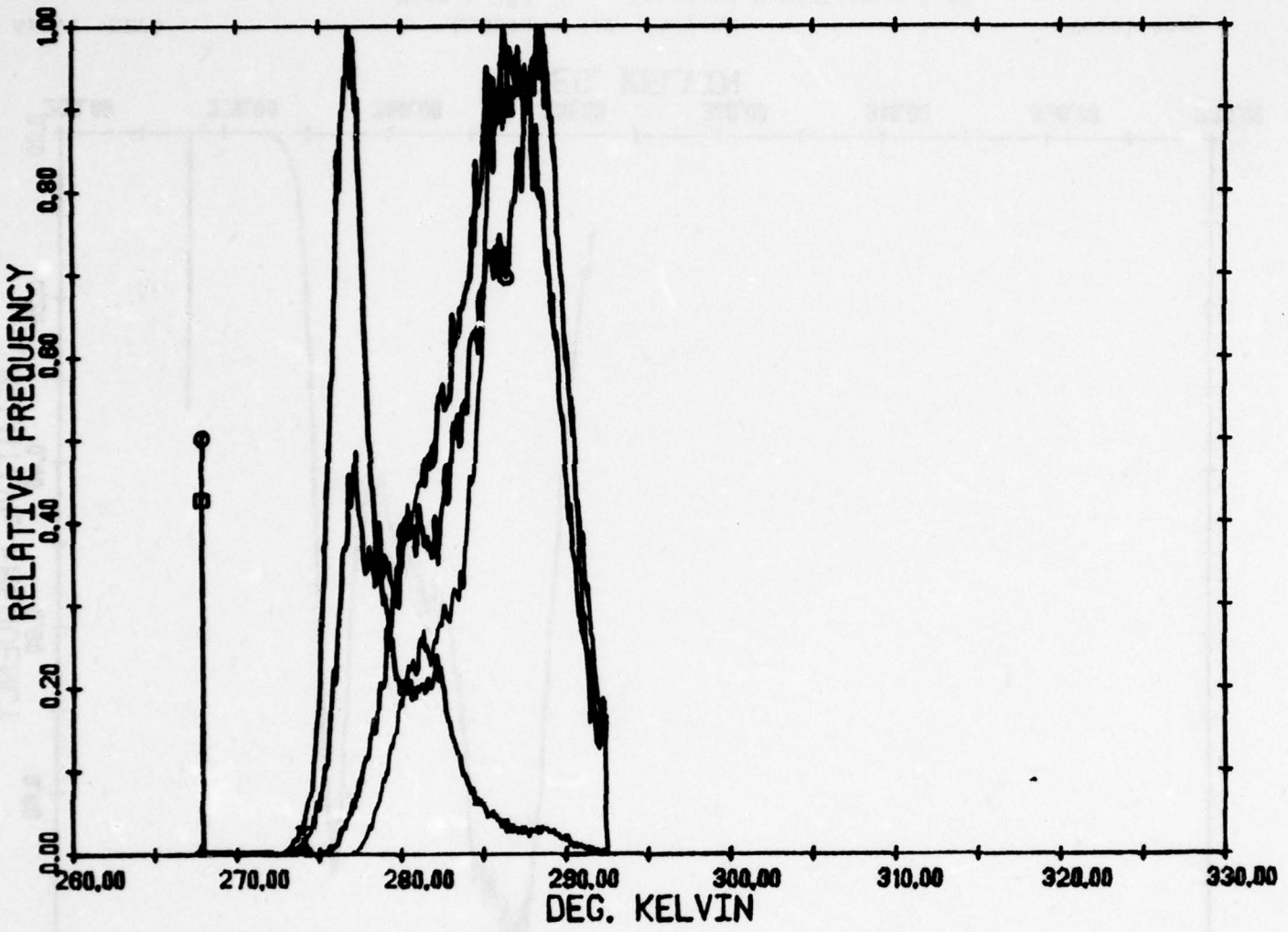

Area: NEVD Lambda = 3.9 - 4.7 μm Subareas

ERIM

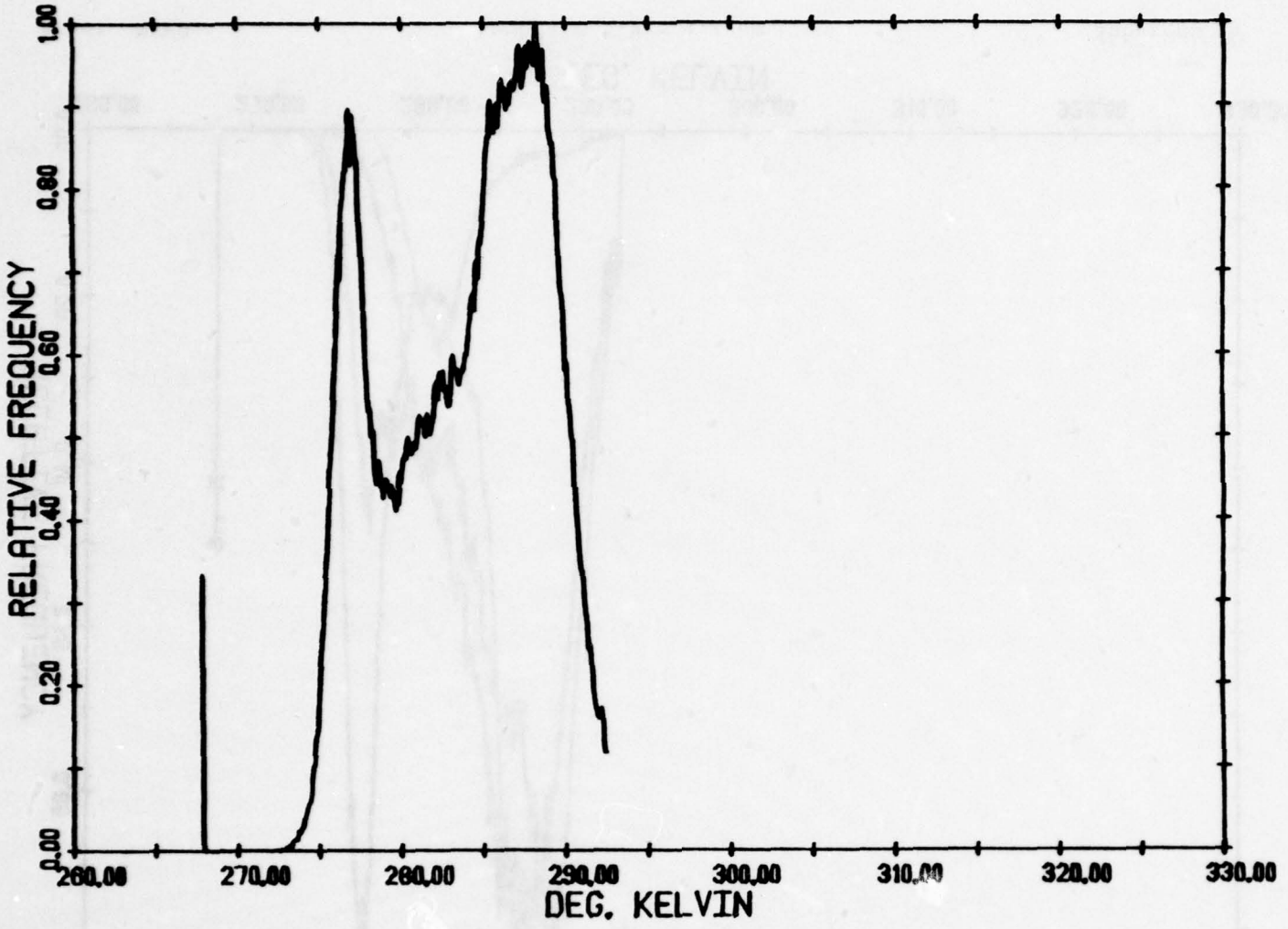

Area: NEVD Lambda = 3.9 - 4.7 μm Total Area

Mean = 283.70 Standard Deviation = 4.80

ERIM

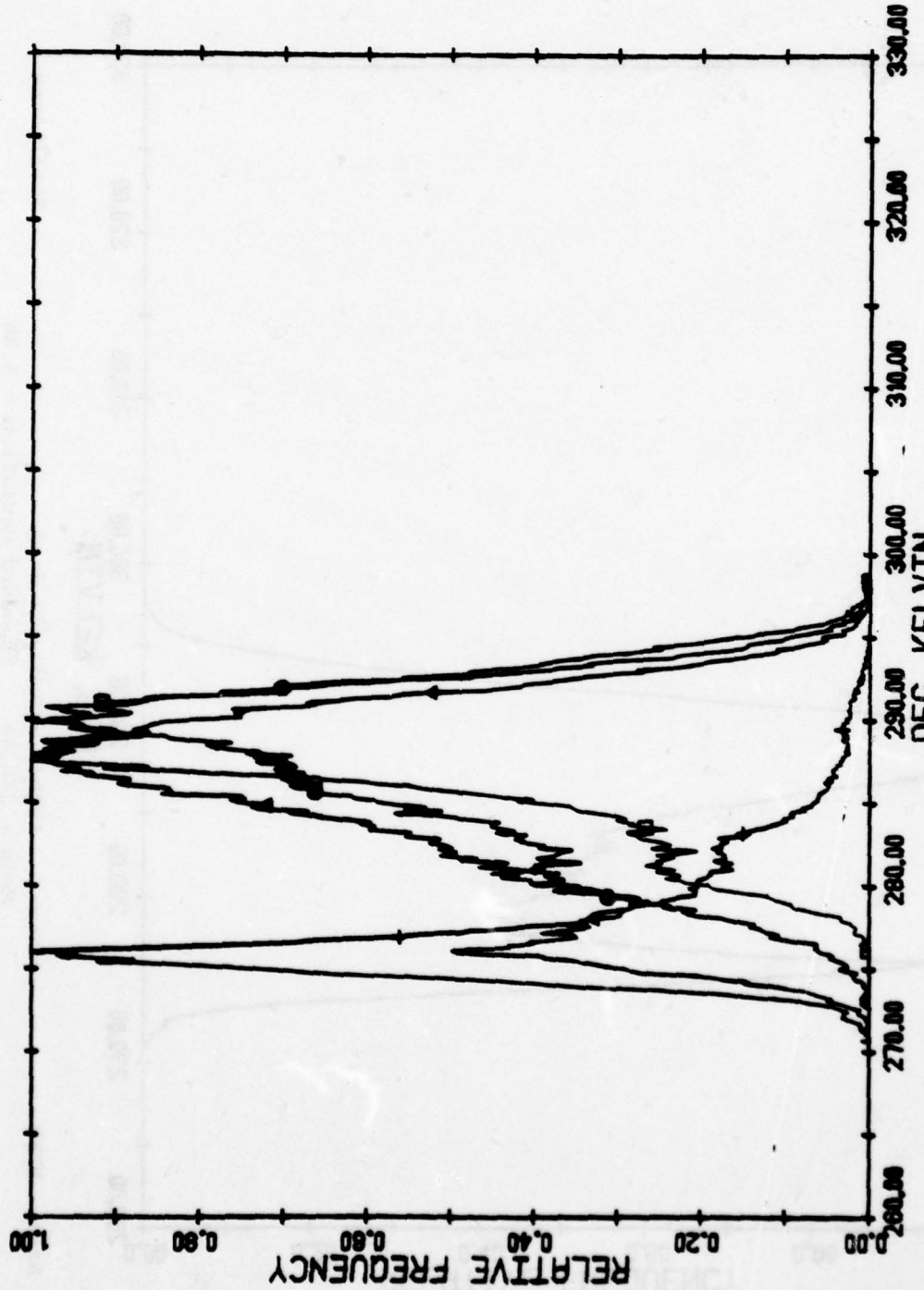
RELATIVE FREQUENCY
0.00
0.20
0.40
0.60
0.80
1.00
260.00
270.00
280.00
290.00
300.00
310.00
320.00
330.00
DEG. KELVIN
Area: NEVD
Lambda = 9.0 - 11.4 µm
Subareas

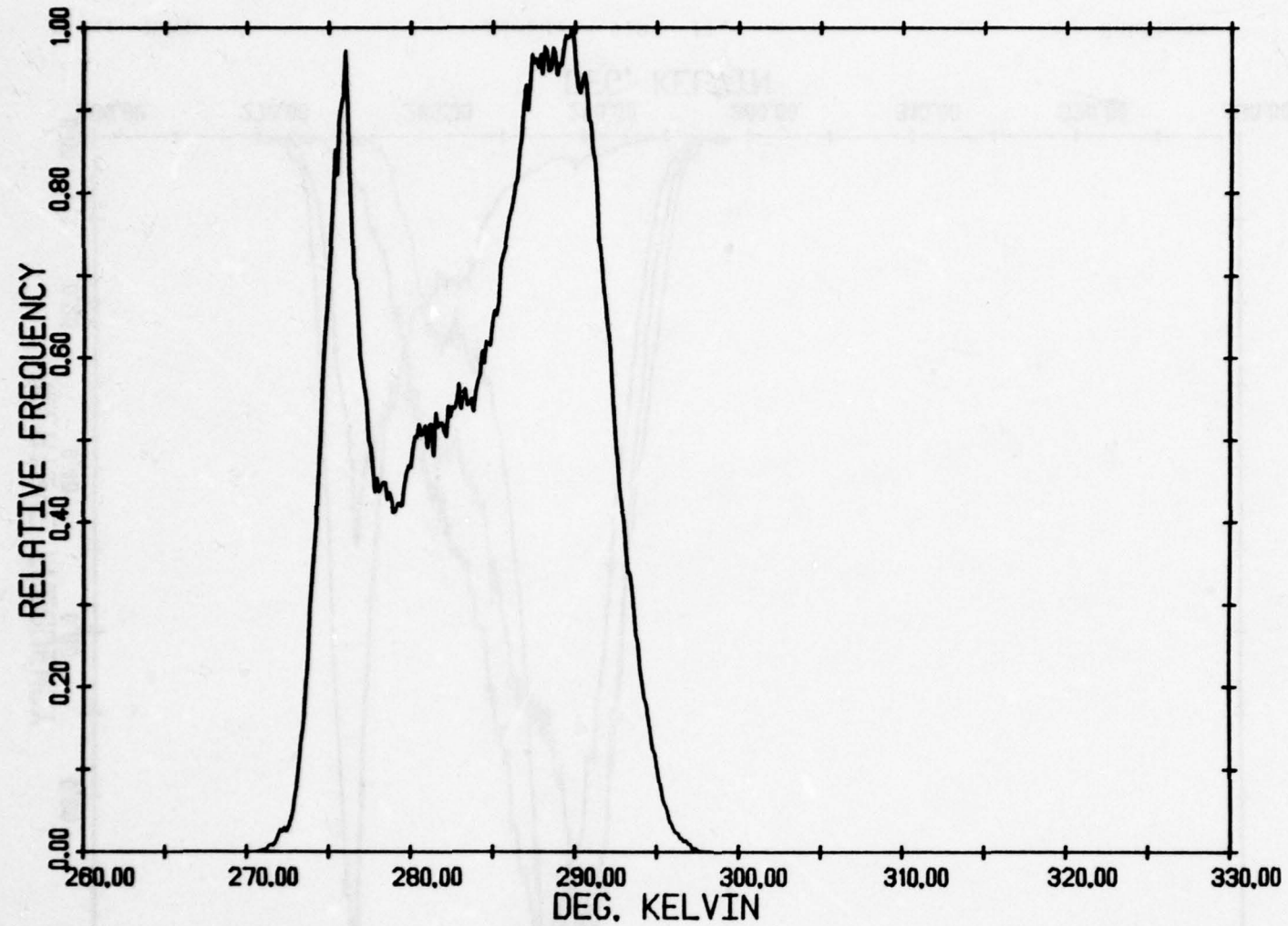

128

ERIM

Area: NEVD Lambda = 9.0 - 11.4 μm Total Area

Mean = 284.44 Standard Deviation = 5.88

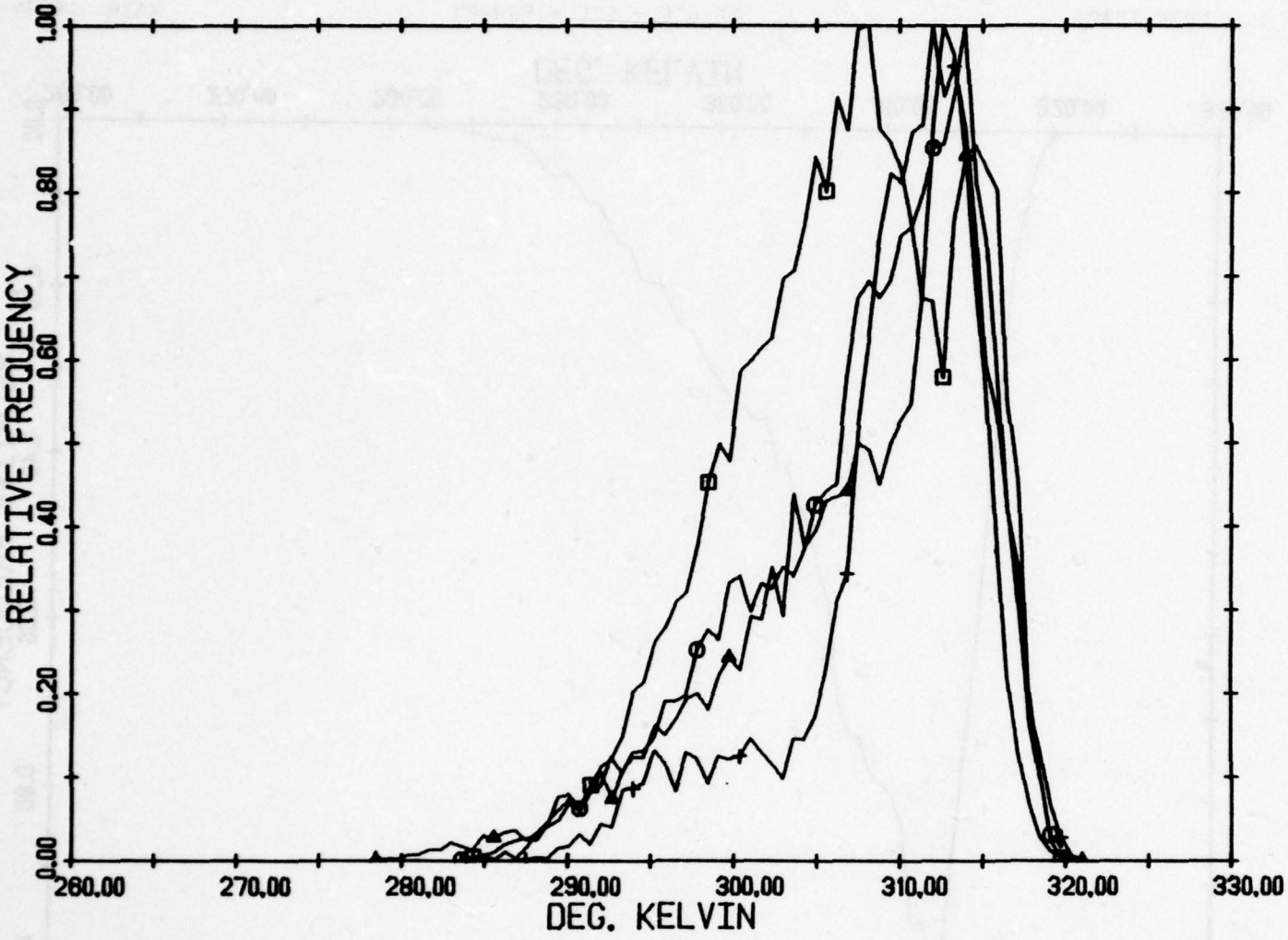

Area: NEVE

Lambda = 3.5 - 3.9 μm

Subareas

ERIM

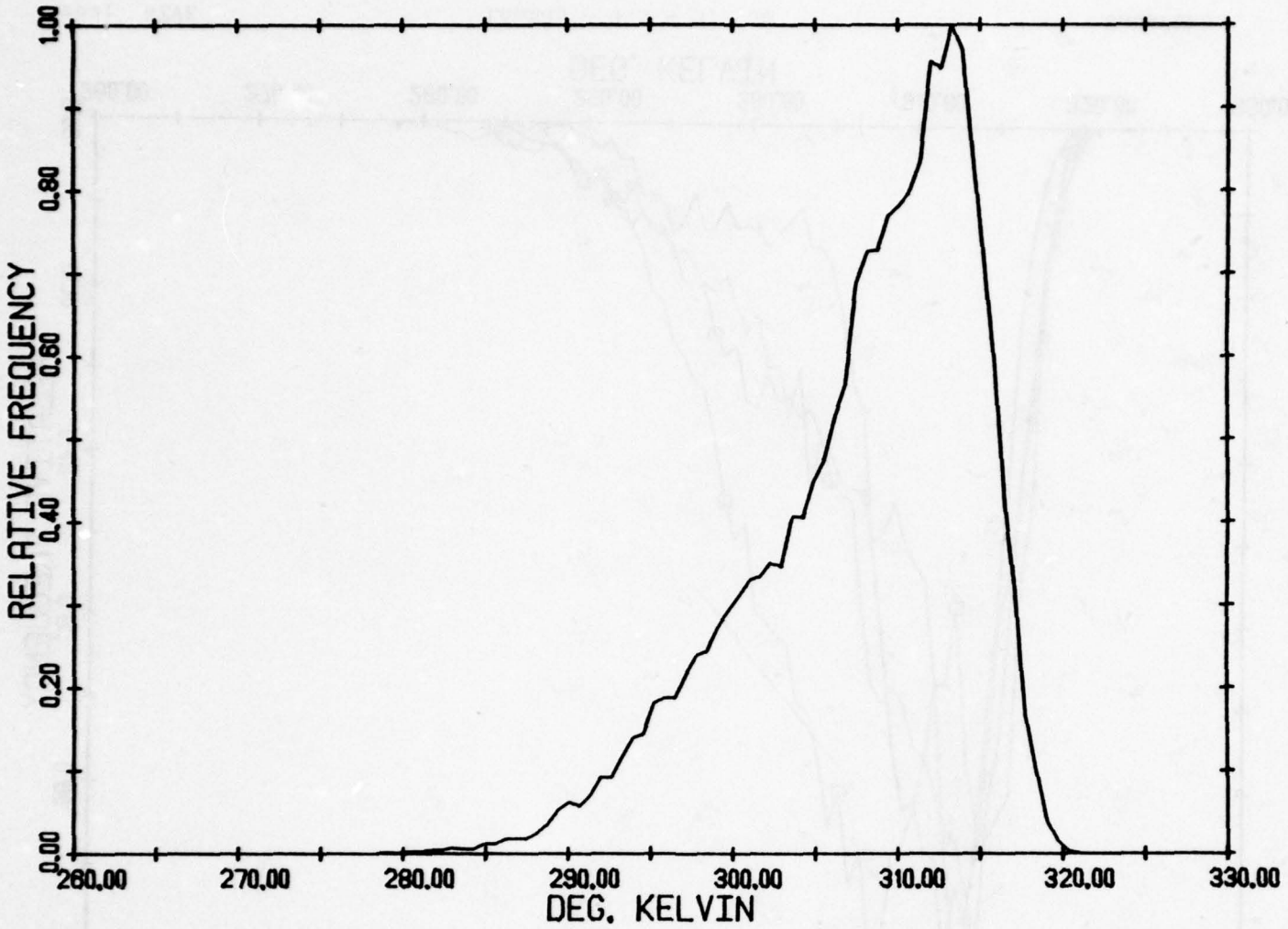

Area: NEVE Lambda = 3.5 - 3.9 μm Total Area

Mean = 307.94 Standard Deviation = 6.70

ERIM

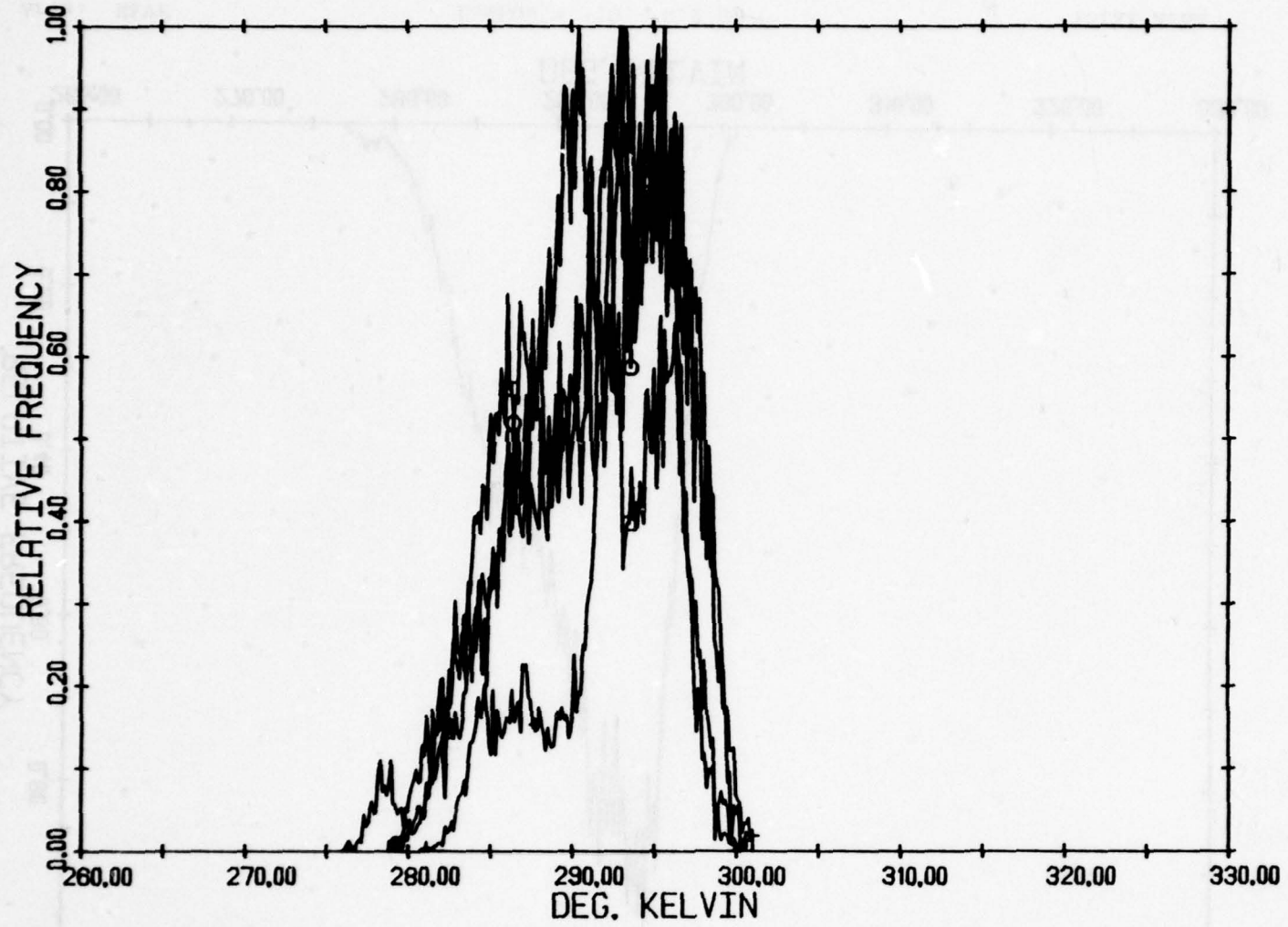

Area: NEVE

Lambda = 3.9 - 4.7 μm

Subareas

ERIM

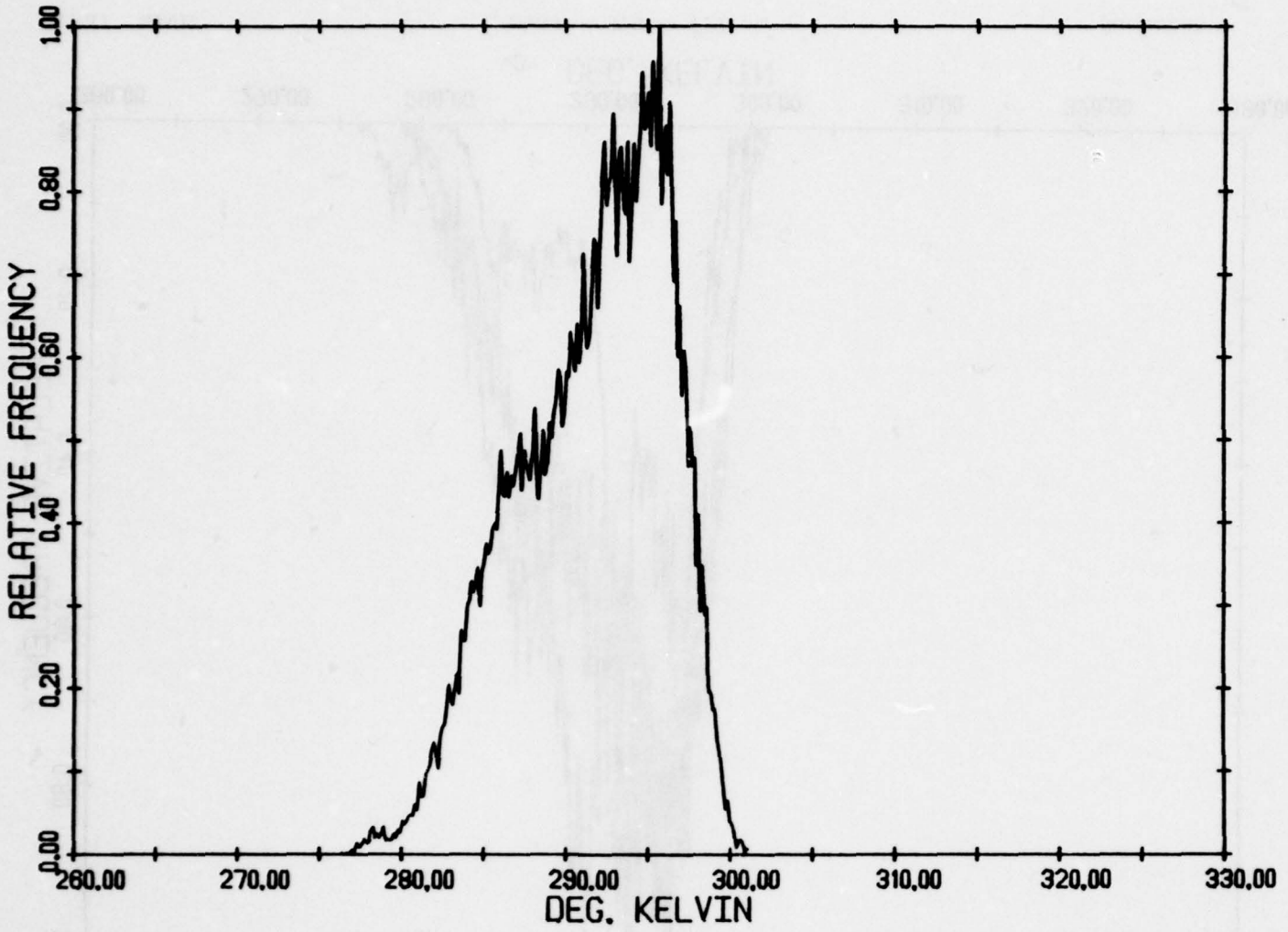

Area: NEVE Lambda = 3.9 - 4.7 μm Total Area

Mean = 291.58 Standard Deviation = 4.47

ERIM

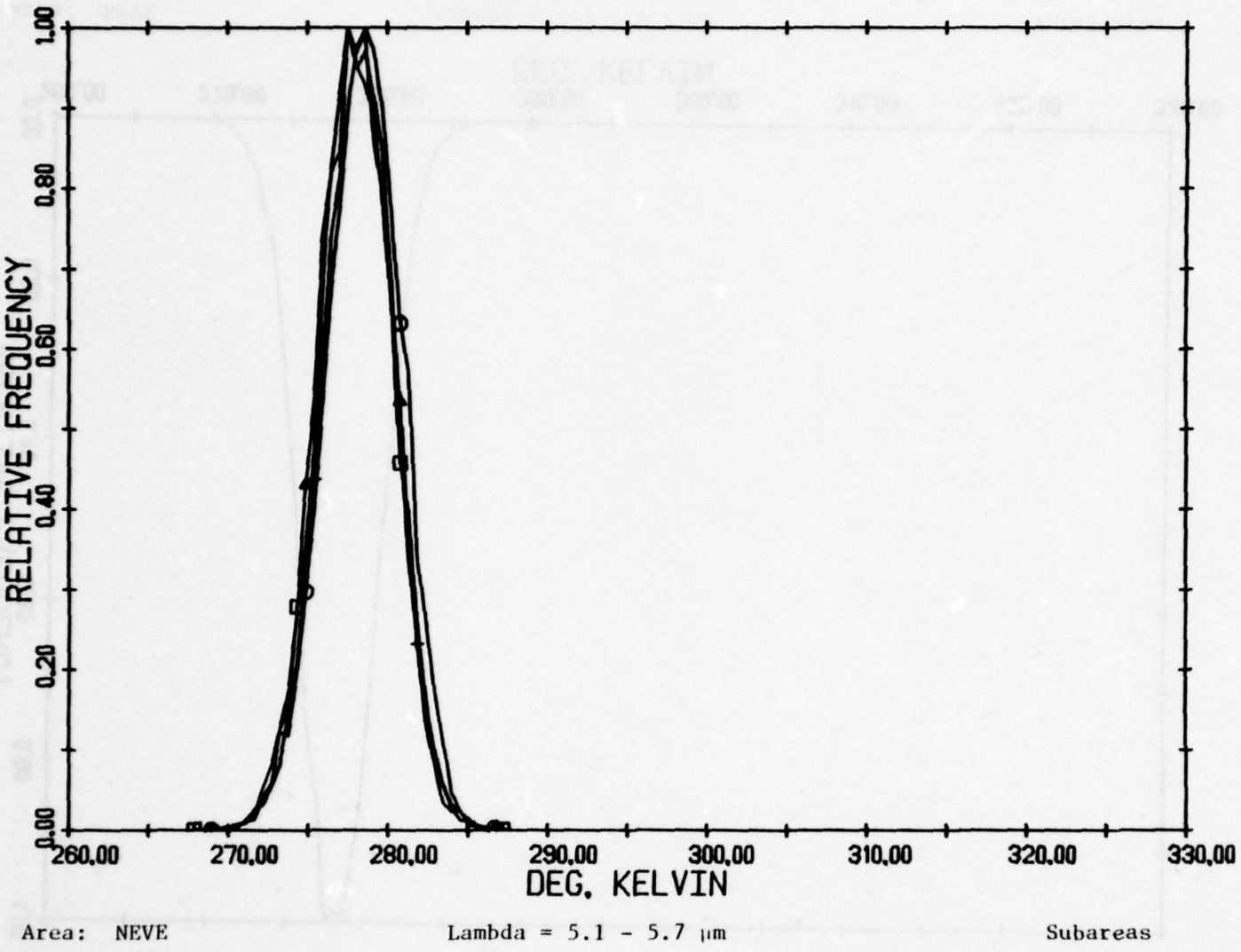

Area: NEVE Lambda = 5.1 - 5.7 μm Subareas

ERIM

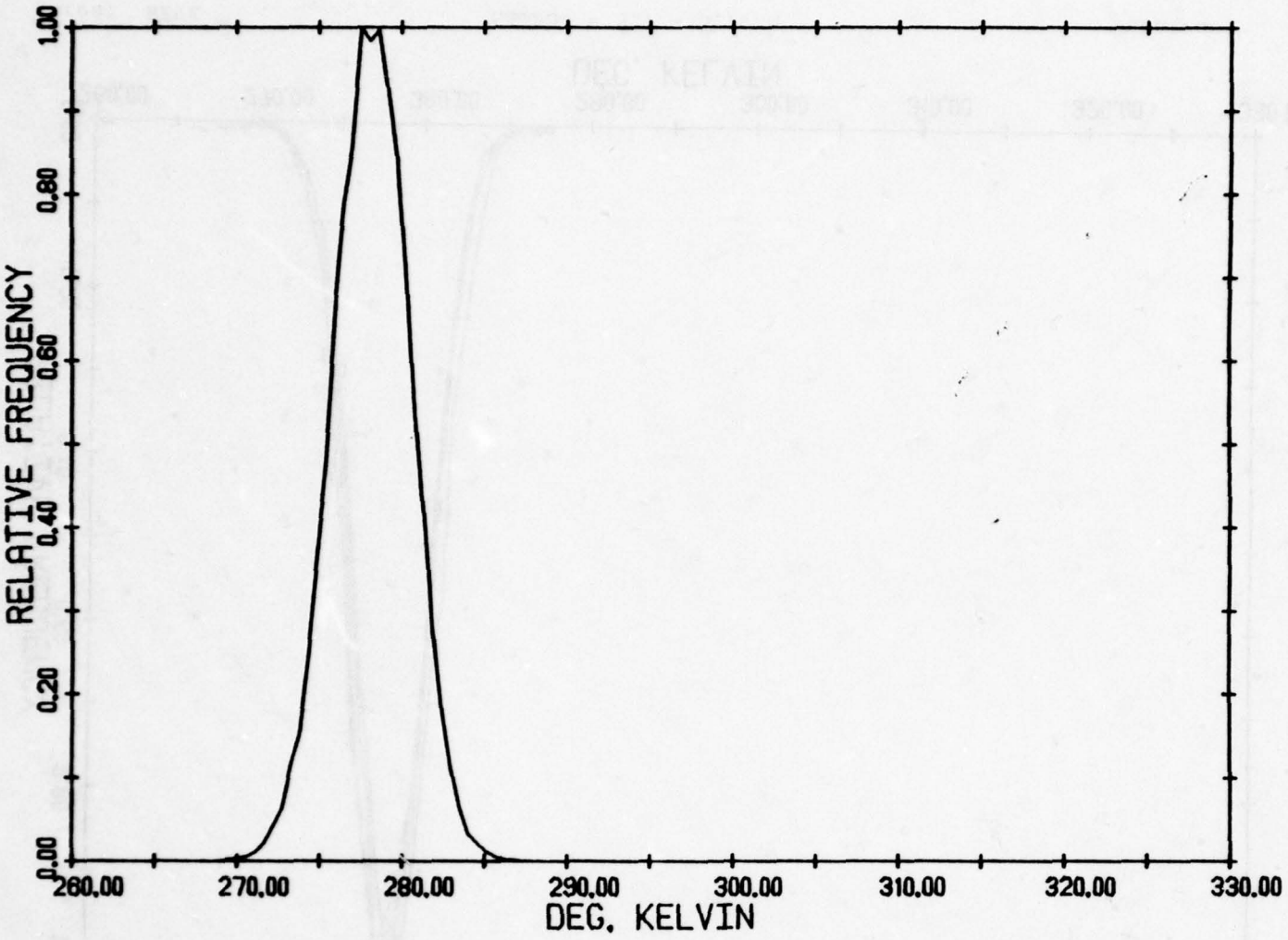

Area: NEVE Lambda = 5.1 - 5.7 μm Total Area

Mean = 278.15 Standard Deviation = 2.31

ERIM

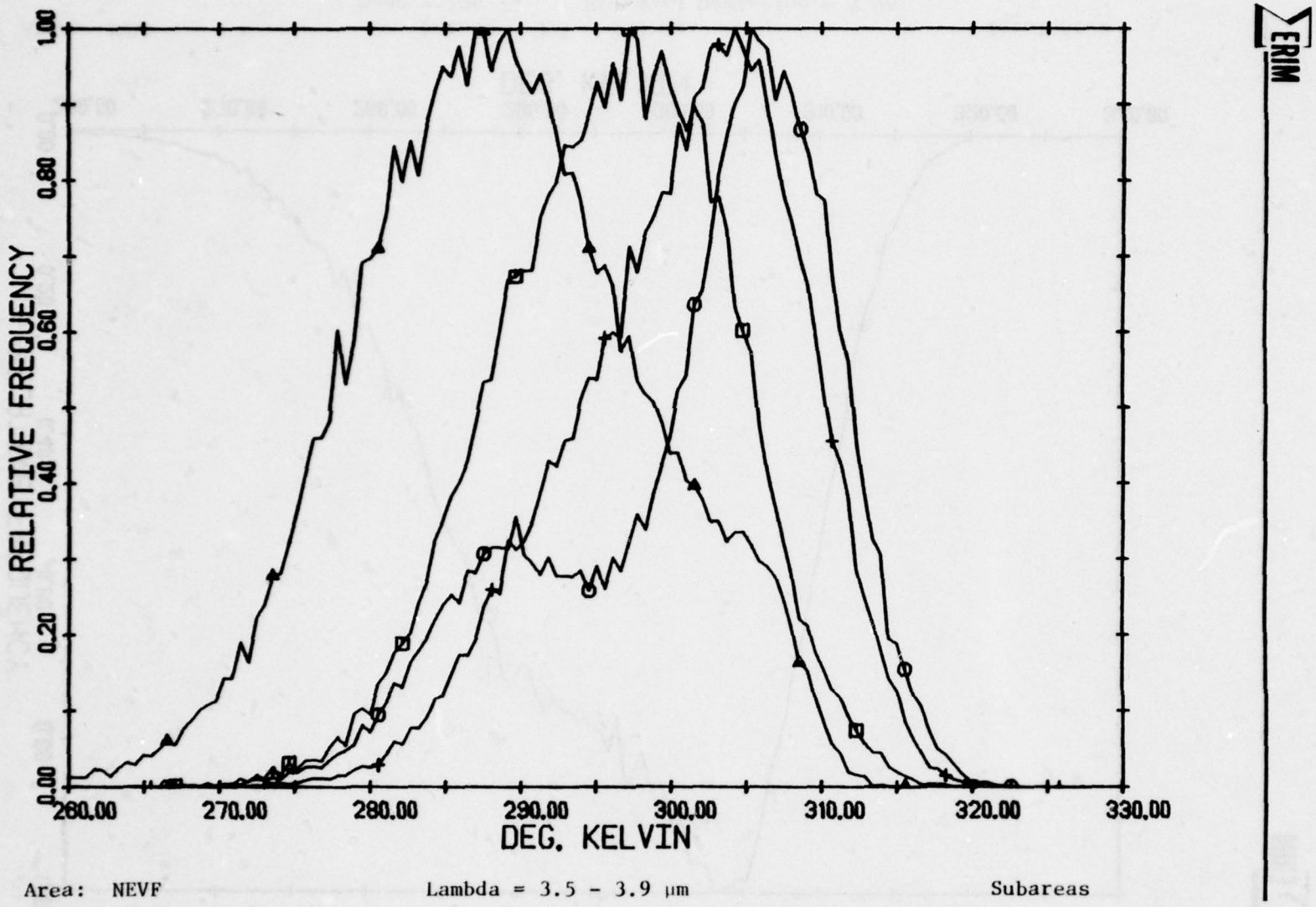

Area: NEVF

Lambda = 3.5 - 3.9 μm

Subareas

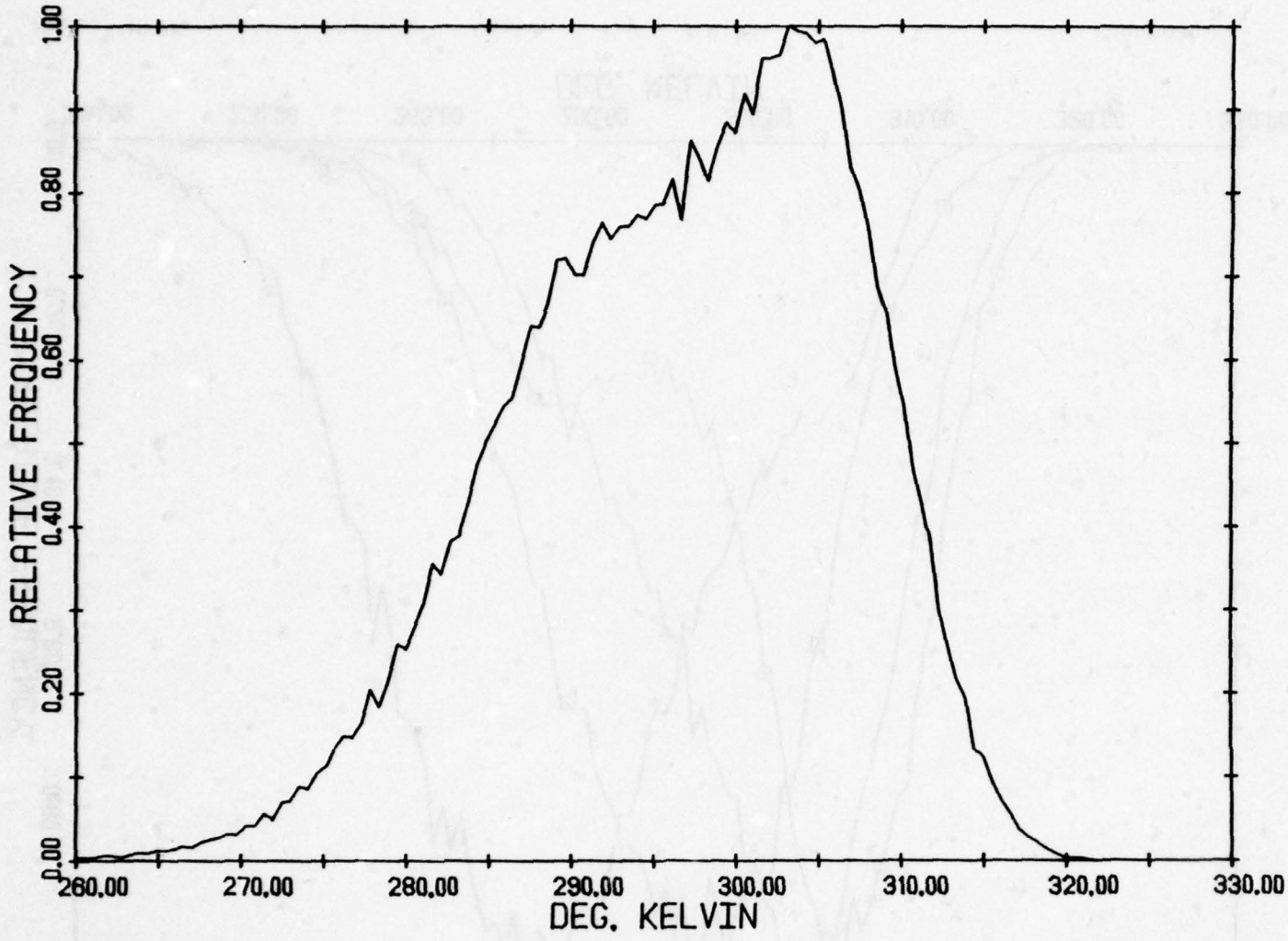

Area: NEVF Lambda = 3.5 - 3.9 μm Total Area

Mean = 296.76 Standard Deviation = 9.94

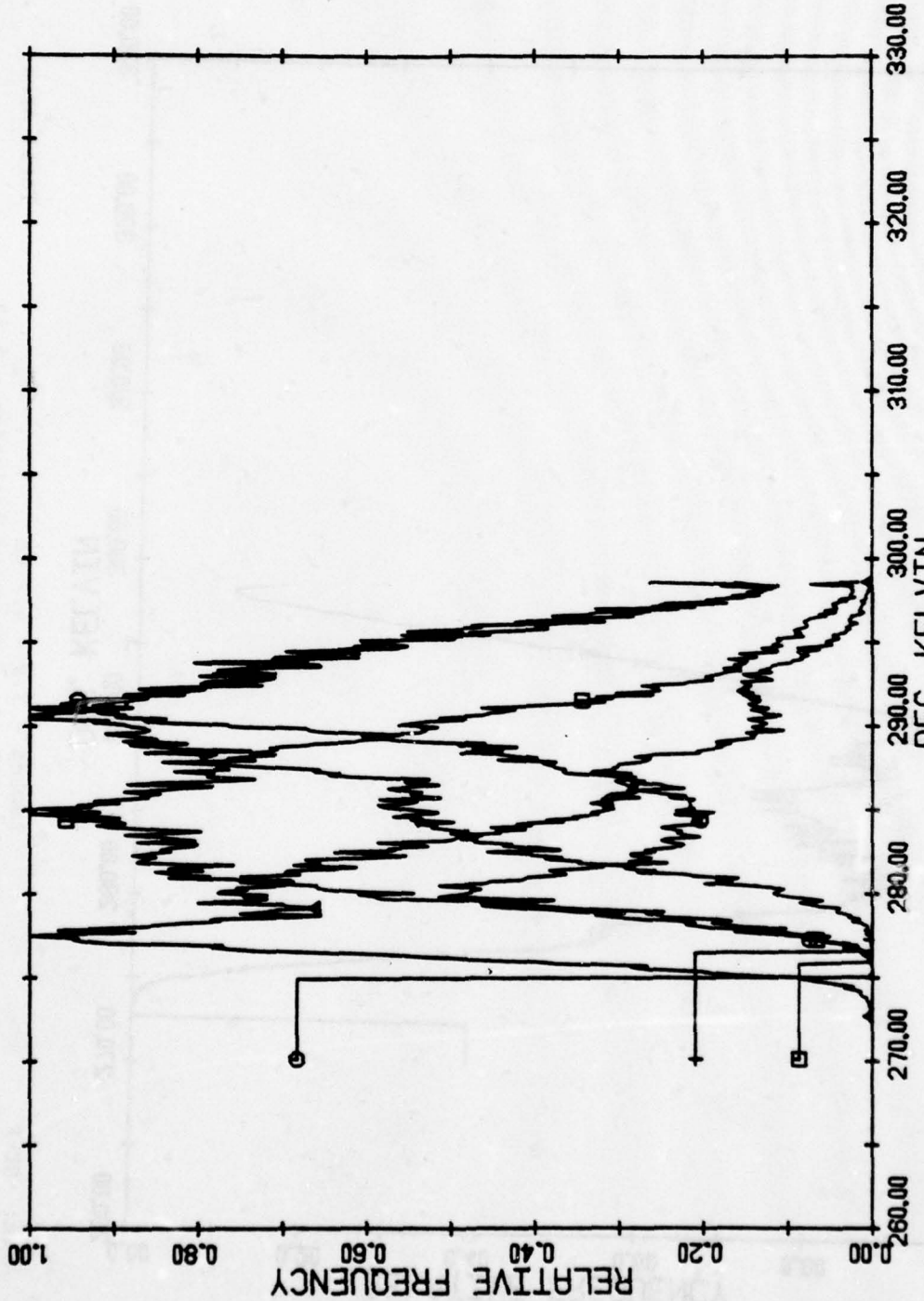

Area: NEVF Lambda = 3.9 - 4.7 μm Subareas

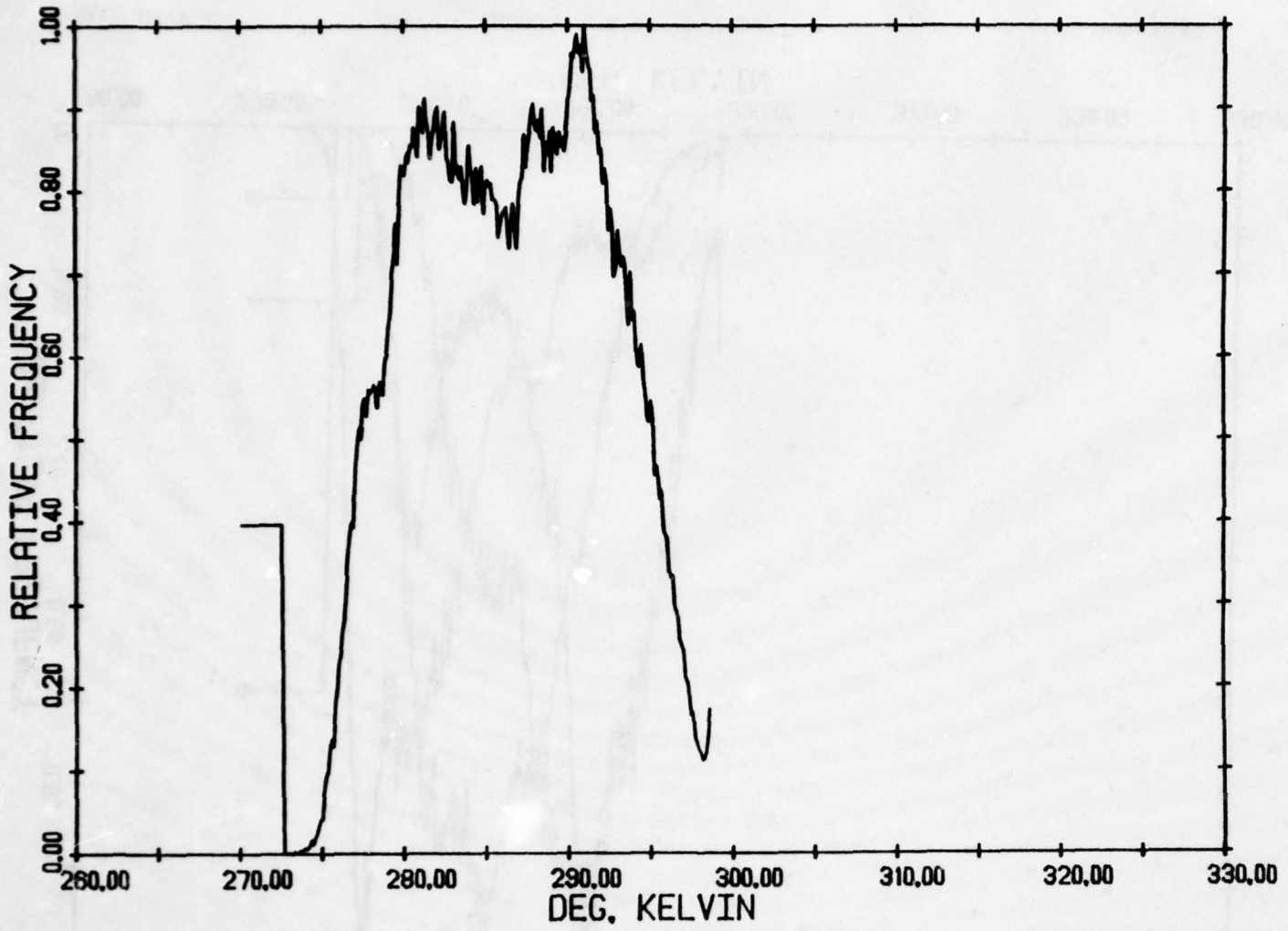

Area: NEVF Lambda = 3.9 - 4.7 μm Total Area

Mean = 286.49 Standard Deviation = 5.68

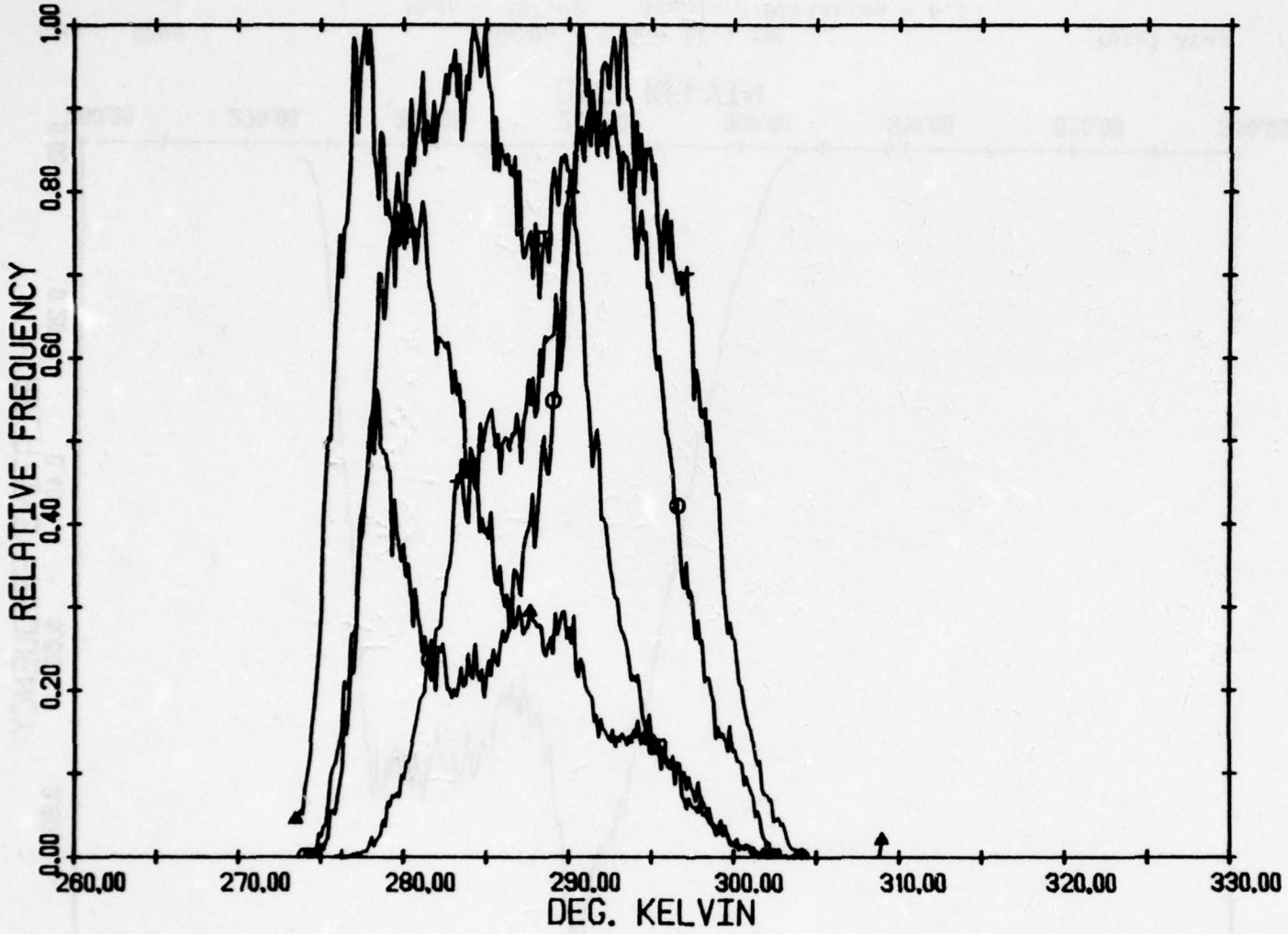

Area: NEVF

Lambda = 9.0 - 11.4 μm

Subareas

ERIM

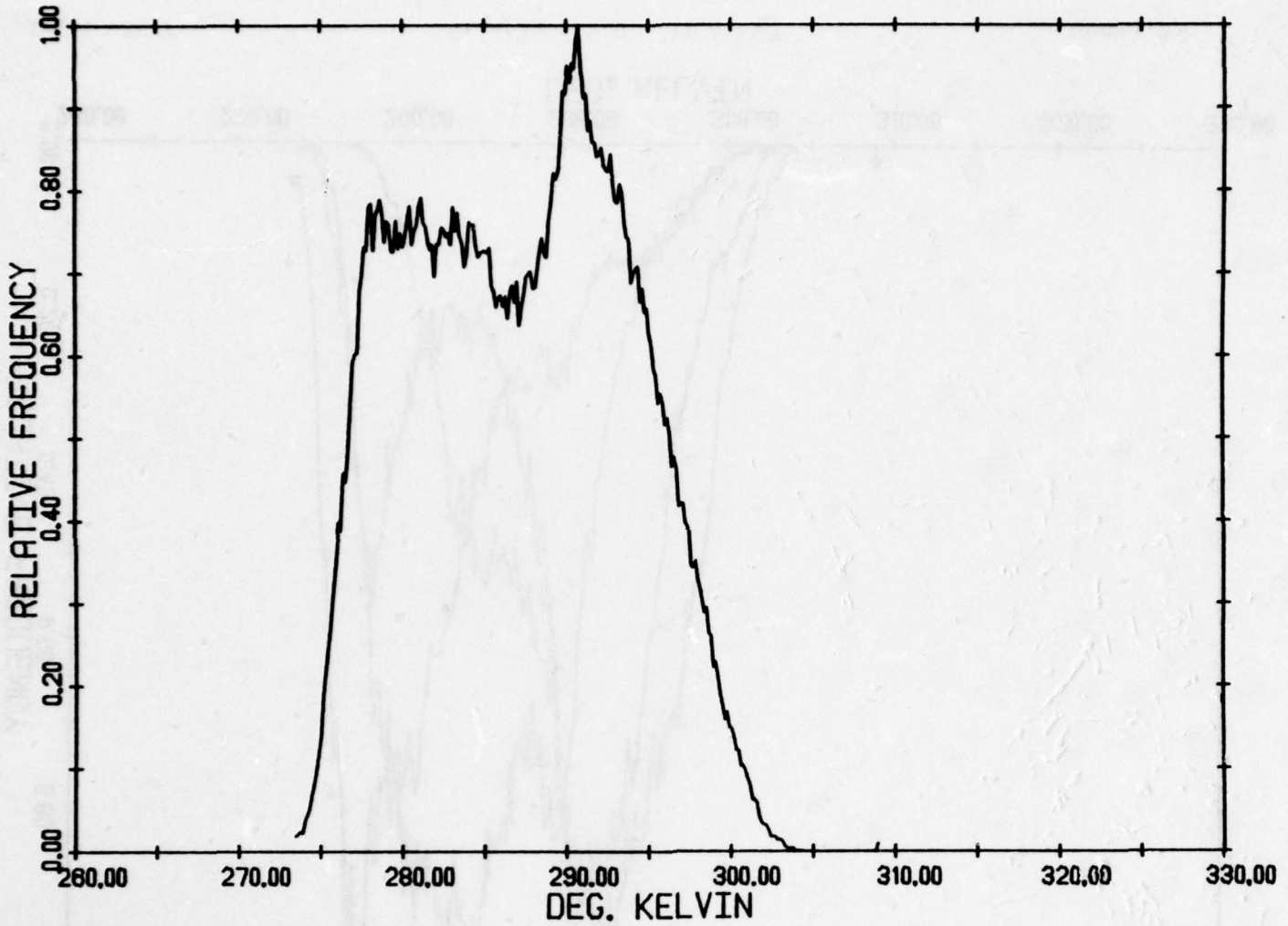

Area: NEVF Lambda = 9.0 - 11.4 μm Total Area

Mean = 287.08 Standard Deviation = 6.53

ERIM

APPENDIX 3

APPENDIX 3

One dimensional power spectra have been measured from the imagery for each of NEVB, NEVC1, NEVC2, NEVD, NEVE, and NEVF. The flight parameters and terrain types for each area are identified in Table 1 in the main report.

The crosstrack power spectra were obtained by averaging the one dimensional power spectrum measured for essentially all of the scan lines in the images. The in-track power spectra were obtained by averaging the one dimensional power spectrum of twenty-five lines taken along the length of the image (along the direction of aircraft flight). These twenty-five lines were equally spaced across the image.

There is a pronounced increase in the power spectral density $(K^2)/(1/M)$ in the NEVB crosstrack data at $6 \times 10^{-2}(1/M)$ especially in the 3.5 - 3.9 μm data. This is not a terrain feature but is due to electrical pickup on board the aircraft. The feature is apparent at $1.5 \times 10^{-2}(1/M)$ in the NEVE data. The feature appears at a lower spatial frequency in the NEVE data because the data were collected at a higher altitude (but the electrical pickup remained at the same temporal frequency).

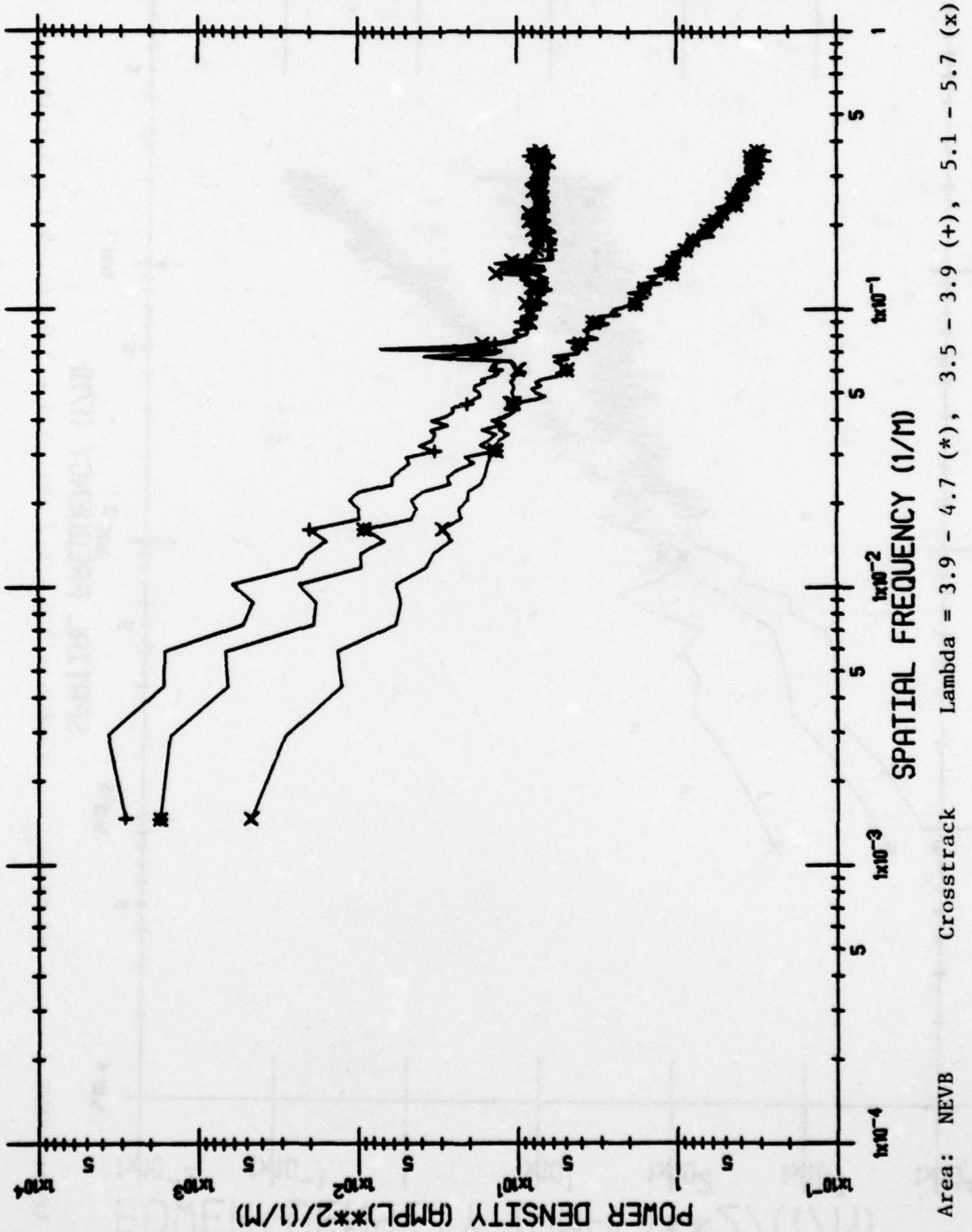

Area: NEVB Crosstrack Lambda = 3.9 - 4.7 (*), 3.5 - 3.9 (+), 5.1 - 5.7 (x)

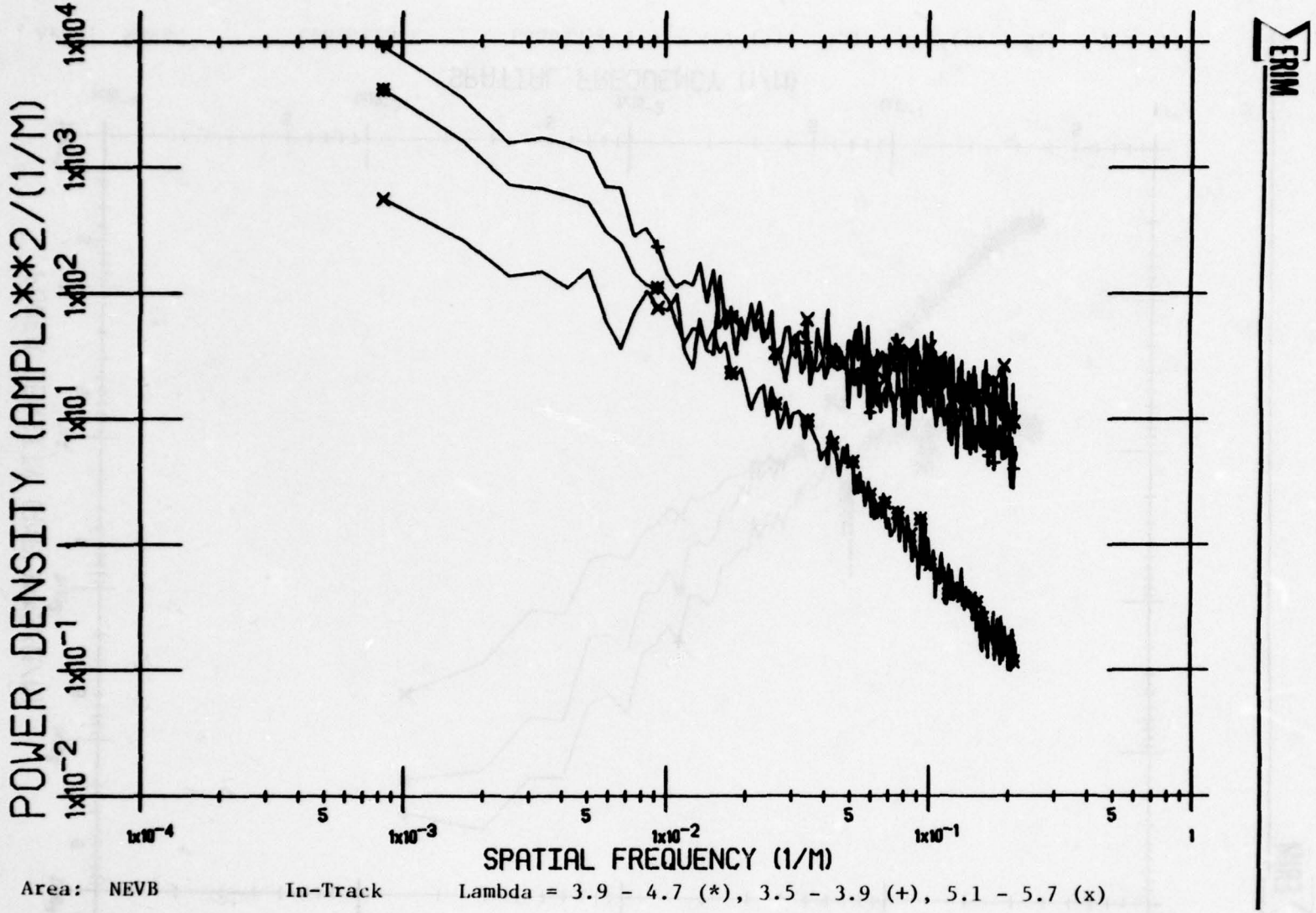

Area: NEVB In-Track Lambda = 3.9 - 4.7 (*), 3.5 - 3.9 (+), 5.1 - 5.7 (x)

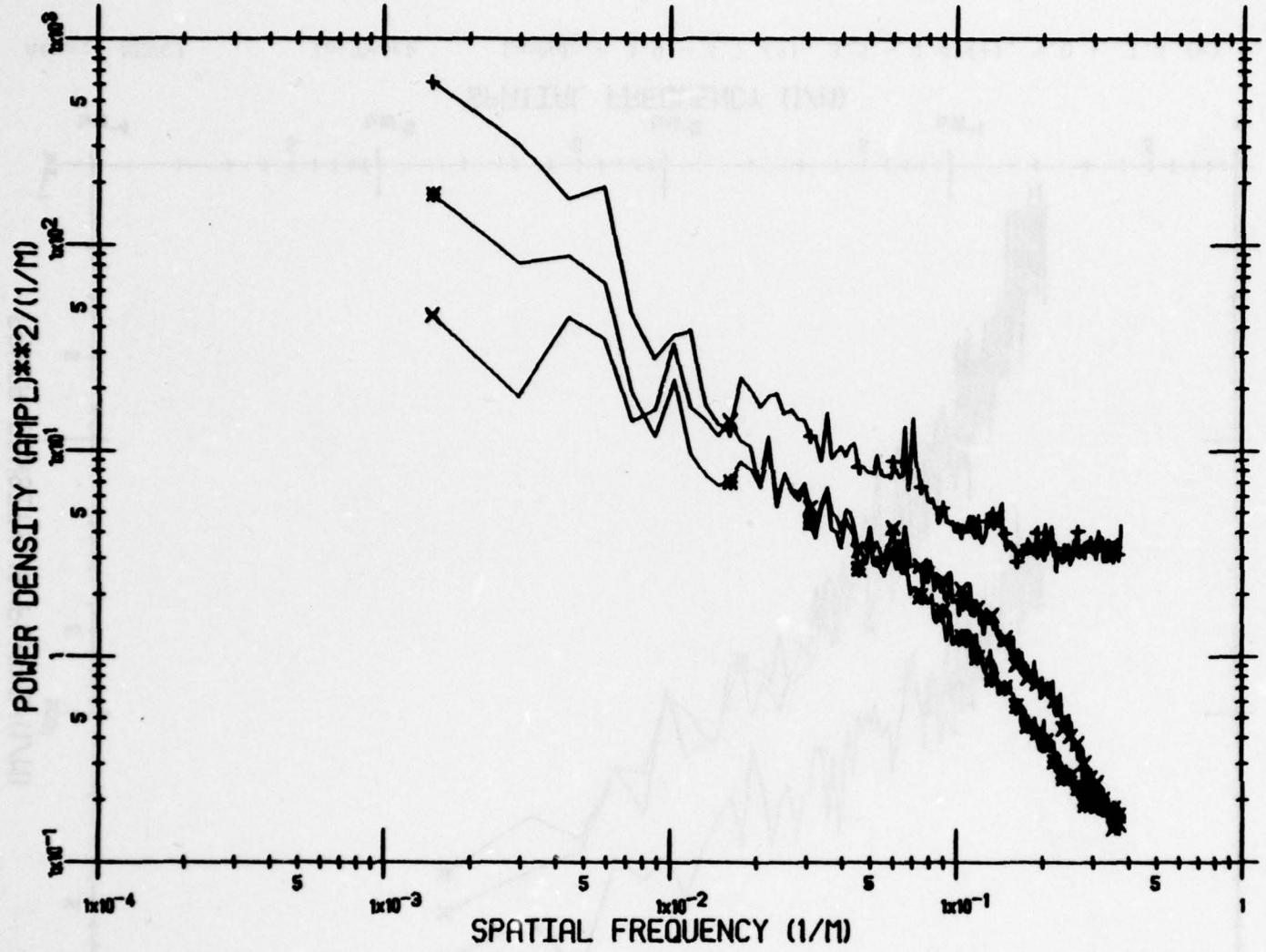

Area: NEVC1 Crosstrack Lambda = 3.9 - 4.7 (*), 3.5 - 3.9 (+), 9.0 - 11.4 (x)

ERIM

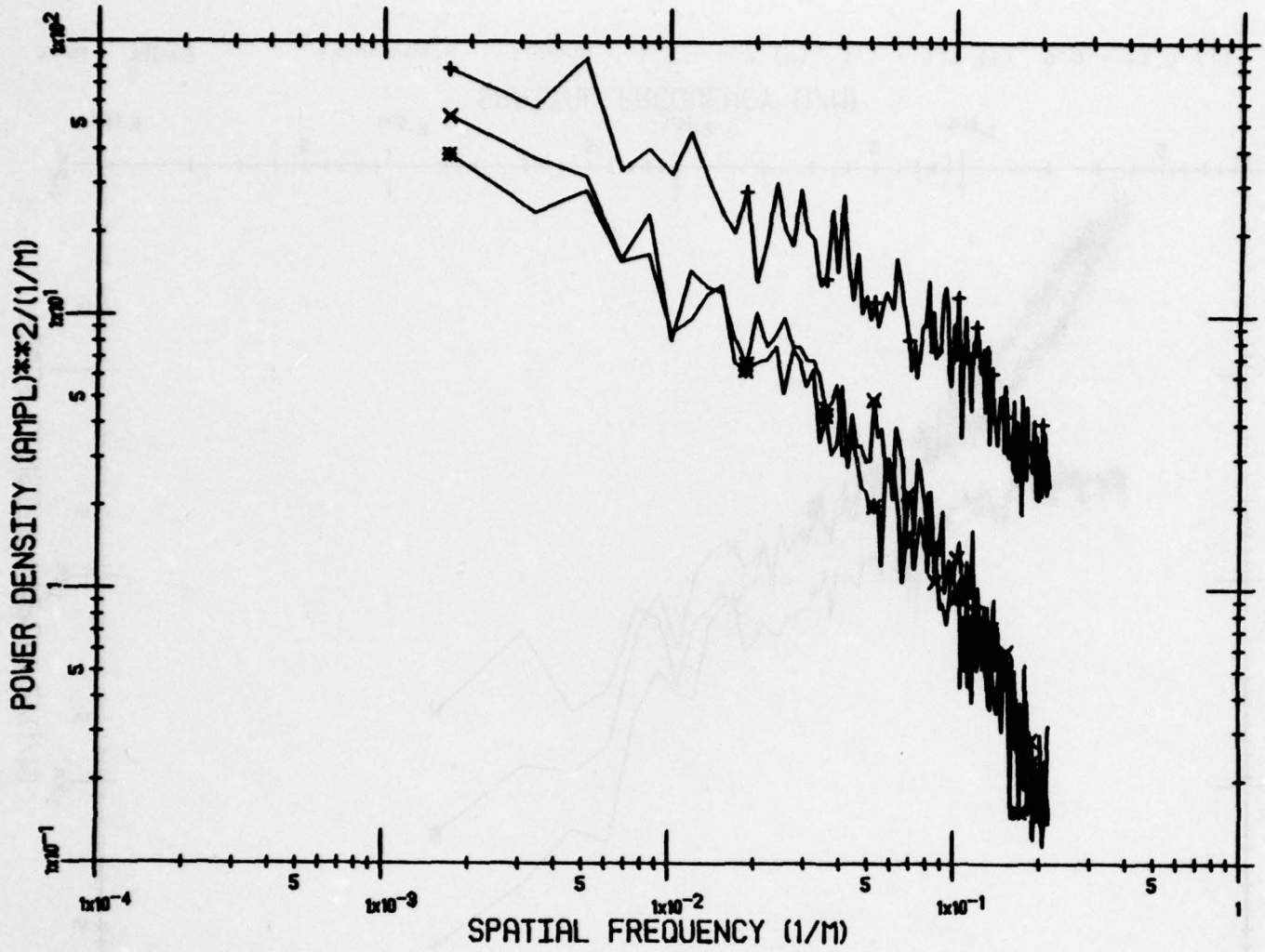

Area: NEVC1 In-Track Lambda = 3.9 - 4.7 (*), 3.5 - 3.9 (+), 9.0 - 11.4 (x)

ERIM

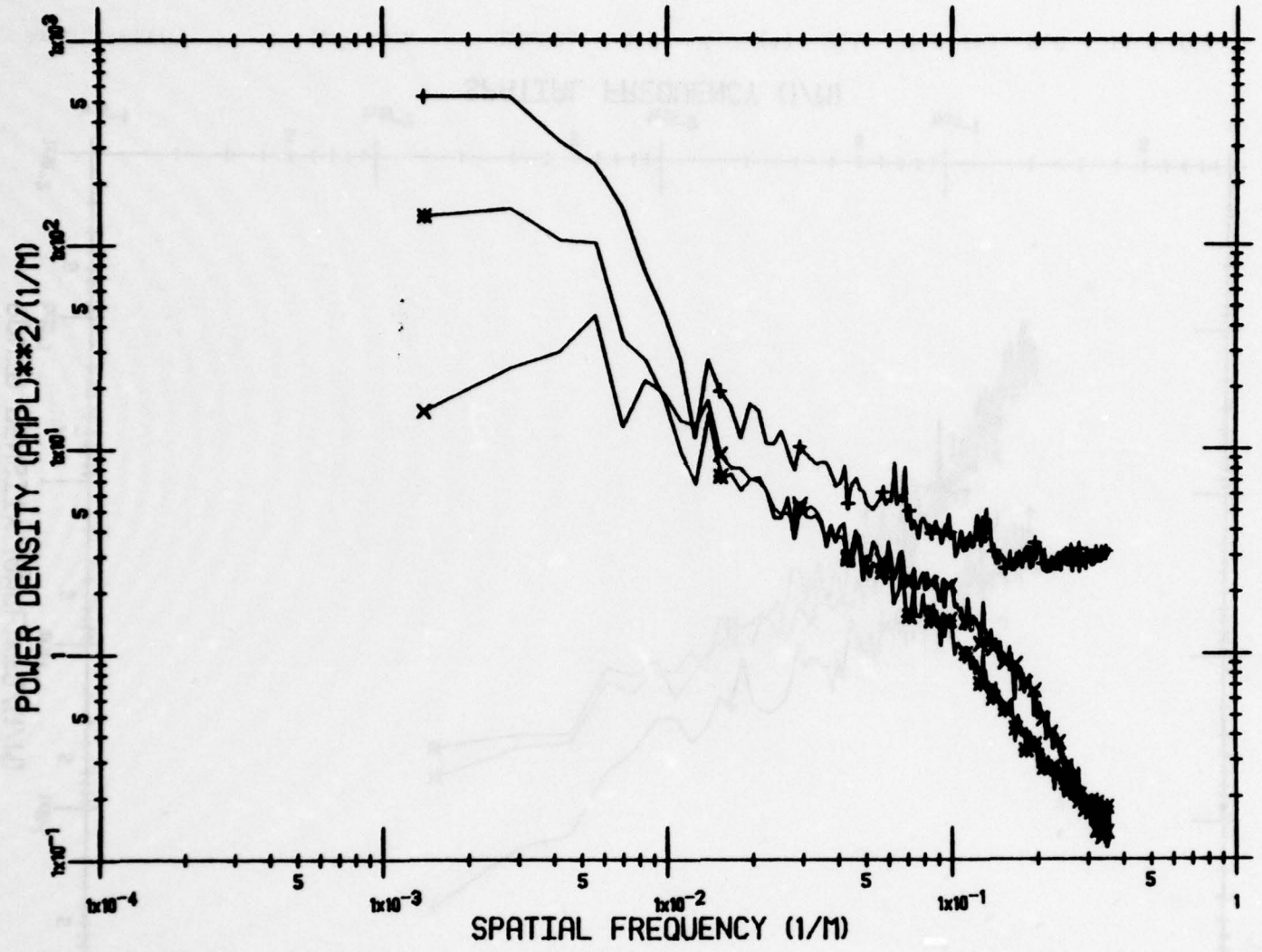

Area: NEVC2 Crosstrack Lambda = 3.9 - 4.7 (*), 3.5 - 3.9 (+), 9.0 - 11.4 (x)

ERIM

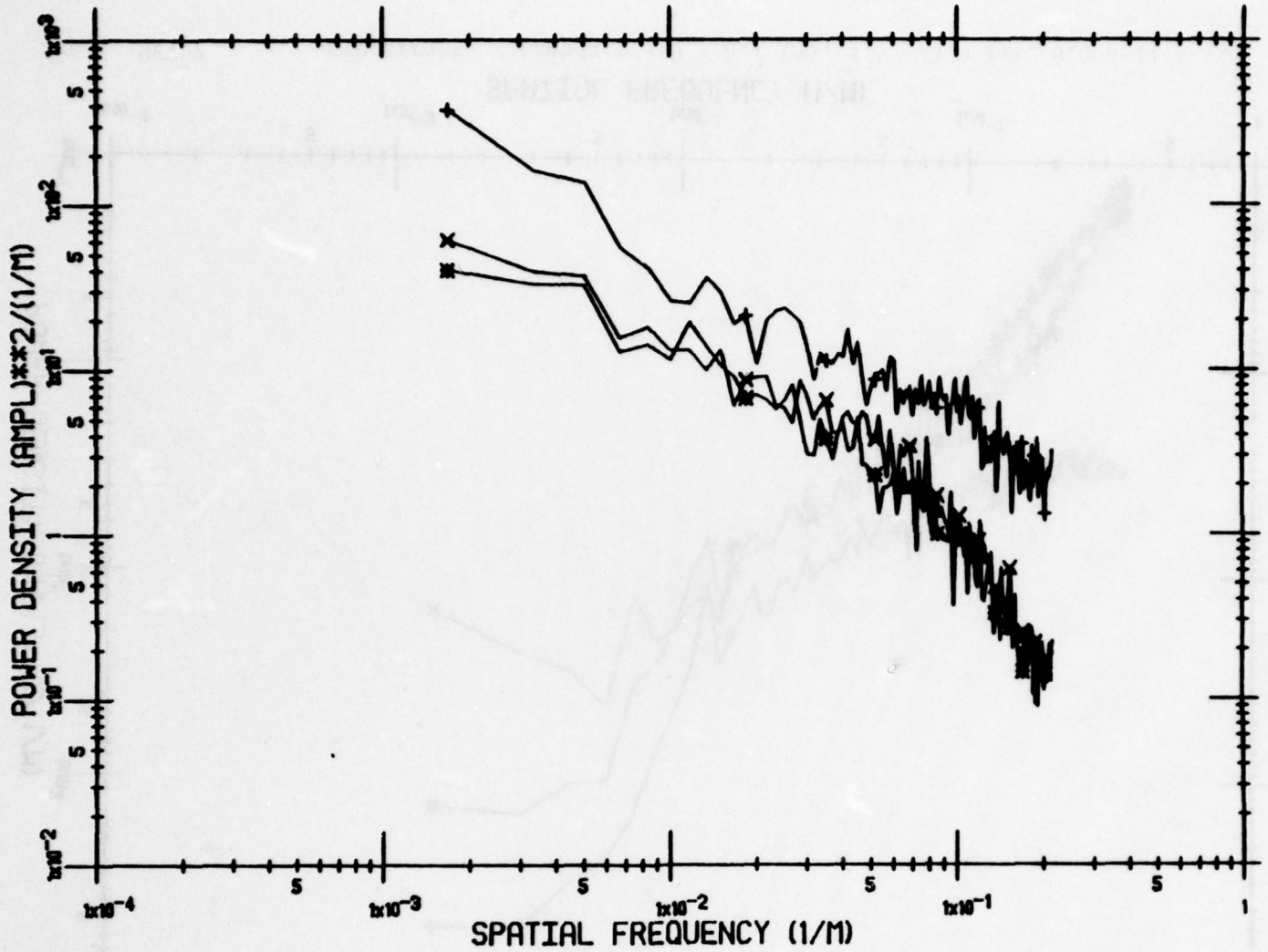

Area: NEVC2 In-Track Lambda = 3.9 - 4.7 (*), 3.5 - 3.9 (+), 9.0 - 11.4 (x)

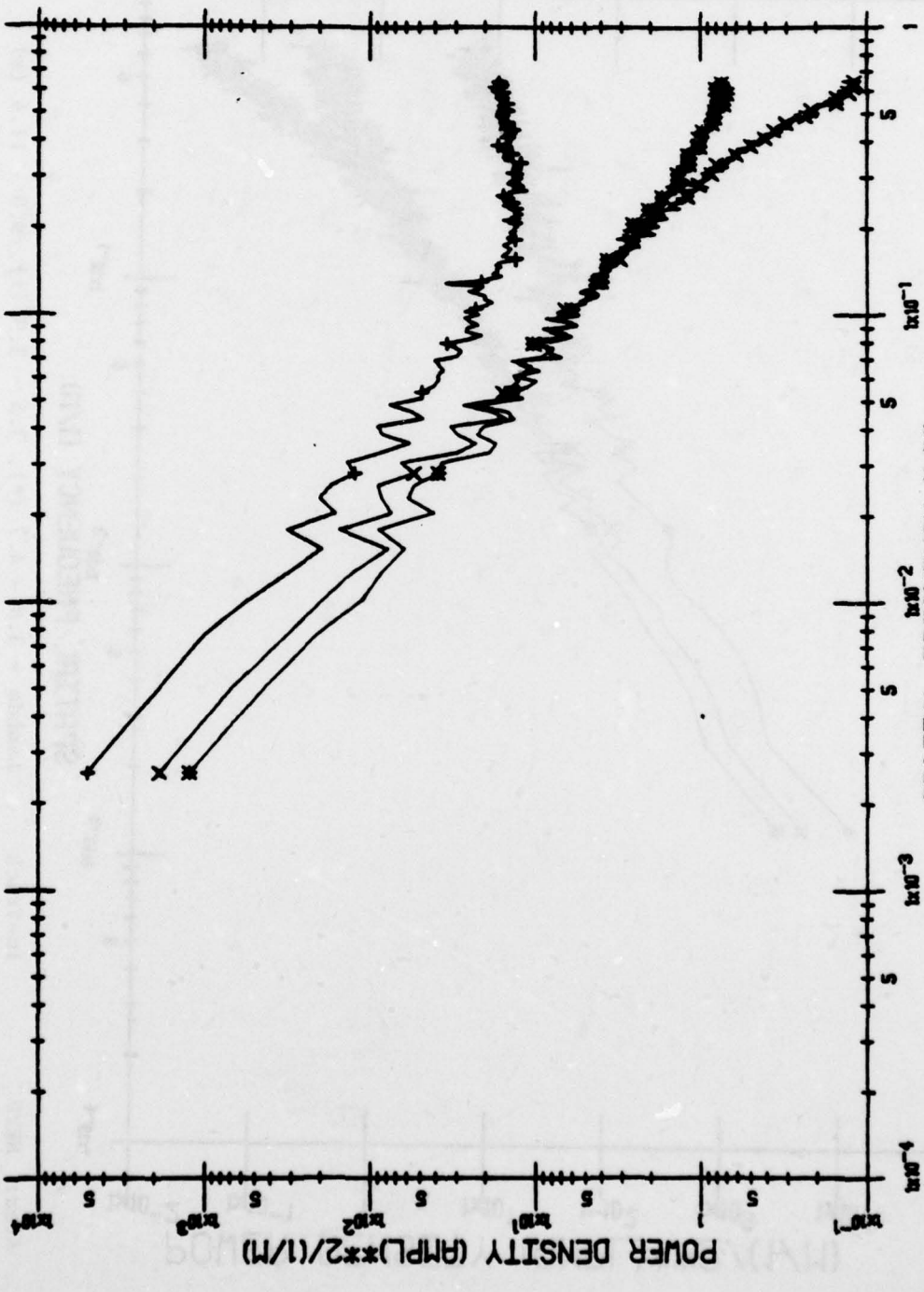

Area: NEVD Crosstrack Lambda = 3.9 - 4.7 (*), 3.5 - 3.9 (+), 9.0 - 11.4 (x)

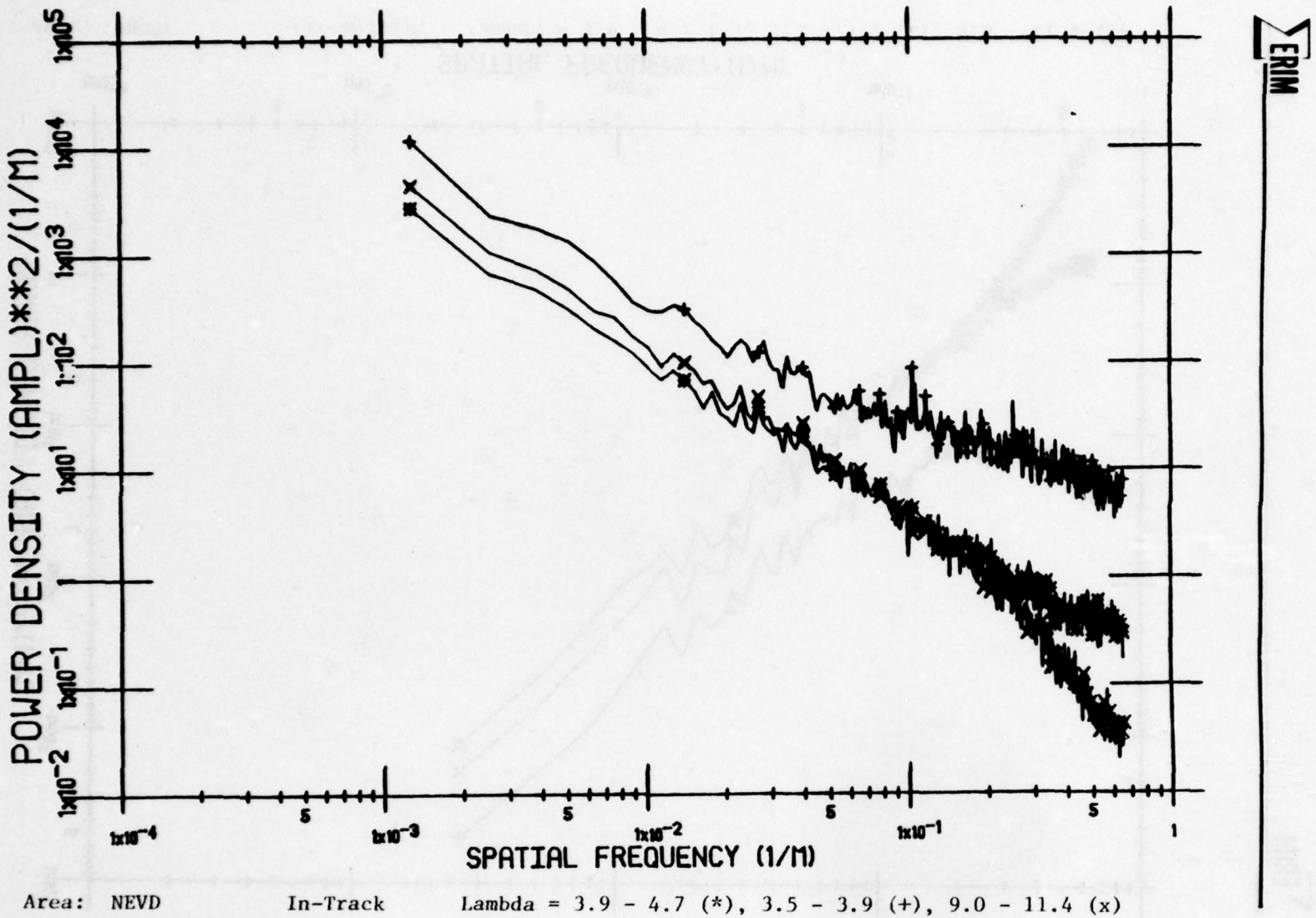

Area: NEVD In-Track Lambda = 3.9 - 4.7 (*), 3.5 - 3.9 (+), 9.0 - 11.4 (x)

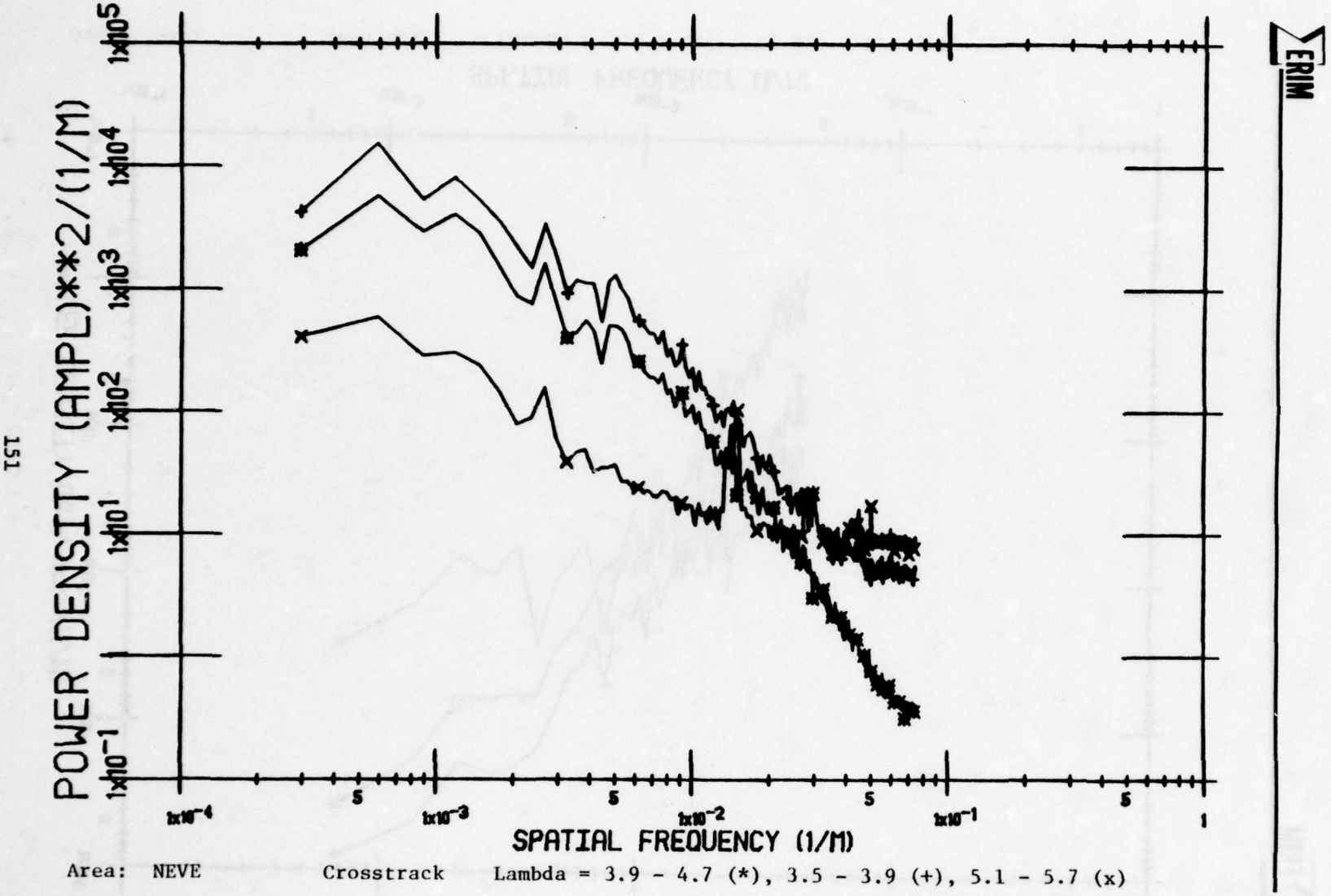

151

Area: NEVE Crosstrack Lambda = 3.9 - 4.7 (*), 3.5 - 3.9 (+), 5.1 - 5.7 (x)

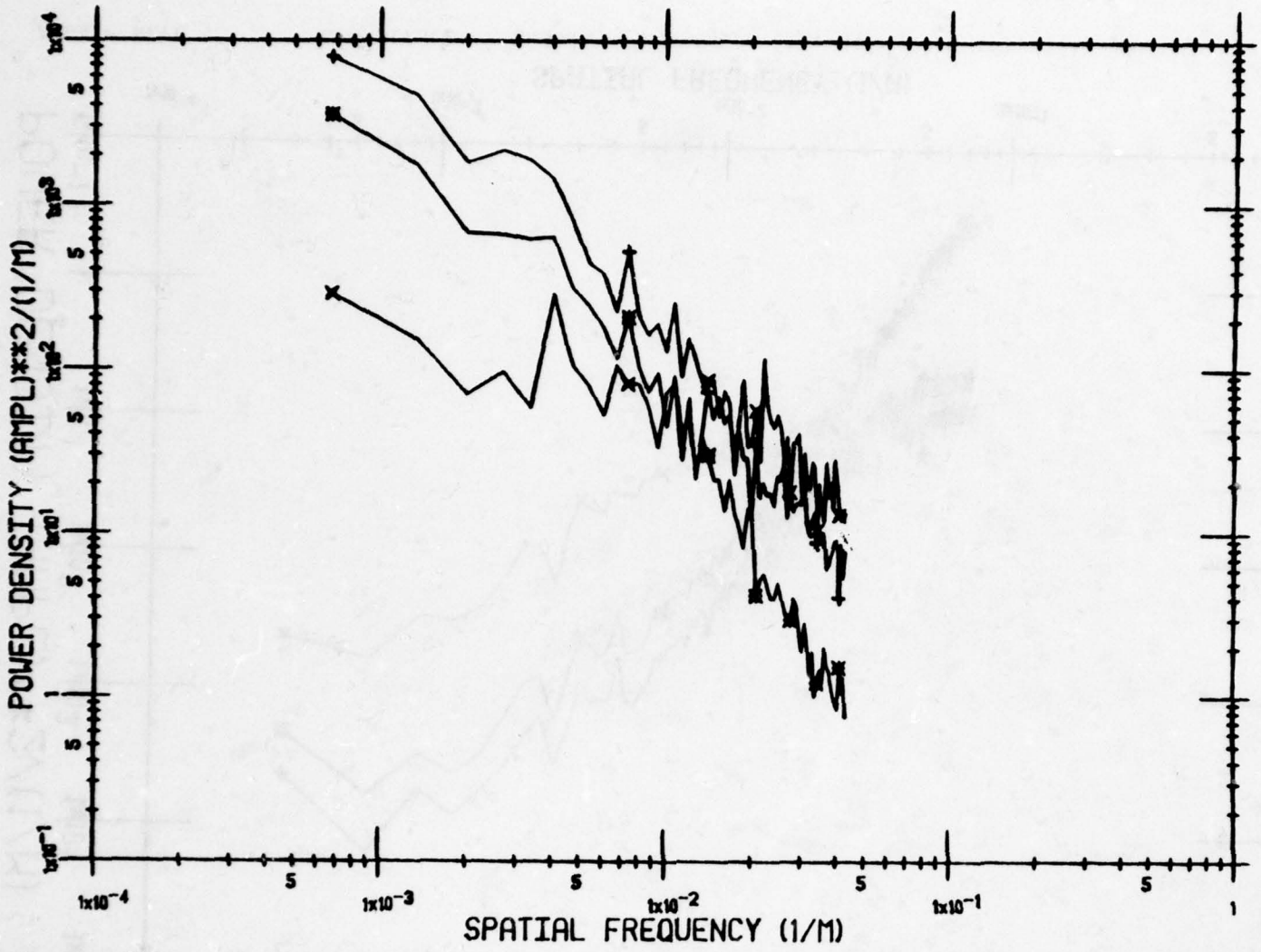

Area: NEVE In-Track Lambda = 3.9 - 4.7 (*), 3.5 - 3.9 (+), 5.1 - 5.7 (x)

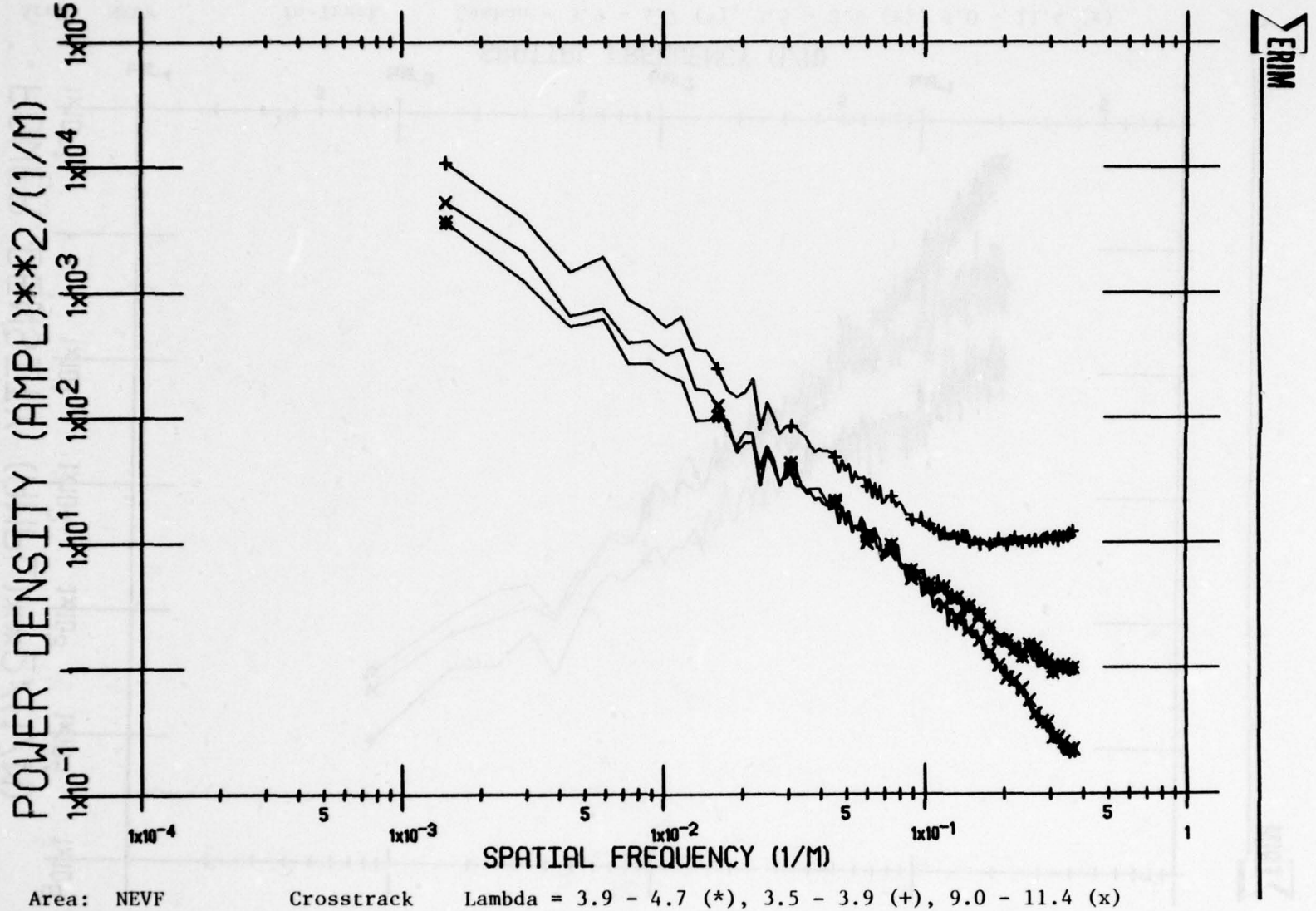

Area: NEVF Crosstrack Lambda = 3.9 - 4.7 (*), 3.5 - 3.9 (+), 9.0 - 11.4 (x)

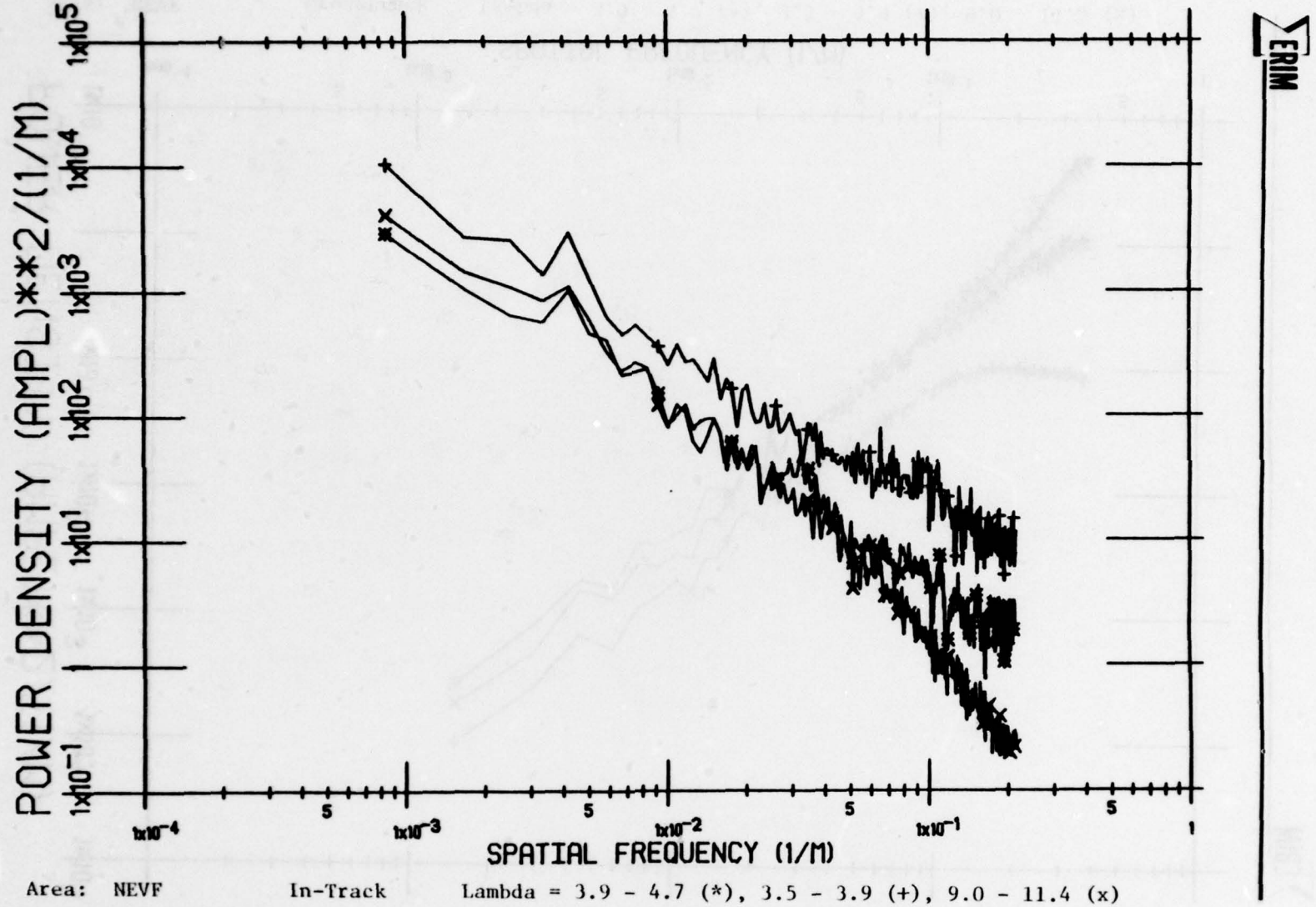

Area: NEVF In-Track Lambda = 3.9 - 4.7 (*), 3.5 - 3.9 (+), 9.0 - 11.4 (x)